Measurement of the Retinal Arteriolar Response to a Hyperoxic Provocation

by Margaret O' Halloran

Supervisor: Prof. Chris Dainty

A thesis submitted in partial fulfilment of the requirements for the degree of Doctor of Philosophy,

Applied Optics, School of Physics,
National University of Ireland Galway

September 2013

Abstract

The endothelium is a monolayer of cells that lines the inner surface of blood vessels; it plays an important role in local blood flow regulation by secreting vasoactive factors, which modulate vascular tone, in response to various agonists and stimuli. Non-invasive stimulation methods can be used to provoke vessels to react (i.e. constricting or dilating), allowing assessment of endothelial function. Such vascular reactivity can be directly visualised in the retinal circulation.

This thesis describes a series of experiments performed to investigate retinal vascular reactivity in a number of different cohorts. This was achieved by measuring the diameter of retinal arterioles, from image sequences obtained using a high-resolution confocal scanning laser ophthalmoscope (cSLO), before and during oxygen breathing and calculating the change in diameter in response to the hyperoxic stimulus. First we describe the image processing techniques used to register, and subsequently average, the image sequences. This is followed by a description of the vessel tracking and vessel diameter measurement algorithms implemented.

In a group of young healthy subjects we investigate whether a reactivity measurement taken from a single, arbitrary measurement site can be considered as representative of the retinal vasculature as a whole. We present results from a group of otherwise healthy smokers, detailing the chronic and acute effects of smoking. The results obtained from healthy older persons are compared to those obtained from the young subjects, to investigate the impact of healthy aging on the magnitude of vasoconstriction. Finally we detail a small clinical study performed to assess the reactivity response in various clinical conditions, such as hypertension, and we discuss the limitations and difficulties of using our experimental protocol and setup in a clinical setting.

Acknowledgements

Firstly I would like to thank my supervisor Chris Dainty for his guidance and support during my PhD studies.

I want to thank Eamonn O' Donoghue for all his advice and for giving me the opportunity to perform my study at the UHG eye clinic. I would also like to thank all the members of staff at the UHG eye clinic for accommodating me during this study, particularly Dr. Sasha Hutchinson.

Thank you to all the members of the Applied Optics Group at NUIG, and to all my friends and family.

Finally, thank you, Edward, for your willingness to be my guinea pig, and your unwavering support.

This research was supported by the National Biophotonics and Imaging Platform, Ireland, and funded by the Irish Government's Programme for Research in Third Level Institutions, Cycle 4, National Development Plan 2007 - 2013 and through Science Foundation Ireland under Grant No SFI/07/IN.1/1906.

Contents

List of Tables

List of Figures

Chapter 1

Introduction

The eye is frequently referred to as a "window" into the body, because the retina uniquely provides an opportunity for the non-invasive, direct visualisation of the human vasculature, thus providing an opportunity to study the effects of various diseases in the microcirculation *in vivo*. The aim of this thesis was to use high-resolution imaging techniques to investigate the retinal arteriolar response to oxygen-breathing in a number of cohorts to assess their ability to regulate blood flow. A short presentation on retinal vasculature and blood flow is therefore necessary to give the reader a global view of the tackled problem. The role of the endothelium in ensuring a blood supply that is commensurate to the needs of the parenchyma will be described. Non-invasive, stimulation methods, which can be used to provoke the vessels to react, thus allowing assessment of endothelial function, are then presented; followed by a description of techniques for measuring blood flow, which have been previously implemented for assessing vascular reactivity. The imaging technique utilised in this project is then detailed and this chapter culminates in a synopsis of the motivation behind this thesis.

1.1 Anatomy and Physiology of Retinal Vessels

The primary function of the cardiovascular system is the rapid and efficient transport of oxygen, nutrients and waste products around the body [4]. Blood is pumped from

Figure 1.1: Diagram depicting the arrangement and structure of blood vessels. Oxygenated blood is pumped from the heart into the aorta, which gives rise to the large named arteries. The large arteries branch into smaller and smaller arteries, which in turn branch into arterioles. The arterioles branch further into a vast number of capillaries, which are the site of nutrient exchange. The capillaries converge into venules, which converge into larger and larger veins, returning deoxygenated blood to the heart. The walls of the blood vessels, except the capillaries, consist of 3 layers or tunics: the tunica intima; the tunica media; and the tunica adventitia. Image adapted from http://goo.gl/rF7l34.

the left ventricle of the heart into the aorta, which gives rise to the large named arteries. These large arteries branch repeatedly into smaller and smaller arteries, which in turn branch into the muscular resistance vessels – the arterioles. The arterioles branch even further into a vast number of thin-walled capillaries, which are the site of nutrient exchange. The capillaries converge into venules, which converge into larger and larger veins, returning the blood to the right side of the heart via the venae cavae [4–6]. The arterioles, along with the capillaries and venules are termed the microcirculation [5–7]. The structure of the blood vessels can be seen in Figure 1.1.

The wall of the blood vessels, except the capillaries, consist of 3 layers or tunics [4]. The innermost layer, at the luminal interface, is the tunica intima. The intima is a single layer of squamous endothelial cells resting on a thin layer of connective tissue [4, 5, 8–10]. The endothelium is involved in the regulation of vascular tone, platelet activity and vascular permeability [4, 8, 10]; its role in blood flow regulation will be discussed in Section 1.4.4. The tunica media, the middle layer, is made up

of smooth muscle cells, elastin and collagen fibres, thereby supplying the mechanical strength and contractile power [4]. The proportion of each of these constituent materials present in the media of a vessel varies depending on the size and function of the vessel [6]. The media is bounded by sheets of elastin, called the internal and external elastic lamina [4]. The outermost layer is the tunica adventitia. The adventitia has no distinct outer border and is composed largely of connective tissue (collagen fibres) which anchors the vessel to the surrounding tissue [4]. In most vessels, this layer also contains nerve fibres [4].

The large elastic arteries, such as the aorta and the common carotid artery, have large lumens, providing little resistance to blood flow and therefore rapidly conduct the blood away from the heart [6]. They also contain large amounts of elastin and fibrous tissue in their walls, allowing them to withstand and dampen the large pressure fluctuations produced by contractions of the left ventricle [5, 6]. As the major arteries branch into smaller and smaller arteries the character of the vessel wall changes; the amount of elastic tissue decreases and the amount of smooth muscle increases, hence these arteries are termed the "muscular arteries" [6]. The increased smooth muscle allows them to alter their tone to control blood flow to the organs.

The smallest arteries branch into the arterioles which supply the capillary bed. The tunica media of arterioles consists predominantly of smooth muscle cells with a few scattered elastic fibres. Arterioles are the main site of resistance in the circulation and are therefore called resistance vessels [4–6]. Due to the abundance of smooth muscle cells, arterioles can regulate their tone to increase or decrease blood flow to match local tissue demand [4, 6]. Structurally the retinal arterioles resemble arterioles found elsewhere in the body, however they lack an internal elastic lamina and have a greater number of smooth muscle cells, which also occur in the adventitia [11–13].

The capillaries are the smallest vessels in the cardiovascular system. Capillary numbers are colossal and they are the site of nutrient exchange [4–7]. Capillaries comprise a single layer of endothelial cells surrounded by a basement membrane and no media or adventitia [4, 6]. This thin wall provides a small diffusion distance between the blood and tissue [4]. Pericytes are embedded in the basement membrane, partially enveloping the outside of the capillary [4, 13–15]. They influence the permeability of the capillary; the more pericytes, the less permeable. Pericytes are also contractile and experimental observations suggest that they contribute to the regulation of microvascular tone [4, 13, 14]. Capillaries are classified as continuous, fenestrated, or discontinuous [4,7]. The continuous capillaries are the most impermeable type of capillary and only allow water and small lipid-soluble molecules to diffuse through [6,8].

Continuous capillaries are present in the retina and they posess tight junctions between their endothelial cells which results in the formation of the blood-retinal barrier [8, 11, 15, 16]. There is an unusually high density of pericytes in retinal capillaries compared to other organs, with a 1:1 ratio of endothelial cells to pericytes [4, 13]. This high density of pericytes is required to maintain the integrity of the blood-retinal barrier [13, 15]. The endothelium cells of fenestrated capillaries are perforated by groups of small pores, called fenestrae, which are bridged by a thin membrane called the diaphragm [4]. The diaphragm allows small molecules and hormones to pass rapidly through to reach the surrounding tissue [4]. Choroidal capillaries are fenestrated in nature and, in contrast to the retinal capillaries, pericytes have been found to be absent in the choroid [8, 11, 17]. Discontinuous capillaries are highly permeable and do not occur in the ocular circulation; they are instead found in tissue where blood cells need to migrate between the blood and the tissue, namely the bone marrow and liver.

Capillaries unite to form venules which in turn converge to form larger and larger veins [4–6]. Their walls are thinner and their lumens larger than those of their corresponding arterioles and arteries. Their thin walls are comprised of an intima, a thin media of smooth muscle and collagen and a thick adventitia of collagen which is often several times thicker than the media [4]. Veins are more numerous than arteries; this fact, together with their larger luminal size, result in approximately two-thirds of the circulating blood being contained in the veins at any one time; they are therefore known as the capacitance vessels [4]. Venous valves are formed from folds of the intima. To prevent the backflow of venous blood, there are numerous valves in the veins of the limbs, where venous flow is opposed by gravity [4, 6]. By contrast, the veins from the head, including those which drain the ocular circulation, lack these valves [4, 6, 8].

1.2 Ocular Circulation

The human eye is supplied by two vascular systems: the retinal and uveal vessels [8, 11, 13, 16, 17]. The uveal vessels include the vascular beds of the iris, the ciliary body, and the choroid [8, 16], which can be identified in Figure 1.2. In humans the ocular vessels are derived from the ophthalmic artery, which is the first branch of the internal carotid artery [8, 16]. The ophthalmic artery branches into the central retinal artery, the posterior ciliary arteries and several anterior ciliary arteries. The central retinal artery enters the optic nerve approximately 10–15 mm behind the eyeball and emerges in the eye at the optic disc, where it divides dichotomously into superior and

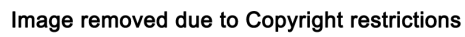

Figure 1.2: Anatomy of the human eye. Top: diagram depicting the simple anatomy of the human eye. Bottom: appearance of the retina when viewed with an ophthalmoscope. Images adapted from http://goo.gl/vjkel and http://goo.gl/xlFsb.

inferior branches [8,11]. These branches again divide in two to give four major retinal arterioles, the superior and inferior temporal and nasal arterioles, which extend out from the optic disc, each one supplying a quadrant of the retina [11,13,16]. The central retinal vein drains the retinal arterioles. The short posterior ciliary arteries supply the

Figure 1.3: Image of the retina demonstrating its multilayered nature. The inner and external limiting membranes are not visible in this image. The choroid and sclera are visible in this image. Image adapted from http://goo.gl/DKWTg.

posterior choroid, while the anterior choroid is supplied by the long posterior ciliary arteries [8]. Choroidal blood drains into the vortex veins [8].

The retina, whose location within the eye and appearance when observed with an ophthalmoscope can be seen in Figure 1.2, is the sensing element of the eye. The retina consists of ten distinct layers, which can be seen in Figure 1.3, through which the light must pass before reaching the photoreceptor layer (the rods and cones). The retinal layers are transparent, however the blood vessels are not. The inner two-thirds

Figure 1.4: Simple diagram depicting the arrangement and location of the vascular beds which nourish the retina. The larger retinal arterioles and venules are located within the nerve fibre layer and are linked through the capillary bed. The capillaries are arranged in interconnecting layers, with a two-layer arrangement in the majority of the retina. The first layer lies in the nerve fibre and ganglion cell layer and the deeper layer extends into the inner nuclear layer. The inner two-thirds of the retina are nourished by the retinal vessels, whereas the outer layers, including the photoreceptors are avascular and nourished by the choriocapillaris in the choroid. Image adapted from http://goo.gl/uGj6y.

of the retina are nourished by the retinal vessels, whereas the outer layers, including the photoreceptors are avascular and nourished by the choroid [8, 13, 16–18]. There are considerable morphological and functional differences between the retinal and choroidal vasculature.

The retinal circulation is an end-artery system without anastomoses [8, 11, 13]. The larger arterioles and venules are located within the nerve fibre layer and are linked through the capillary bed, where each capillary measures approximetely 5–7 μm [8, 11, 13, 16, 17]. The capillaries are arranged in interconnecting layers, with a two-layer arrangement in the majority of the retina [8]. The first layer lies in the nerve fibre and ganglion cell layer and the deeper layer extends into the inner nuclear layer [8, 11, 13]. A simple diagram of the retinal vascular arrangement is seen in Figure 1.4. In the cen-

tral part of the retina, these capillary layers become more dense and become three- or four-layered [8]. Towards the peripheral retina the capillary network is reduced to a single layer, and at the extreme periphery the inner retina is avascular and nourished by the choroid [8]. An avascular zone also exists centrally in the fovea, which enables light to reach the central photoreceptors without encountering the opaque blood vessels [8,11]. The choroidal capillaries have a considerably larger calibre than the retinal capillaries at $\geq$10 μm [8,17]. Blood flow in the retinal vasculature is characterised by a low perfusion rate, as opposed to the choroid which has the highest perfusion rate of all vascular beds in the body. The oxygen extraction is equally contrasting between the two vascular beds, with the retinal vasculature exhibiting a high oxygen extraction of approximately 40%, while the arteriovenous oxygen difference in the choroid is just 3–5% [8, 17, 18]. Approximately 65% of the oxygen consumed by the retina is supplied by the choroid [8, 17]. Retinal blood vessels lack any innervation distal to the lamina cribrosa, unlike the choroid which is under neural control [8, 13, 18, 19]. Consequently retinal blood flow is regulated entirely by local control mechanisms, which will be discussed in more detail in Section 1.4.

1.3 Blood Flow

Blood flow is defined as the volume of blood transported per unit time [4]. The flow, Q, of a liquid through a cylindrical tube (including the flow of blood through a vessel), is directly proportional to the difference in pressure between the inlet (pressure P_1) and outlet (pressure P_2) of the tube, and is inversely proportional to its resistance [4–6]:

$$Q = \frac{(P_1 - P_2)}{R} \tag{1.1}$$

where resistance describes the degree of difficulty the blood experiences passing through the tube [4–6]. This is referred to as Darcy's law of flow, which is analogous to Ohm's law in electrical circuits [7, 20]. From this basic law we can see that there are only two ways to alter blood flow – either the pressure gradient (the difference between arterial and venous pressure) or the resistance must be modified. Therefore, for a given pressure gradient, if resistance decreases, blood flow increases; and if resistance increases, blood flow decreases.

Darcy's law can be applied to describe the relationship between flow, pressure and resistance in the systemic circulation by making some substitutions. First, blood flow through the systemic circuit is equal to the cardiac output (CO), which is the volume

of blood being pumped by the heart per unit time [4, 6]. The pressure gradient is the difference between the mean arterial pressure (BP_m) and the central venous pressure (CVP) [4, 6]. The CVP is approximately equal to atmospheric pressure, and as blood pressure is conventionally expressed as pressure above atmospheric pressure, CVP $\cong$ 0; thus, the pressure gradient is approximately equal to BP_m [4, 6]. Finally, the resistance in the systemic circuit is the total peripheral resistance (TPR) [4, 6]. Substituting these variables into Darcy's law we obtain [4, 6]:

$$CO \cong \frac{BP_m}{TPR} \tag{1.2}$$

Rearranging this expression we have:

$$BP_m \cong CO \times TPR \tag{1.3}$$

From this equation we can see that the mean arterial blood pressure is determined by the cardiac output and the total peripheral resistance.

Blood flow in the retina can also be described by Darcy's law. As in other vascular beds the pressure gradient or perfusion pressure depends on the difference between the local arterial blood pressure (P_a) and the local venous pressure (P_v) [8, 19]. As P_v is approximately equal to the intraocular pressure (IOP), we have [8, 19]:

$$Q \cong \frac{P_a - IOP}{R} \tag{1.4}$$

where (P_a - IOP) is termed the ocular perfusion pressure [8]. When in a sitting or standing position P_a is about two-thirds of BP_m, due to the drop in blood pressure between the heart and the ophthalmic artery [8, 13].

What parameters determine the resistance, R, in the above equations? The French physician J. L. M. Poiseuille studied the flow of water in glass capillary tubes and derived the following equation:

$$R = \frac{8\eta L}{\pi r^4} \tag{1.5}$$

which is called Poiseuille's law [4,7]. G. H. L. Hagan, a German engineer, also theoretically derived this equation, independently of Poiseuille, therefore this law is sometimes referred to as the Hagan-Poiseuille law [20]. This law tells us that resistance increases as the length of the tube (L) and the viscosity (η) of the liquid increases, but resistance decreases as the radius (r) of the tube increases. Changes in vascular resistance are rarely due to changes in vessel length, as this parameter is essentially

constant [5, 6, 13]. Vascular resistance increases as blood viscosity increases, however, under normal physiological conditions viscosity does not change significantly [5, 6]. This leaves changes in the radius of blood vessels as the main contributor to variable resistance in the circulation.

By combining Darcy's law and Poiseuille's law we obtain:

$$Q = \frac{(P_1 - P_2)}{R} = \Delta P \frac{\pi r^4}{8\eta L} \tag{1.6}$$

From this expression we can clearly see that blood flow is highly sensitive to the radius of the vessel. A small change in the radius of the vessel will have a large effect on blood flow, because it is proportional the the fourth power of the radius. Therefore, if the radius of a vessel doubles, blood flow increases 16-fold. This underlines the importance of accurately measuring vessel diameter when assessing blood flow.

As flow is also equal to the velocity (v) of the fluid times the cross-sectional area (A) of the tube, when determining blood flow *in vivo*, blood velocity and the diameter of the vessel are measured and flow is calculated via:

$$Q = v \times A = v \times \pi r^2 \tag{1.7}$$

This is more practical than measuring ΔP, η, L and r and calculating blood flow via Poiseuille's equation. Various techniques for measuring blood velocity and vessel diameter *in vivo* in the retina will be described in Section 1.6.

1.4 Blood Flow Regulation

From Poiseuille's equation, in the last section, we saw that blood flow is strongly influenced by the radius of the vessel – a small change in r has a large effect on flow, due to the r^4 term. Vessel calibre is controlled by the tension exerted by the vascular smooth muscle in the tunica media, this is called the vascular tone [4]. Changes in vascular tone modulate vessel calibre, thereby regulating blood flow. A contraction of the vascular smooth cells increases vascular tone, constricting vessels, thereby reducing blood flow; while relaxation of the vascular smooth muscle cells results in a decrease in vascular tone, vasodilation, and an increase in blood flow [4]. The various mechanisms responsible for the control and regulation of vascular tone fall into two categories: extrinsic and intrinsic [4]. Extrinsic regulation includes regu-

lation mechanisms from outside the organ or tissue. Extrinsic regulatory mechanisms include vasomotor nerves and vasoactive hormones, such as angiotensin II, adrenaline and vasopressin [4]. Intrinsic regulatory mechanisms originate entirely from within the organ or tissue. Intrinsic regulation is brought about by: the myogenic response; vasoactive endothelial secretions; metabolic factors; and autacoids, such as histamine, bradykinin, serotonin, prostaglandins and leukotrienes (autacoids are mainly involved in pathological events, such as inflammation and bleeding) [4].

These regulatory mechanisms regulate blood flow in a hierarchical fashion. The lowest rank in this regulatory hierarchy is the myogenic response to changes in transmural pressure. The middle rank is composed of vasoactive factors secreted by the endothelium, vasoactive metabolites and autacoids. The highest rank represents extrinsic regulation, which can alter or override the intrinsic regulation represented in the lower layers [4]. The general strategy is that the extrinsic control mechanisms provide adequate arterial pressure for all organs in the systemic circulation, while an individual organ or tissue regulates how much blood flow it needs at any given time, through intrinsic mechanisms, optimising tissue perfusion and nutrient exchange [4, 19].

1.4.1 Blood Flow Regulation in the Eye

Histological studies and stimulation experiments have revealed that the vascular beds of the uvea are richly innervated, but that the retinal vasculature is devoid of vasoactive nerves distal to the lamina cribrosa [8, 13, 15, 19, 21, 22]. Therefore the retinal vessels are not under extrinsic regulatory control mechanisms and blood supply to the retina is entirely controlled via local regulatory factors. Intrinsic control mechanisms keep retinal blood flow constant in the face of variations in perfusion pressure and alter flow in response to changes in the metabolic needs of the tissue [8,15,21,22]. The exact interaction of myogenic and metabolic mechanisms by which retinal blood flow is regulated still remain to be precisely elucidated however [23]. In contrast to the retina, the choroidal circulation is under neurogenic control, but studies have demonstrated that reductions in perfusion pressure, due to a reduction in blood pressure or an increase in IOP, elicit a corresponding decrease in choroidal blood flow [8,13,15,19]. This indicates that choroid lacks myogenic autoregulation. Choroidal vessels do respond to increases in CO_2, and may therefore be expected to demonstrate some level of metabolic regulation [8].

1.4.2 Myogenic Autoregulation

The myogenic response was first described by Sir William Bayliss is 1902, hence it is sometimes referred to as the Bayliss effect [4]. It is the mechanism by which blood flow is maintained constant in the face of changes in perfusion pressure [13,24]. An increase in perfusion pressure (which in the eye depends on the arterio-venous pressure gradient and the IOP) results in an increase in transmural pressure. This stimulates a reflex contraction of smooth muscle cells in the media, which decreases the diameter and returns blood flow to its original level [4, 23]. A decrease in perfusion pressure elicits a fall in transmural pressure, which evokes vasodilation, reducing resistance and restoring flow to its steady state [4, 23]. Autoregulation operates over a limited pressure range however and an acute change in perfusion pressure will lead to an alteration of blood flow. For example, previous studies have found that increases in BP of 40%, induced by isometric exercise, increases blood flow [8,23]. Therefore, changes in perfusion pressure, within the physiological range, have little effect on steady state blood flow, thereby protecting the organ from fluctuations in arterial blood pressure, stabilising tissue perfusion and capillary filtration pressure [4, 25]. Autoregulation does not mean that blood flow cannot be altered. Metabolic vasoactive factors can reset the myogenic autoregulatory mechanism to operate at a different, but still autoregulated level [4].

1.4.3 Metabolic Regulation

Metabolic regulation adjusts vascular resistance so that blood flow maintains the concentration of metabolites within a narrow range [7]. Factors associated with an increase in the metabolism of the tissue, such as an accumulation of metabolites (for example potassium ions, H^+ ions, adenosine, ATP, phosphate ions and hydrogen peroxide), an increase in concentration of CO_2, or an increase in O_2 consumption, results in vasodilation and an increase in blood flow [4, 13]. Conversely a decrease in the levels of metabolites and CO_2 or excess O_2, indicates that blood flow is surplus to the requirements of the tissue or organ; this triggers an increase in vascular tone resulting in a decrease in blood flow. Metabolic regulation is graded, so blood flow varies almost linearly with the metabolic demands of the parenchyma [4]. For example, breathing pure oxygen constricts retinal blood vessels, reducing blood flow; while flickering light increases retinal neuronal activity, resulting in vasodilation and a corresponding increase in blood flow [8]. Autoregulation is defined as "the ability of a vascular bed to maintain blood flow to the tissue or organ under conditions of vary-

ing perfusion pressure", so metabolic regulation should not technically be referred to as autoregulation; however it is commonly called "metabolic autoregulation" [4].

1.4.4 The Endothelium

The vascular endothelium consists of a monolayer of cells that line the intimal surface of all blood vessels [8, 10]. Crucially they are located between the circulating blood and the vascular smooth muscle cells in the media. Over the past several decades it has been recognised that the endothelium plays an important role in vascular permeablility, vascular tone, platelet activity and coagulation [4, 8, 10]. The endothelium acts as a selective, semi-permeable membrane between the circulating blood and the tissue [4]. In the retinal vasculature the endothelial cells contain tight junctions, forming the blood-retinal barrier [8]. This barrier prevents non-lipid soluble substances passing through the endothelium from the blood [8]. Endothelial cells also sense the pulling/tugging force exerted by the flow of blood on the luminal suface of the vessel [4, 7, 26]. The magnitude of shear stress depends on the velocity of the blood flow and the viscosity of the blood [4, 7, 26]. When shear stress increases, the endothelium is stimulated to release nitric oxide, causing vasodilation and reducing shear stress [4, 26, 27]. Some of the endothelial secretions influence blood clotting, with nitric oxide and prostacyclin inhibiting platelet aggregation and thus preventing blood clotting (thrombosis), while von Willebrand factor promotes clotting [4, 8]. The important role played by the endothelium in the modulation of vascular tone, was first suggested by the pioneering work of Furchgott and Zawadski [28]. They discovered that vascular relaxation elicited by acetylcholine in rabbit aorta was lost if the endothelium was damaged or removed [28–30]. Subsequent investigations have identified numerous vasoactive factors released by the endothelium, which act on the adjacent smooth muscle cells in the media to evoke vasodilation and vasoconstriction. It is now recognised that the endothelium plays a primary role in local blood flow regulation. The importance of endothelial integrity has been emphasised by the discovery of abnormal endothelium-dependent vasodilation and vasoconstriction in diseases such as hypertension and diabetes mellitus. The roles of endothelium are thus many, diverse and vitally important [4]. In this thesis we are primarily interested in the role it plays in modulating vascular tone, therefore we will now briefly decribe some of the vasoactive factors synthesised by the endothelium.

Nitric Oxide

In 1980 an endothelium-derived vasodilating factor was discovered by Furchgott and Zawadski, this substance was identified as nitric oxide by Palmer et al. in 1987 [4,31,32]. Nitric oxide (NO) is both lipid and water soluble and so is a freely diffusible [4]. NO is generated continuously by a constitutively produced enzyme, endothelial nitric oxide synthase (NOS) [4,8,10,31,33]. NOS cleaves the nitrogen groups from the amino acid L-arginine and combines it with oxygen to form NO [4,7,8,10,31,33,34]. NO diffuses into the vascular smooth muscle cells, resulting in vasodilation [31,33,35]. NO has a short half-life, surviving a matter of seconds, before degradation [4,7,10]. Normally, the primary stimulus for NO production is the shear stress exerted by flowing blood [4, 10, 33]. NO expression can be enhanced by agonists such as the inflammatory autacoids, including bradykinin, thrombin and substance P, which induce vasodilation via an increase in NO production [4, 8, 10, 31, 33]. Besides its vasodilating properties, NO also displays anti-atherogenic actions by inhibiting smooth muscle cell proliferation and migration, platelet aggregation and leukocyte adhesion [4,10,31,35]. It is believed that reduced NO availability may contribute to atheroma formation [4,35]. NO production can be inhibited by analogues of L-arginine, including L^G-monomethyl-L-arginine (L-NMMA), thus providing a useful tool to investigate NO production [10, 31, 34]. Basal NO synthesis is continuous, so inhibitors of NO generation causes vasoconstriction [4,10,36]; therefore L-NMMA can be used to investigate basal NO production. L-NMMA has also been used to demonstrate that flicker-induced vasodilation is mediated by increased NO synthesis [36,37].

Prostacyclin

Prostacyclin (PGI_2), like NO, is a vasodilator produced by the endothelium, which also has anti-thrombotic properties [4,7,8,10,33]. Its production is continuous, and can be enhanced by inflammatory agents such as thrombin [4].

Endothelial Hyperpolarising Factor

The existence of another vasodilator was discovered when it was observed that some endothelium-dependent dilation persists even when nitric oxide and prostacyclin production pathways are blocked [4, 33]. This factor was termed 'endothelium-hyperpolarizing factor' (EDHF), as the response involves smooth muscle cell hyperpolarization [4]. The identity of this factor remains controversial [4]. The stimuli for EDHF production include inflammatory agents, such as bradykinin, and possibly

shear stress [4].

Endothelin

Endothelin (ET) was discovered by a Japanese group in 1989 [4]. It is the most potent vasoconstrictor that has been found [4, 7, 13]. ET is a 21-amino-acid peptide with three known isoforms: endothelin-1 (ET-1); endothelin-2 (ET-2); and endothelin-3 (ET-3) [7, 8, 10, 31, 38]. Endothelin-1 is produced by the endothelium and is the primary isoform acting in the cardiovascular circulation [4, 39]. Two receptors mediate ET activity: ET_A and ET_B, both of which have been found in the vascular smooth muscle cells of the retinal vessels [7, 8, 13, 31, 38, 40]. ET_A has a high affinity for ET-1 [40]. When ET-1 activates an ET_A receptor on the vascular smooth muscle the resulting rise in Ca^+ triggers vasoconstriction [4, 31, 33]. Basal levels of ET-1 are low [10, 33], but a previous study demonstrated that the administration of an inhibitor of ET production evoked a small vasodilation in the human forearm [4]. This indicates that low levels of ET-1 are continuously secreted and make a small contribution to basal vascular tone. ET receptor blockers, such as BQ-123 (ET_A receptor blocker) and Bosentan ($ET_{A/B}$ receptor blocker) provide a means of investigating ET-1 activity [31, 40]. Oxygen breathing has been shown, in numerous studies, to elicit vasoconstriction and a reduction in blood flow in the retina. This response has been shown to be mediated by the ET-1–ET_A pathway, as a previous investigation has demonstrated that ET_A blockade, by BQ-123, diminishes the vascular response to hyperoxia [7, 8, 13, 38, 40].

Cyclooxygenase Products

The endothelial cyclooxygenase products induce vasoconstriction, they include thromboxane, prostaglandins and superoxide anions [7, 10, 33].

1.5 Retinal Vessel Provocation Techniques

As discussed in the last section, the retinal vasculature will attempt to compensate for disturbances in perfusion pressure or alterations in metabolism to ensure an adequate blood supply to the tissue. Administering an artificial disturbance (provocation) to blood flow provides us with the opportunity to assess the funtional health of the vessels. Vascular reactivity is defined as the magnitude of change in a haemodynamic parameter (e.g. vessel diameter, blood flow velocity or volumetric blood flow) in

response to such a provocation [7, 41].

Numerous techniques exist to assess the ability of the vasculature to respond to a stimulus, such as flow mediated dilation (FMD). FMD is currently the most widely used technique, and it facilitates the *in vivo* investigation of endothelial function in the brachial artery [42]. In this technique the provocative stimulus is created by inflating a sphygmomanometric (blood pressure) cuff to suprasystolic pressure to occlude arterial inflow for a designated length of time (of the order of a few minutes) [26, 27, 42]. This results in downstream ischaemia, causing vasodilation of the tissue arterioles [4, 26, 27]. Therefore upon cuff deflation, the increase in shear stress in the brachial artery, caused by the increase in flow due to vasodilation in the downstream arterioles, results in enhanced NO production and vasodilation of the brachial artery (reactive hyperaemia) [4,26,27,42]. The magnitude of the change in blood flow, from before cuff inflation to after cuff deflation, is measured using ultrasonographic techniques [27, 42]. This technique only provides large artery information, however, which cannot necessarily be extended to the microcirculation [37]. This technique is also limited by technical difficulties: ultrasound systems have a limited spatial resolution, are technically challenging to use, requiring significant training and subsequent data evaluation involves a subjective component [27, 42].

The retinal vasculature provides the ideal opportunity to investigate reactivity in the microvasculature, as this vascular bed can be directly imaged. Provocative stimuli that have thus far been used in studies assessing retinal vessel reactivity include: blood pressure elevation; IOP alteration; postural change; flickering light; and O_2 or CO_2 inhalation.

1.5.1 Change in Ocular Perfusion Pressure

The ocular perfusion pressure can be altered by a change either in arterial pressure or IOP; therefore a number of techniques are available to provoke a change in perfusion pressure. Numerous studies have used isometric exercise to induce a sharp rise in blood pressure [23, 43, 44]. Isometric exercises are exercises performed in static positions and in most studies this involves the participants holding weights [37]. Due to the sharp increase in blood pressure and heart rate evoked by these exercises, this type of provocation would not be suitable in some patients, such as those with high blood pressure or heart disease. Hence this stimulus may not be suitable for clinical studies. Another method which can induce an increase in ocular arterial pressure is postural change. In the upright position, blood pressure falls as you move distally above the

level of the heart due to gravity [4]. The difference between the mean arterial pressure and the arterial pressure in the retina is approximately 20–25 mm Hg [8]. Therefore, changing the postural position of a study subject from an upright to a supine position increases the arterial pressure in the eye, thereby elevating the ocular perfusion pressure [4]. Tachibana et al. [45] used this technique in their study. Ocular perfusion pressure can also be modified by altering the IOP. This can be achieved by placing a pressure cup on the sclera and increasing the negative pressure to the cup resulting in an increase in IOP [46]. A drawback of this technique, however, is that an increase in IOP cannot be induced without causing considerable discomfort and anxiety in the study participant. These three provocation methods can be used to assess myogenic autoregulation in the retinal vessels.

1.5.2 Increase in Metabolism

It has been observed that flickering light increases retinal neural activity, thereby increasing the metabolism of the tissue [19, 47]. This increased metabolic demand elicits vasodilation and a subsequent increase in blood flow to ensure the blood supply meets the needs of the tissue [42]. A large number of researchers now use this flickering light stimulus to study retinal vascular reactivity. The flicker stimulus in previous studies was generated either by introducing an additional light source to the instrument being used to assess blood flow, or by inserting an optoelectronic shutter into the optical path of a fundus camera to interrupt the fundus illumination on alternate video frames [37]. Different protocols with regard to the frequency, length and duration of flicker stimulation have been used, but the measurement time is generally, approximately 6 minutes, with 8 Hz and 12.5 Hz being the most commonly used flicker frequencies [37]. Upon cessation of the flicker stimulus the vessel diameter is observed to contract to below the baseline diameter, before returning to its pre-flicker level [48,49]. Previous investigations have demonstrated that administration of the nitric oxide synthase inhibitor, L-NMMA, diminishes this flicker-induced vasodilatory response, thus indicating the response is mediated by enhanced NO production [37]. There are some limitations associated with this provocation technique. Firstly, because of the different stimulation protocols that have been used, the comparability of results is limited. Also, the frequency of the flickering light is within the frequency range which can potentially trigger an epileptic fit [50].

1.5.3 Alteration of Blood Gas Concentration

That retinal vessels react to variations in blood gases to maintain an adequate oxygen supply to the tissue and to ensure sufficient removal of metabolic waste from the tissue. In this way, high levels of O_2 (hyperoxia) produce vasoconstriction and low levels result in vasodilation; while high concentrations of CO_2 (hypercapnia) elicit vasodilation and low levels result in vasoconstriction [8,13,21,40,51]. Previous studies observed that administration of gases with increased CO_2 levels (gas mixtures of 92% O_2 + 8% CO_2 and 90% O_2 + 10% CO_2) were poorly tolerated by participants, with reports of headache and dizziness [52,53]. Also, gas mixtures with elevated CO_2 or decreased O_2 may be hazardous for subjects with retinopathy or vascular disease, which may prevent such protocols being extended to clinical studies [54]. Provocation through breathing 100% O_2 has been used by numerous studies to investigate endothelial function, with no reports of adverse reactions. Previous investigation has revealed that the marked constriction induced by hyperoxia is mediated, at least in part, by ET-1 [40].

For our experiments we decided to use oxygen breathing as the provocation stimulus to evoke a retinal vascular reaction. This stimulus method was chosen because oxygen breathing induces minimal discomfort and anxiety to the subjects, and also poses minimal risk to their well-being. There are also no contraindications preventing an oxygen-breathing protocol from being extended to a clinical study. The oxygen delivery system used is detailed in Section 3.2.3, page 62.

1.6 Techniques for measuring ocular blood flow in humans

Vascular reactivity in the human retinal circulation has previously been studied using a number of techniques for assessing ocular blood flow. Currently there is only one commercially available instrument with the ability to measure volumetric retinal blood flow, but a number of other instruments are available which measure parameters which reflect blood flow. To date retinal vascular reactivity has not been assessed using high-resolution imaging techniques. Techniques which have thus far been used in human retinal vascular reactivity studies will now be detailed.

1.6.1 Blue Field Entoptic Technique

The blue field entoptic technique was first introduced by Petrig and Riva in 1980 [16, 55]. This method uses the blue field entoptic phenomenon to investigate leukocyte dynamics in the perifoveal vessels [7, 17, 55, 56]. The blue field entoptic phenomenon is most visible when gazing into a blue light source with a narrow optical spectrum centred at approximately 430 nm [17, 51, 56]. Under these conditions a subject will perceive many tiny corpuscles moving around in an area 10° to 15° of arc radius centred at the fovea [7, 17, 51, 56]. This phenomenon is caused by the different absorption properties of red and white blood cells – red, but not white blood cells absorb the short wavelength light [7, 17, 56]. Therefore a leukocyte passing through a vessel is perceived as a flying corpuscle [17, 56]. Retinal haemodynamic parameters are extracted by showing a simulated particle field to a subject under study. They then compare the simulation field to their own entoptic observation and adjust the number and velocity of the particles in the simulation to match their own perception. In this way, retinal leukocyte density and velocity is estimated [7, 17, 51, 56]. This method is therefore subjective in nature and is highly dependent on subject cooperation [16, 17, 51, 55, 56]. Also, it is the flow of leukocytes that is assessed with this technique, as opposed to red blood cells, and it is not clear whether leukocyte flow is proportional to erythrocyte flow in all clinical conditions [17, 51, 52, 56]. A further limitation is that any subjects with poor visual acuity will be unable to observe this phenomenon [17].

1.6.2 Pulsatile Ocular Blood Flow Techniques

The ocular volume and intraocular pressure (IOP) vary during the cardiac cycle [7, 17, 56, 57]. This observation has lead to the development of two techniques which assess the changes in ocular volume and IOP during the cardiac cycle, to estimate pulsatile ocular blood flow (POBF) [7, 17, 56, 57]. Pneumotonometry measures changes in IOP during the cardiac cycle. The maximum IOP during the cardiac cycle is called pulse amplitude and the variation in IOP with time is used to calculate POBF [7, 17, 56, 57]. The second method for assessing POBF involves measuring the changes in distance between the cornea and the retina during the cardiac cycle using an interferometric method [17, 56, 57]. This phenomenon is termed ocular fundus pulsation [17, 56]. The distance between the cornea and the retina decreases during systole and increases during diastole, and the maximum distance change during the cardiac cycle is called the fundus pulsation amplitude (FPA) [17, 56, 57]. The main limitation for both of

these techniques is that only the pulsatile amplitude of blood flow that is measured as opposed to blood flow directly [7,17,56].

1.6.3 Laser Doppler Techniques

Laser Doppler velocimetry (LDV) is a well known technique for the non-invasive measurement of retinal blood flow velocity in large vessels, based on the optical Doppler effect [56, 58]. In LDV a retinal vessel is illuminated by a high coherence laser beam [17]. The laser light is scattered by the vessel wall as well as the erythrocytes flowing through the vessel [17]. The light which is scattered by the moving blood cells is shifted in frequency; this frequency shift is proportional to the velocity of the blood [16, 22, 56, 58, 59]. The light scattered from the vessel wall is not shifted in frequency [59]. As blood flows fastest in the centre of the blood vessel and slows towards the vessel wall, the backscattered light consists of a range of frequency shifts corresponding to the range of blood cell velocities within the vessel [17,22,56,59]. The maximum frequency shift corresponds to the maximum velocity at the centre of the vessel [17, 22, 56, 58, 59]. The absolute maximum velocity at the centre of the vessel can be determined with bidirectional LDV, which uses two photodetectors separated by a known angle [17,22,56,58,59].

Laser Doppler techniques have also been applied to assess blood flow in the microvasculature in a similar manner to that used in LDV [16]. In this technique, which is called laser Doppler flowmetry (LDF), the laser beam is directed away from visible vessels and is focused on the vascularised tissue [13, 58]. Scattering of the light incident on the moving blood cells is frequency shifted, while light scattered by the stationary tissue is unshifted but leads to a randomisation of light directions impinging on the red blood cells, leading to a broadening of the Doppler shift spectrum [17,56,58]. From this spectrum relative measures of red blood cell velocity, volume and blood flow are calculated [13, 17, 56, 58]. Interindividual comparisons with LDF are not advised, however, as measures of blood flow are calculated in relative units and absolute values are influenced by the scattering properties of the tissue, of which there is considerable variation between subjects [56, 60]. A further limitation is that it is likely that Doppler shifted light from both the retina and the choroid contribute to the received signal [17,51,56].

Scanning laser Doppler flowmetry (SLDF) combines the principles of LDF and scanning laser opthalmoscopy [17,56,58,61]. The Heidelberg Retina Flowmeter (Heidelberg engineering, Heidelberg, Germany) is a commercially available SLDF system.

During the laser scanning process the haemodynamic parameters are calculated at each point to build up a two-dimensional map of retinal and optic disc blood flow [17,51,56,58]. The limitations related to LDF measurements also apply to SLDF [17]

1.6.4 Laser Speckle Technique

Laser speckle is an interference pattern that can be observed when coherent light is scattered from a diffuse surface [62]. When the coherent light is focused on a moving object, the speckle pattern varies. In this way, when the ocular fundus is illuminated with laser light the rate of speckle variation can be used to provide an estimate of blood cell velocity [17, 56]. Tamaki et al. [63, 64] have presented an instrument for estimating blood velocity in the human retina by assessing speckle variation on the fundus. The device consists of a fundus camera equipped with a diode laser of wavelength 808 nm [7, 63, 64]. The fundus is illuminated with a halogen lamp [7, 63, 64], and the laser beam is focused on an area of the fundus with no visible vessels [63,64]. Statistics are used to derive haemodynamic information from the variations in the speckle pattern. The ratio of the average of the speckle intensity (I_{mean}) to the difference between I_{mean} and the speckle intensity for successive measurements is defined as normalised blur (NB). NB is nearly equivalent to the reciprocal of speckle contrast and quantifies the blood cell velocity [7, 63, 64]. There are a number of limitations associated with this method. As this method does not provide an absolute measure of blood velocity interindividual comparison is ill-advised [63]. Also as vessel diameter measurements are not possible with this method, volumetric blood flow determination is not possible [17,56].

1.6.5 Retinal Vessel Analyser (RVA)

The Retinal Vessel Analyser (RVA) is a commercially available system (Imedos, Jena, Germany), which consists of a Zeiss FF450 fundus camera (Zeiss, Jena, Germany), a digital video camera, a real time monitor and a personal computer with image-analysis software for measuring retinal vessel diameters [37,49,65]. The illumination source is a halogen bulb; a green filter is placed in the illumination pathway to enhance contrast for vessel visualisation [66, 67]. The image field angle is 30° [67] and each pixel subtends approximately 12.5 μm [37]. Pupil dilation is necessary for adequate image quality [37,66]. The RVA uses an image-analysis algorithm, which, once the operator has selected a vessel of interest, continuously assesses the vessel diam-

eter. This software can also correct for slight eye movements to track the vessel of interest [65,66] and automatically remove data when image quality is poor, for example during blinks [65,66]. The RVA can also include the capacity to provide a flicker provocation [66]. A flicker stimulus is achieved by interrupting the fundus illumination using an optoelectronic shutter [37,66]. The RVA was developed for the analysis of the larger retinal vessels, and due to the limited resolution of the system, it is not recommended that this instrument be used to measure vessels with a diameter less than 90 μm [66–68].

1.6.6 Canon Laser Blood Flowmeter CLBF

The Canon Laser Blood Flowmeter (CLBF), model 100 (Canon, Toyko, Japan), can simultaneously measure vessel diameter and blood flow velocity, thereby allowing it to calculate volumetric blood flow in absolute units [59]. The maximum velocity of blood cells at the centre of the vessel is determined using bidirectional laser Doppler velocimetry [22,59,69]. A green stripe from a 543 nm He-Ne laser, which is oriented perpendicular to the vessel of interest, is used by a vessel tracking system to track the vessel of interest, stabilising the measurement site. It is also utilised to measure the vessel diameter using computer analysis [22,69–71]. Diameter measurements are corrected for possible magnification effects using axial length measurements (operator input) and refractive error measurements made by the CLBF itself [22,69,70]. The CLBF can measure vessels $\geq$80 μm in diameter [72].

1.7 High-Resolution Imaging Technique used to Assess Retinal Arteriolar Reactivity in this Thesis: the Modified HRT-Classic

In this thesis, retinal imaging was performed with a manufacturer-modified HRT-classic (Heidelberg Engineering, Heidelberg, Germany), which is a confocal scanning laser opthalmoscope (cSLO). Confocal scanning laser ophthalmoscopy is an imaging technique based on confocal microscopy, applied to retinal imaging to provide high-quality images of the fundus.

The term 'confocal' refers to the confocal aperture placed in the plane conjugate to the depth of the retina that is being imaged. This pinhole limits the reflected light that

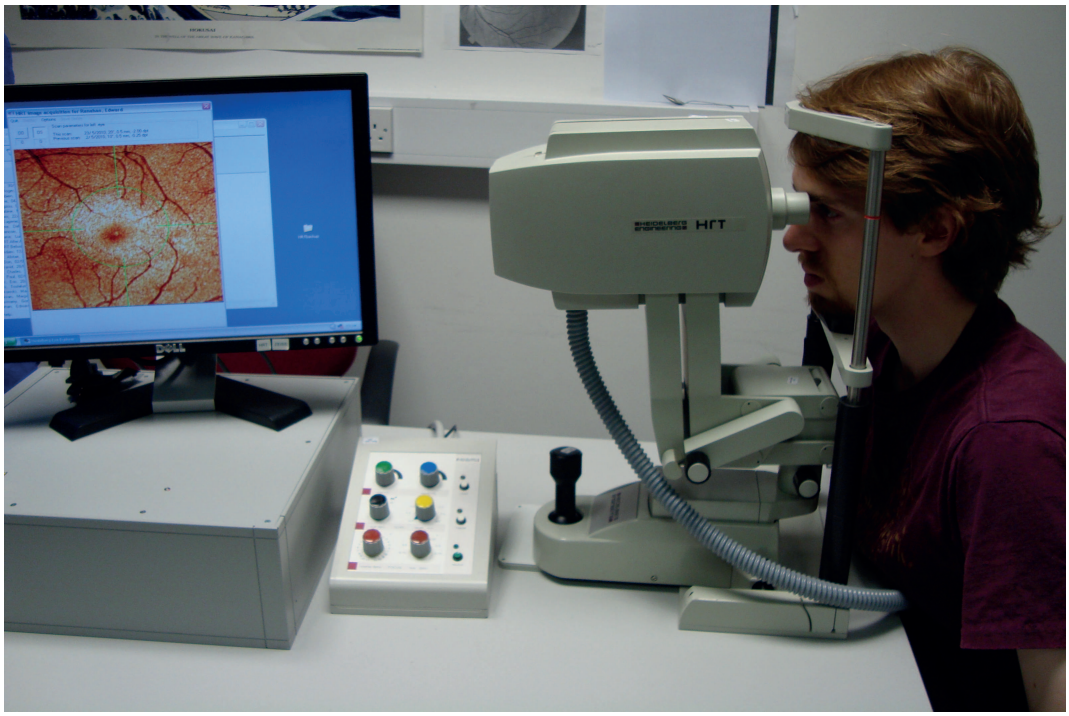

Figure 1.5: The modified HRT-classic.

reaches the detector to a narrow range centred around the focal plane in the retinal layer of interest [73]. In Figure 1.6 it can be seen that light coming from depths deeper or shallower than that conjugate to the pinhole are blocked, thus preventing spurious light coming from retinal layers, other than the layer of interest, from reaching the photodetector (which is an avalanche photodiode in the modified HRT-classic). This provides the system with the capability of optical depth sectioning. Optical sectioning through the tissue is achieved by incrementally moving the pinhole to vary the depth of the focal plane in the tissue, thereby acquiring a layered 3-D image [73]. Each layer of this 3-D image represents an image obtained at a focal plane, as the focal plane was shifted through the tissue. We obtained images at a single focal plane to obtain a video of the vasculature.

Figure 1.7 shows an image of the HRT optics block and a schematic diagram of its optical setup. The modified HRT-classic images using a 675 nm diode laser. During image acquisition, at any given instant, only one point on the retina is illuminated. Therefore, to acquire a 2-D image, the emitted light beam must be swept over the retina. The emitted beam is scanned in the x and y axes along the plane of focus perpendicular to the optic axis (z-axis) using two oscillating mirrors [73]. In this way an

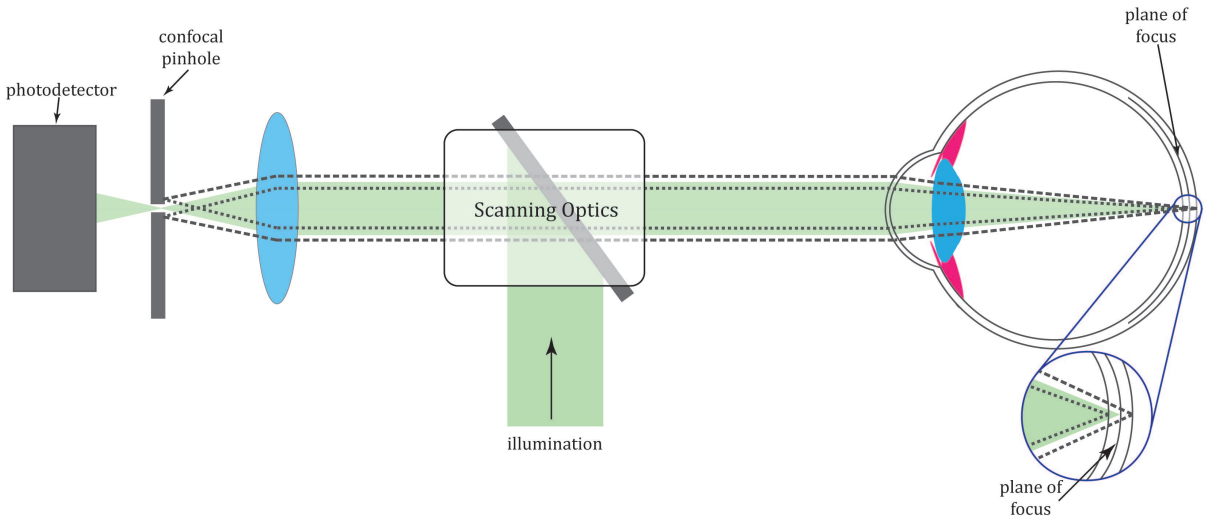

Figure 1.6: Schematic diagram of a confocal scanning laser ophthalmoscope. The confocal aperture (pinhole) is placed in the plane conjugate to the depth of the retina that is being imaged. This pinhole limits the reflected light that reaches the detector to a narrow range centred around the focal plane in the retinal layer of interest. Light coming from depths deeper or shallower than that conjugate to the pinhole are blocked, thus preventing spurious light coming from retinal layers, other than the layer of interest, from reaching the photodetector. This provides the system with the capability of optical depth sectioning.

image is recorded point-by-point, over time, as the the region of interest is scanned in a raster-like fashion [74]. In the modified HRT-classic the fast scan is in the horizontal direction, with a scanning rate of 8 kHz, while the vertical scan rate is 30 Hz. It scans in 'double scan' mode, which means that two lines of an image are obtained in one complete cycle of the fast horizontal scanner [73]. This means that the first line is recorded as the scanner moves from left to right and the second line is acquired as the beam scans back from right to left [73]. The velocity of the horizontal scan varies across a scan-line, therefore the image line is recorded during the relatively linear portion of the scan, to minimise distortion in the resultant image. Some distortion still occurs, however, and we corrected for this using a Matlab®-based algorithm, which is described in detail in Section 2.1.

The acquisition time for a single image is 32 ms. A sequence of 32 frames was acquired at a single focal plane to obtain a video of the retinal vasculature. The acquisition time for a sequence of 32 frames is: 32 frames $\times$ (32 ms + 16 ms) = 1.5 s, where 16 ms is the resetting time between frames.

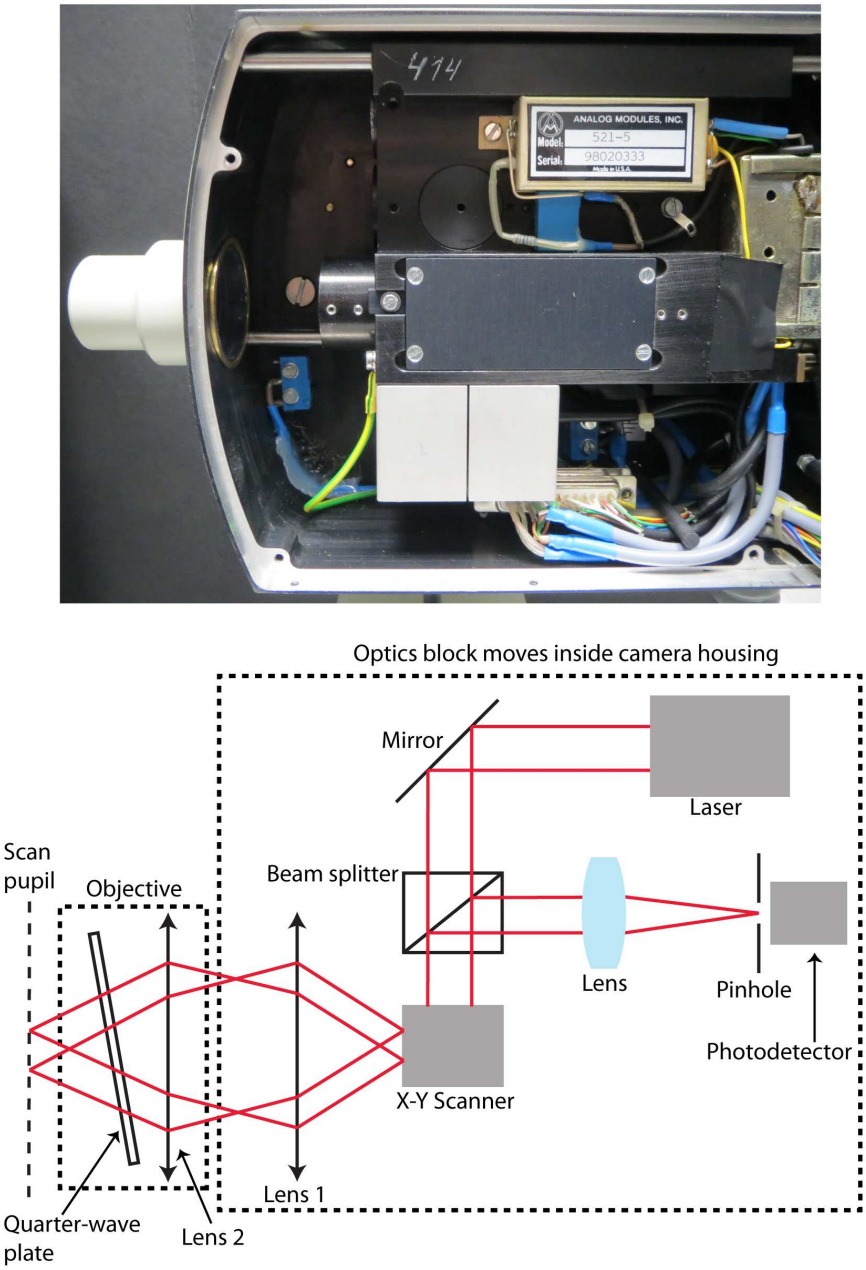

Figure 1.7: Top: image of the HRT optics block. Bottom: schematic diagram of the optical set-up of the HRT.

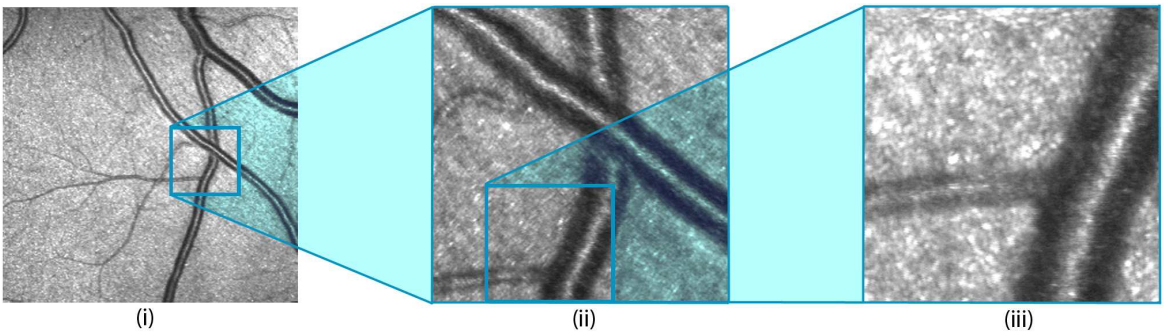

Figure 1.8: Images of the same portion of the retina taken at the different fields of view (FOV) of the modified HRT-classic. (i) 10° FOV, (ii) 2° FOV and 1° FOV

The modified HRT-classic could originally image with a 10°, 15°, or 20° FOV, but it was modified such that it could image at the smaller FOVs of 10°, 2°, or 1°. Thus, it is capable of very high resolution imaging of the retina. Images taken at each FOV of the modified HRT-classic can be seen in Figure 1.8. Images are 256 × 256 pixels. Ocular refraction can effect image magnification, but each pixel subtends approximately 10 μm at the 10° FOV, 2 μm at the 2° FOV, and 1 μm at the 1° FOV.

We measured vessel calibre in the high-resolution images we acquired from the modified HRT-classic using Matlab®-based algorithms, which are described in detail in Chapter 2. We did not obtain velocity measurements, so volumetric blood flow could not be calculated. However, according to the Hagan-Poiseuille law, discussed in Section 1.3, blood flow is proportional to the pressure gradient, ΔP, and the fourth power of the radius, r^4. As the provocative stimulus used in our experiments was oxygen-breathing, which does not alter blood pressure or IOP [12, 21, 25, 46, 52, 75, 76, 76–78], we believe it is reasonable to use vessel diameter changes as a good surrogate measure for blood flow changes in response to hyperoxia. The sensitivity of blood flow to changes in diameter, due to the r^4 term, underlines the importance of accurately measuring changes in diameter in retinal vascular reactivity studies. However, the quantification of vessel calibre changes has been limited by the resolution of the techniques used to date, with previous studies assessing vessels measuring $\geq$80 μm. Using the high resolution modified HRT-classic allowed us to investigate the reactivity response of retinal arterioles with diameters as small as 40 μm.

1.8 Thesis Motivation

The endothelium is a monolayer of cells that lines the inner surface of blood vessels. The endothelium plays an important role in local blood flow regulation by secreting

vasoactive factors, which modulate vascular tone, in response to various agonists and stimuli. Non-invasive, stimulation methods can be used to provoke vessels to react (i.e. constricting or dilating), allowing assessment of endothelial function. Such vascular reactivity can be directly visualised in the retinal circulation and has already been assessed using a variety of measurement techniques; however, to our knowledge, high resolution imaging techniques have thus far not been utilised. There has been growing interest in the study of endothelial function since it was found to be abnormal in cardiovascular diseases, such as hypertension and diabetes. Reliable assessment of endothelial function could improve understanding, and could potentially facilitate early diagnosis, risk prediction and treatment monitoring in these diseases. Knowledge is required of as many factors as possible that affect endothelial function in order to assess it in pathological conditions. However, studies have reported contradictory results in relation to many of the investigated factors hypothesised to influence the vascular response to stimuli. The motivation behind this thesis is to accurately measure the magnitude of retinal arteriolar constriction in response to hyperoxia, using a high-resolution confocal scanning laser ophthalmoscope and image processing techniques in a bid to improve understanding of endothelial function and to clarify previous equivocal results. In this thesis we investigate whether a reactivity measurement taken from a single, arbitrary site can be considered as representative of the retina as a whole. We present results on the chronic and acute affects of smoking in otherwise healthy individuals. We present our findings on the impact of healthy aging on the magnitude of vasoconstriction. Finally, we detail a small clinical study performed to assess the reactivity response in hypertensive and diabetic patients and discuss the limitations and difficulties of using our experimental protocol and setup in a clinical setting.

Chapter 2

Image Processing

In this chapter, the image processing techniques implemented to measure retinal arteriolar diameters in the image sequences acquired from the modified HRT-classic are described. The first step is desinusoiding, which is required to remove the horizontal distortion in the images caused by the varying velocity of the scanner in the HRT. The image registration technique used to align the images is then described, followed by image averaging of the registered image sequences. The semi-automated vessel tracking and diameter measurement algorithm is then detailed. The chapter concludes with a description of the video processing techniques which were attempted to extract velocity information from the image sequences.

2.1 Desinusoiding

Raw videos were first processed to correct for distortions due to raster scanning. The scanning laser ophthalmoscope (SLO) employs a resonant scanner and a sensor that captures pixels at a constant rate. The velocity of the scanner varies sinusoidally across each scan line, which results in a horizontal distortion in raw videos. The velocity of the scanner is slowest at the left and right edges of the frame and fastest in the centre; thus there are more pixels per retinal area toward the edges compared to the centre. The result of this can be seen in Figure 2.1, which is an image of the callibration grid used to estimate the distortion. The lines at the edges of the image

are thicker and more widely spaced, while those at the centre are narrower and more closely spaced. To remove this distortion, the horizontal warp from videos of the calibration grid was measured, using a Matlab®-based algorithm.

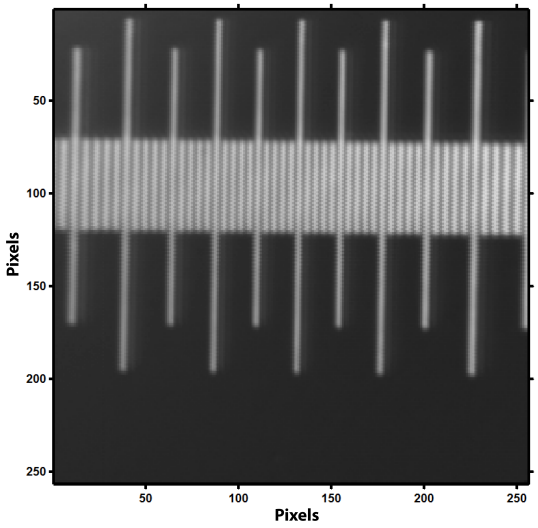

Figure 2.1: Raw image of the calibration grid. The velocity of the scanner in the modified HRT-classic varies across each scan line, being slowest at the edges of the images and fastest at the centre. This results in more pixels per retinal area toward the edges compared to the centre of the images. This is clearly evident in this image of the calibration grid as the lines at the edges of the image are thicker and more widely spaced, while those at the centre are narrower and more closely spaced.

The video of the calibration grid was first imported to the Matlab® program and the 32 frames of the video were averaged to produce a single, high signal-to-noise image (see Section 2.4, page 47). An intensity profile through the lines of the grid was extracted (horizontally across the image at row 100 in Figure 2.1). The positions of the maximum intensity pixels, which correspond to the lines in the image, were then determined. The blue line plotted in Figure 2.2 shows the line positions calculated across the image and the red line represents the position of the lines if the velocity of the scanner had been constant and the lines were equidistant.

Figure 2.3 describes the pixel acquisition in an SLO. The pixels are acquired at constant intervals. Pixel 1 is acquired at t_1. Δ, duration, in the diagram is the time to acquire all 256 pixels in a horizontal line of an image. The interval between pixel acquisition is then the duration divided by the number of intervals, $\frac{\Delta}{255}$. Therefore, pixel i is acquired at $\left(t_1 + \frac{\Delta}{255} \cdot (i-1)\right)$. The time between line acquisition is, however, not constant. It is required that (Line 3 - Line 2) = (Line 2 - Line 1) etc.. Thus we need to

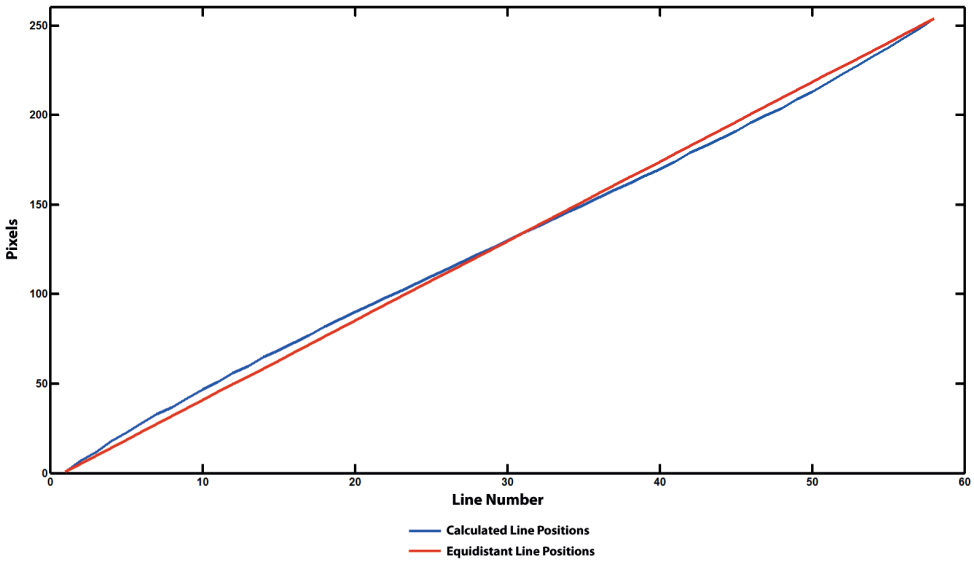

Figure 2.2: Plot of the actual, calculated line positions (blue line) and the equidistant line positions, which would have been obtained if the velocity of the scanner been constant (red line).

find t_1 and Δ which would give equally spaced lines.

A cost function was constructed which calculates a parameter f, which was large when the lines are irregularly spaced and small (close to zero) when they were evenly spaced. The cost function was then passed into a simplex search algorithm along with the initial guesses for t_1 and Δ and the maxima positions. The simplex search algorithm then iteratively altered t_1 and Δ until f was minimised, giving t_1 and Δ which would transform the images to give evenly spaced lines. An equation in the general form was required:

$$f(x) = \alpha \times sin(\beta x + \gamma) + \varphi \tag{2.1}$$

We had:

$$f(x) = \alpha \times sin\left(t_1 + \frac{\Delta}{255} \cdot (i-1)\right) + \varphi \tag{2.2}$$

Along with the constraint:

$$\begin{aligned} f(1) &= 1 \\ f(256) &= 256 \end{aligned} \tag{2.3}$$

This constraint allowed us to map the first and last pixel of the original image to

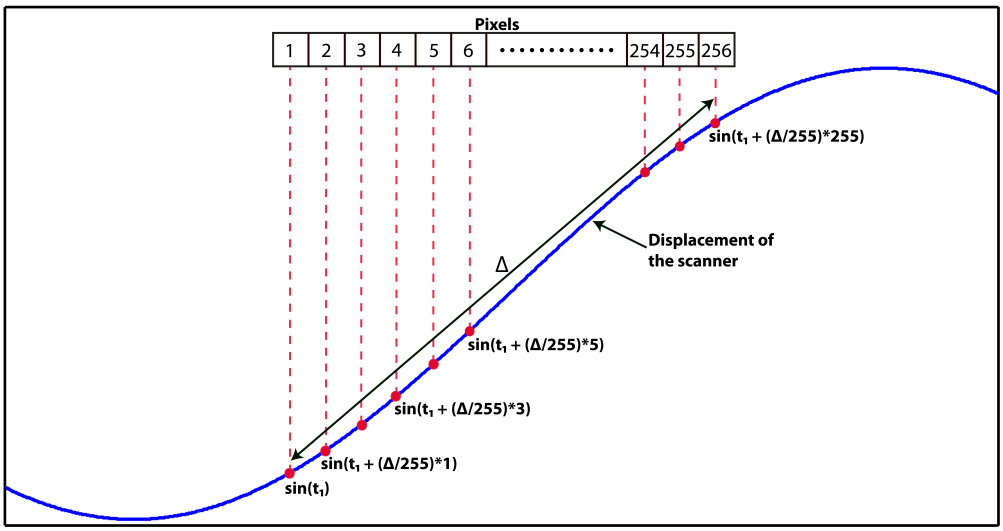

Figure 2.3: Pixel acquisition in the SLO. The pixels are acquired at constant intervals. Pixel 1 is acquired at t_1. Δ, duration, is the time taken to acquire all 256 pixels in a single, horizontal scan line of an image. The interval between pixel acquisition is then the duration divided by the number of intervals, $\Delta/255$. Therefore, pixel i is acquired at $(t_1 + \Delta/255.(i-1))$.

the first and last pixel of the dewarped image. t_1 and Δ had been estimated, so this allowed us to calculate parameters α and φ and then subsequently to calculate β and γ.

$$\alpha = \frac{255}{sin\,(t_{256}) - sin\,(t_1)} \tag{2.4}$$

$$\beta = \frac{t_{256} - t_1}{255} \tag{2.5}$$

$$\gamma = t_1 - \frac{t_{256} - t_1}{255} \tag{2.6}$$

$$\varphi = 1 - \frac{255 \times sin\,(t_1)}{sin\,(t_{256}) - sin\,(t_1)} \tag{2.7}$$

So $f(x) = \alpha^* sin\,(\beta x + \gamma) + \varphi$ gave the transformation necessary to transform the original image into the dewarped image with evenly spaced line grating. The transformation could be implemented in a forward or inverse manner. Each pixel from the original image could be directly transformed using the estimated mapping function.

This approach is the forward method. Pixels in the original image do not neccessarily correspond to pixels in the dewarped image, so interpolation to evaluate the original image on the grid defined by pixels in the dewarped image is required. However, the transformed pixels of the original image are irregulary spaced in the dewarped coordinate system. Therefore, the inverse transformation is generally preferred since it allows interpolation of the original image using the regular sample grid of the original image itself. Therefore, to implement an inverse transformation we have:

$$f^{-1}(x) = \frac{arcsin\left(\frac{x-\varphi}{\alpha}\right) - \gamma}{\beta} \tag{2.8}$$

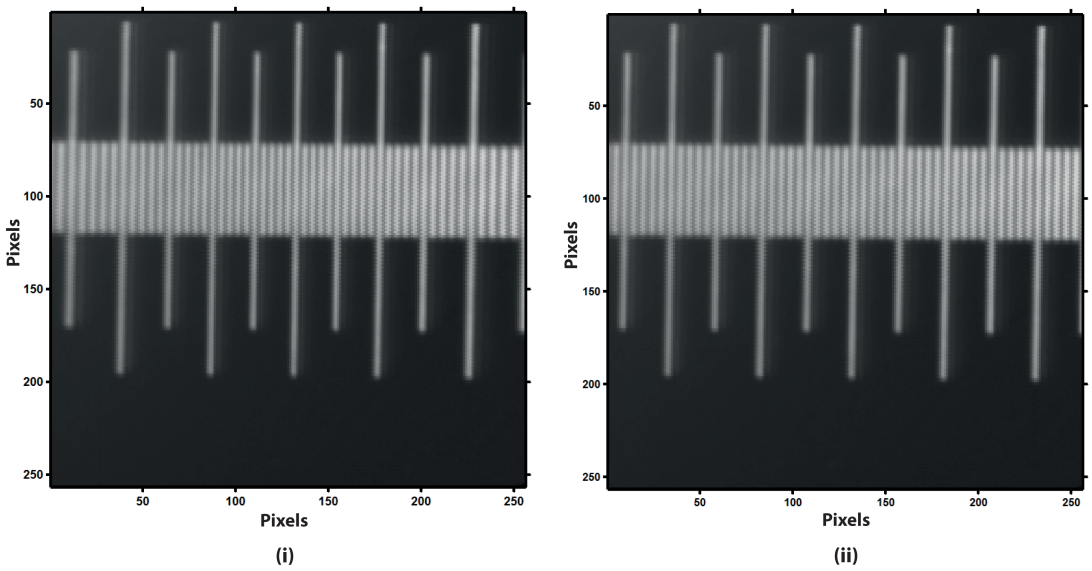

Figure 2.4: Comparison of (i) original and (ii) desinusoided images of the calibration grid. After desinusoiding the lines in the image are equally spaced and of equal thickness.

Comparing the original image to the dewarped image in Figure 2.4, it appears that the lines in the desinusoided image are now equally spaced and of equal thickness across the image. To examine the result of desinusoiding more carefully the desinusoided images of the calibration grid were imported into the algorithm to determine the position of the maxima. The positions of the maxima in the desinusoided image were plotted along with the positions of the maxima if the velocity of the scanner had been constant and the maxima were equidistant, Figure 2.5. It can be seen that the lines lie on top of each other and there appears to be little deviation. The actual line

positions have a mean absolute deviation from the equidistant line positions of 0.28 pixels.

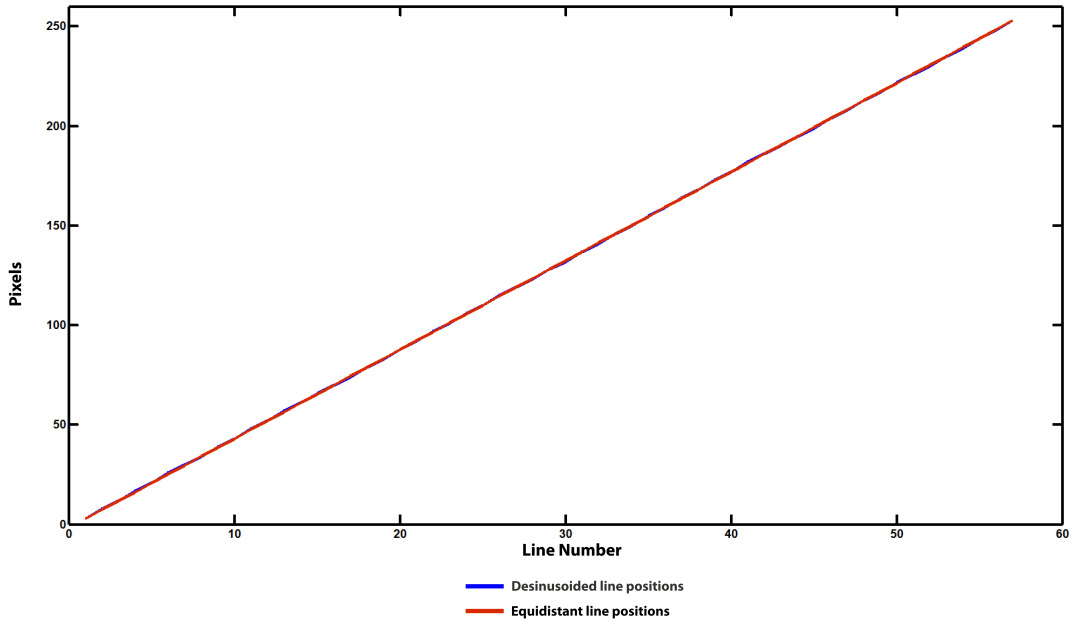

Figure 2.5: Plot of the dewarped line positions (blue line, barely visible under red line) and the equidistant line positions, which would have been obtained if the velocity of the scanner had been constant (red line).

2.2 Fixational Eye Movements

The eye is constantly moving, even during attempts to fixate on a stationary target. Three main types of eye movement occur during visual fixation in humans: tremor, drift and microsaccades. They are collectively know as fixational eye movements. Typically an eye that is attempting to fixate steadily will exhibit a slow drift, which can be thought of as a slow continuous walk over the retina, which will be interrupted periodically by a large, rapid movement, which is a microsaccade. An additional tremor component can also be found. Tremor is a fast, jerky movement of small amplitude in the range 5-20 arcsec and high frequency of 30-100 Hz [74, 79–83]. Drifts have large amplitudes, 1-12 arcmin [81], with speeds of 5-20 arcmin/s [80]. Microsaccades have amplitudes between 1 and 20 arcmin with mean speeds in the order of 10-75 deg/s [74, 79–81]. All retinal imaging systems suffer from these eye movements; however, these distortions are particularly apparent in adaptive optics

ophthalmic instruments and the modified HRT classic, as the distortion scales with the magnification of the instrument [74,79,80].

To maintain safe retinal exposures low illumination levels are used, so the signal in a single frame is quite low. High signal-to-noise frames can be obtained by averaging a sequence of images. To do this, to obtain stabilised videos of the retina, or to analyse retinal motion, the images must first be registered to compensate for the fixational eye movements. Eye motion that occurs during image acquisition produces distortions that are unique in each frame of the image sequences acquired by scanning techniques because the images are captured over time from a scanning focused beam. These distortions, which can be extreme if a microsaccade occurs during acquisition as can be seen in Figure 2.6, make registration of the images recorded by the HRT non-trivial.

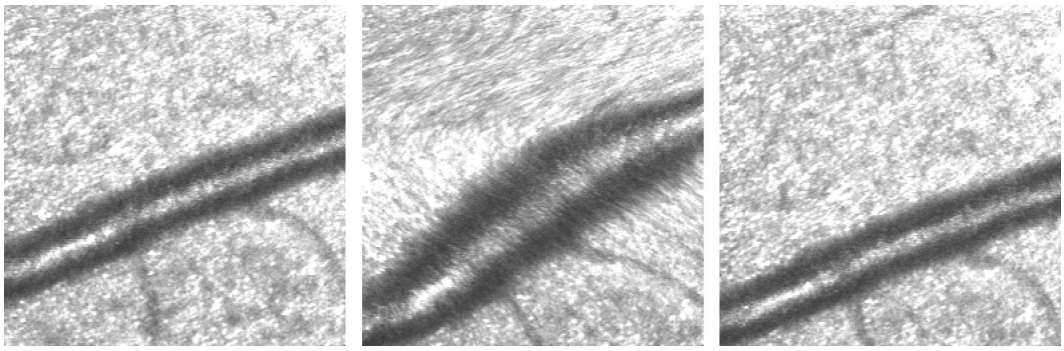

Figure 2.6: Example of extreme distortion that can occur in scanning techniques. These are three sequential images taken from a sequence obtained by the modified HRT classic. The second image shows severe distortion due to a microsaccade which occured during image acquisition.

2.3 Image Registration

Image registration methods attempt to align two or more images of the same scene taken under different conditions. The need to register images has arisen for a range of tasks in different fields. For example, registration is necessary for integrating information taken from different instruments to provide enhanced visualisation of the scene. This is common in medical imaging. Images which show anatomical body structure, such as MRI, CT and ultrasound, are registered with images which show functional and metabolic activity, such as PET, SPECT and magnetic resonance spectroscopy. The results have been applied to improve accuracy in treatment planning for radiation therapy and to facilitate better surgical planning. A different scenario

arises when images are taken at different times. In this situation the aim is to find and evaluate changes in the scene between the acquisition of images. Satellite images can be aligned to detect environmental changes. In medical imaging it can be applied to monitor tumour evolution. A different objective for aligning images taken at different times arises in astronomy, and indeed in our case. A large number of images of the scene are taken fractions of a second apart with the same instrument. These images are registered so they can be averaged to produce a single, higher signal-to-noise image, see Section 2.4.

There is no universal method which can be applied to all registration tasks due to the diverse range of images which need to be registered. However, most image registration algorithms consist of the following basic stages:

- Feature detection.
- Feature matching.
- Transformation function estimation.
- Applying the transformation function to align the images.

The feature detection step extracts the information in the images that will be used for matching. Edges, contours, line intersections and corners are commonly detected features for registration. Once extracted, the correspondance between the features in the reference and template images are determined using various similarity metrics. The reference image is the image to which all the other "template" images are aligned. The parameters of a transformation function to map the points in the template image to their corresponding points in the reference image are estimated using the information obtained in the feature matching step. Finally, the template image is aligned with the reference image by application of the estimated function.

2.3.1 Intensity-based methods

Intensity-based methods, also known as template matching and area-based and correlation-like methods, are thus called because the feature detection step is omitted and matching works directly with image intensity. In intensity-based matching, the template image is shifted point-by-point over every pixel of the reference image. At each location a similarity metric is computed. The template image is said to match the reference image at the position where a distinct peak of the similarity measure is

located. An example of a distinct maximum peak obtained at the location of matching can be seen in Figure 2.8, page 40.

Correlation-like match metrics are frequently used. The correlation measures are derived from another, more intuitive match metric, which calculates the sum of differences squared between the template and the reference image at every location:

$$d(m,n) = \sum_x \sum_y [f(x,y) - t(x-m,y-n)]^2 \tag{2.9}$$

where f is the reference image, t is the template image positioned at m,n, the summation is taken over x,y under the template. When the template is shifted to the location where it is most similar to the reference the differences between their intensity values at each pixel will be smallest at this location. Therefore this measure decreases with the degree of similarity.

If this measure $d(m,n)$ is expanded into its quadratic terms we obtain:

$$d(m,n) = \sum_x \sum_y \left[f^2(x,y) - 2f(x,y)t(x-m,y-n) + t^2(x-m,y-n) \right] \tag{2.10}$$

The template energy term $t^2(x-m,y-n)$ is constant irrespective of location. If the reference energy term, $f^2(x,y)$, is also constant at every position, then the remaining product or cross-correlation term determines the similarity between the reference and the template images:

$$c(m,n) = \sum_x \sum_y f(x,y)t(x-m,y-n) \tag{2.11}$$

This measure increases with the degree of similarity. There are however three caveats to using Eq. 2.11 for registration.

- The local reference image energy term $f^2(x,y)$ is rarely constant and therefore matching can fail, as the correlation where the reference and template are an exact match may be less than the correlation at some arbitrary position, where the reference frame contains a bright spot.
- The range of $c(m,n)$ is dependent on the size of the template. As the size of the template increases, the range of $c(m,n)$ increases.
- Eq. 2.11 varies with changes in image amplitude. For example, if all the intensity values of $f(x,y)$ are doubled, for the same template image, the values of $c(m,n)$

are doubled.

To overcome these difficulties the reference and template are normalised yielding the correlation coefficient:

$$cc(m,n) = \frac{\sum_x \sum_y \left[f(x,y) - \bar{f}_{m,n}\right]\left[t(x-m,y-n) - \bar{t}\right]}{\sqrt{\sum_x \sum_y \left[f(x,y) - \bar{f}_{m,n}\right]^2 \sum_x \sum_y \left[t(x-m,y-n) - \bar{t}\right]^2}} \tag{2.12}$$

where $\bar{t}$ is the mean of the template and $\bar{f}_{m,n}$ is the mean of the reference under the template. As with cross correlation, the correlation coefficient also obviously increases with the degree of similarity and a high value of $cc(m,n)$ indicates a good match between the reference and template, when the template is centred at (m,n). The correlation coefficient has the added advantage that it gives a similarity measure on an absolute scale ranging from $[1,-1]$. Therefore, by computing $cc(m,n)$ for all translations by shifting the template pixel-by-pixel this method can be used to register images which are misaligned by a rigid translation.

2.3.2 Cross Correlation in the Frequency Domain

Correlation is a popular match metric in many registration problems because the correlation theorem enables it to be efficiently computed in the frequency domain. The correlation theorem may be regarded as a special case of the convolution theorem. If $F(u,v)$ is the Fourier transform of $f(x,y)$ and $T(u,v)$ is the Fourier transform of $t(x,y)$, the correlation theorem states

$$f(x,y) \circ t(x,y) \Leftrightarrow F^*(u,v)\,T(u,v) \tag{2.13}$$

where $\circ$ denotes correlation and F^* denotes the complex conjugate of F. This means that the correlation of two functions in the spatial domain is equivalent to multiplying the Fourier transforms of the functions and computing the inverse Fourier transform of the result [84]. This gives an alternative way to compute the correlation between images. The main reason this operation can be more efficient than performing correlation in the spatial domain is due to the fast Fourier transform (FFT). If the template is very small it is more efficient to directly implement correlation in the spatial domain. As the size of the template increases it becomes substantially faster to perform correlation in the frequency domain. There is a major drawback however, the correlation coefficient, which is preferred in template matching, does not have a simple, efficient

expression in the frequency domain. This drawback was overcome in a paper by Lewis [85]. In this paper, the numerator of Eq. 2.12 was reduced to correlation in the frequency domain using the FFT by precomputing the mean of the template, as it is constant irrespective of (m,n). Looking at the denominator, the template expression $\sum_x \sum_y [t(x-m,y-n)-\bar{t}]^2$ could also be precomputed, leaving the problematic expression $\sum_x \sum_y \left[f(x,y)-\bar{f}_{m,n}\right]^2$. The local reference image mean and local reference image energy must be calculated at each (m,n). By constructing tables of the reference image running sum and energy, the expression $\sum_x \sum_y \left[f(x,y)-\bar{f}_{m,n}\right]^2$ can be computed with substantially fewer operations. This technique has dramatically reduced the computational cost of using the correlation coefficient for template matching.

2.3.3 Patch Registration

Registration of retinal images acquired using scanning techniques is much more complex than implementing a simple rigid translation to align the images. This is due to fixational eye movements during the acquisition of each image. However, during short time intervals, retinal motion can be well-approximated by a simple translation. This has lead to patch-based correlation methods being used to register SLO images [79, 80, 86]. Because the direction of the fast scan in the SLO is horizontal, it is assumed that a single horizontal scan line is unaffected by fixational eye motion and is essentially a snapshot of the retina. Thus each template image is partitioned into patches that extend horizontally across the entire image but extend just a few lines of the vertical extent of the image (the direction of the slow scanner), as seen in Figure 2.7. Correlation is then calculated between each patch and the reference image to obtain approximations of motion within the frames.

Is the assumption that retinal motion in a patch is negligible and a rigid translation can be used to register individual patches to the reference valid for the modified HRT classic? As explained in the next section, patches would ideally extend just 1 line vertically, but in practice, typically extend 9 lines vertically. According to the eye movement data from Section 2.2, retinal features could be displaced 0.001–0.02 μm in a single line and 0.009–0.18 μm in a 9 line patch due to tremor, 0.003–0.012 μm in 1 line and 0.027–0.111 μm in a 9 line patch due to drift. Given that these values are much less than a pixel (at the 2° FOV 1 pixel is approximately equal to 2 μm), it is reasonable to assume that the retinal motion due to tremor or drift can be neglected within a 9 line patch. However, if a microsaccade occurs retinal features could be displaced 0.4–7.9 μm in a single line and 3.4–71.3 μm in a 9 line patch. In this event the assumption that

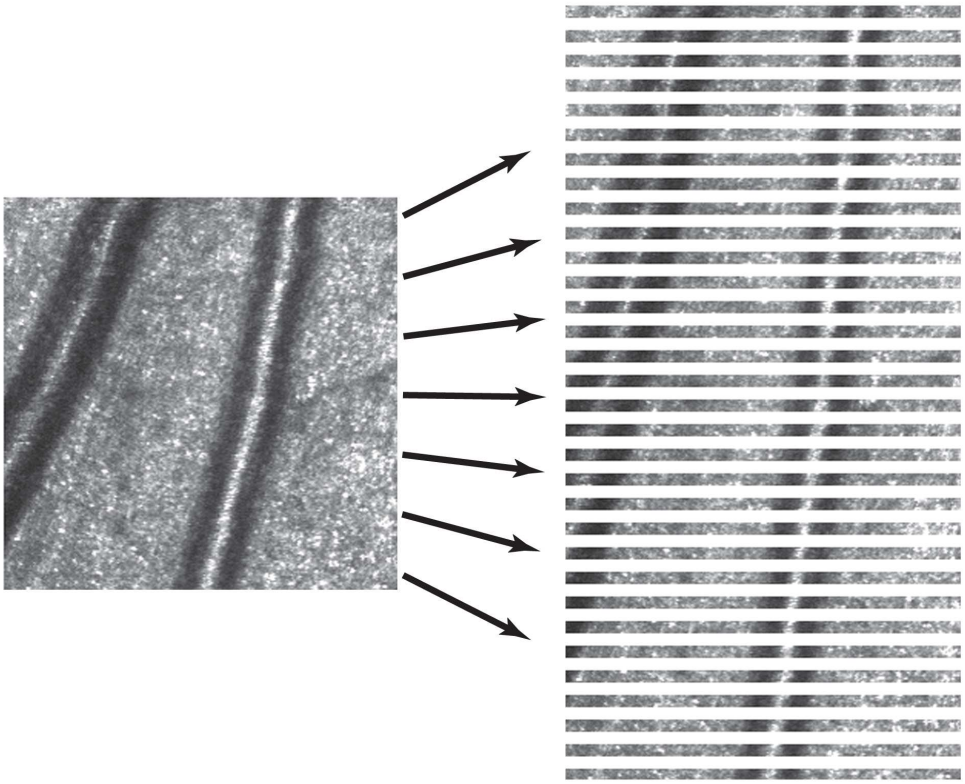

Figure 2.7: Image is split into patches which extend fully across the image horizontally and are a fraction of the vertical extent of the image.

retinal motion can be neglected within a 9 line patch is invalid, and registration for the image fails. Large microsaccades are relatively rare however, and only 1 image in a sequence of 32 is lost in such an event. Therefore, it was considered that the simplification of assuming that a patch of 9 lines could be considered as undistorted due to fixational eye movements was acceptable, as opposed to implementing a more complex and computationally demanding algorithm.

2.3.4 Algorithm to register modified HRT-classic images

It is the correlation coefficient computed in the frequency domain which was used as the match metric in the Matlab® based algorithm to register sequences of images from the HRT. It is necessary to use the correlation coefficient to make shift estimations robust to intensity fluctuations. Such intensity fluctuations are very common in image sequences obtained from ophthalmoscopes due to subject misalignment, tear film break-up etc.. Another useful property of the correlation coefficient is that it has an absolute range $[-1,1]$. This was used to delete frames which did not sufficiently

match the reference image by discarding images whose maximum correlation coefficient did not reach a set threshold. This could be due to insufficient overlap between the reference and template images, which occured when the eye wandered too far away from the fixation target, or due to extreme warping in the template image.

Videos of an image sequence at each stage of registration can be viewed at:
www.moeohanahan.wordpress.com/image-registration.
These videos can also be viewed from the DVD provided.

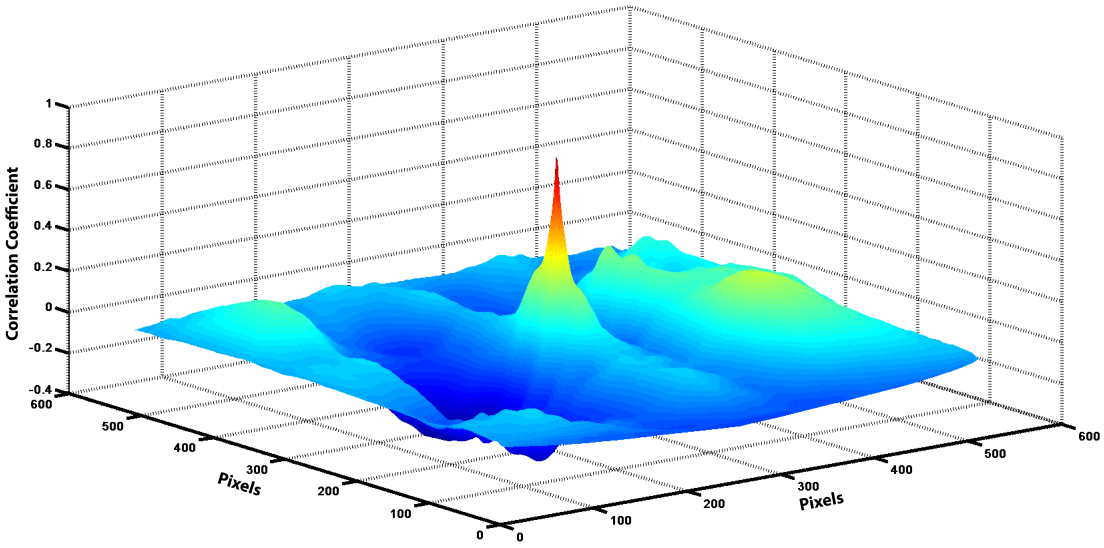

Figure 2.8: Correlation peak obtained in "full-image" matching. The correlation coefficient is calculated for every possible translation between the reference and the template image. The correlation coefficient increases with the degree of similarity and a high value indicates a good match. Therefore, the location of the peak gives the displacement needed to optimally register the template image to the reference image.

Before importing the desinusoided image sequence into the registration algorithm, frames where blinks had occured, resulting in the intensity dropping to zero in the images throughout the blink, were manually deleted. The first step in the registration algorithm was to implement a "full-image" alignment. The first image in a sequence was normally taken as the reference image, unless it showed visible signs of distortion. Then the correlation coefficient for every possible translation between the reference and each of the subsequent template images in the sequence was calculated to estimate the inter-image eye movement. The maximum of the correlation coefficient for each template image was determined and the location of the peak gave the

displacement which was needed to optimally register the template image to the reference image. Figure 2.8 shows an example of a correlation coefficient peak obtained from full-image registration. If the correlation coefficient for any of the template images was not greater than a set threshold the image was discarded. The remaining images were aligned by a simple rigid translation, determined by the calculated shift estimates. Due to the movement of the eye there are areas of the retina, at the edges of the frames, that are not present in all the images. Because of this, when the images are registered a border is introduced around each of the frames so that the registered images will be the same size. This effect can be seen in the video – *Full-Image Registered Image Sequence*. The size of the borders depends on the magnitude of the eye motion. The registered sequence is therefore cropped. The regions of the retina that are not common to all the frames are deleted, thereby eliminating the boundary effects due to the image stabilisation. The result of this can be seen in the video – *Cropped Image Sequence*.

As explained in Section 2.3.3, the images obtained through scanning techniques, such as in the HRT classic, suffer warping as each image is captured over time and is not a snapshot of the retina. Therefore a patch-based registration scheme was implemented. Ideally, each patch would extend just 1 line vertically, however in most sequences such patches fail to register due to noise. A compromise between having enough data to reliably match the patches and obtaining the most accurate within frame motion estimates must be reached. After testing many sequences it was empirically decided to use patches which were typically 256 across by 9 pixels vertically. This problem is illustrated in Figure 2.9. Figure 2.9 (i) shows the correlation coefficient matrix for a 1 line patch. Figure 2.9 (ii) shows the correlation coefficient matrix for a 9 line patch of the same region of the same template image. From this it can be seen that a more defined peak is obtained when more data is used for matching.

When implementing the patch registration to remove the warping within frames the cropped sequence was used. The image which was taken as the reference for the full image registration was again taken as the reference image. The correlation coefficient was calculated for every possible translation between the reference and each individual patch. The maximum correlation coefficient was determined for each patch and the shift estimate to optimally register the patch to the reference image was calculated. Patches where the correlation coefficient did not reach a certain threshold were discarded.

Once the x- and y- shifts for each patch were estimated cubic spline interpolation was used to calculate a y-shift for each line and linear interpolation to calculate an x-shift

for each line. The corresponding transformations were then applied to the template images to align them to the reference image.

Figure 2.10 (i) shows the inter-frame eye motion estimates that were obtained for a typical sequence, where no images were discarded due to blinks or insufficient matching. The images were acquired at a 2° FOV, so each pixel corresponds to 28 seconds of arc or approximately 2 μm of planar distance on the retina. Figures 2.10 (ii) and (iii) show the x- and y- motion estimates plotted individually against time. The intra-frame motion estimates are included in these plots. The 1.5 s duration corresponds to the acquisition time for a sequence of 32 images. Negative values in the y/vertical direction represent upward movement with respect to the reference and negative values in the x/horizontal direction represent movement to the left with respect to the reference. In Figure 2.10 (i) the red circle indicates the starting position $(0,0)$, the reference image. One can clearly see a general upward drift along with an initial drift to the left followed by a drift to the right. Figures 2.10 (ii) and 2.10 (iii) show that tremor occured in all the frames and was of similar magnitude in each image. The missing data in plots 2.10 (ii) and (iii) is due to a lack of recorded data during the resetting time or "flyback" between frames, and due to loss of data due to cropping.

The images first undergo a full-image registration as removing the inter-frame eye-motion makes the patch-based, intra-frame registration more robust. To demonstrate this, patch-based registration was applied to an image sequence which had been full-image registered (it had also been cropped), and on the same image sequence which had only been desinusoided. In both cases the first image was taken as the reference image. Figure 2.11 show the correlation coefficient matrices obtained for a 9 line patch of the same region of images (i) 5 and (ii) 27, from the full-image registered sequence. From the shift estimates obtained from the full-image registration it is known that image 5 had not translated with respect to the reference image, while image 27 had translated 17 pixels horizontally and 8 pixels vertically from the reference image. It can be seen that a well defined peak is still obtained, for the patch from image 27, towards the end of the sequence when the template image had moved considerably with respect to the reference image. Figure 2.12 shows the correlation coefficient matrices obtained for a 9 line patch of the same region, of the same images, but from the desinusoided sequence. It can be seen in (i), for image 5, that a well defined peak is obtained from the desinusoided sequence when the template image has not moved considerable with respect to the reference. However, as the template image moves further from the reference image the peak becomes considerable diminished, as demonstrated in Figure 2.12 (ii).

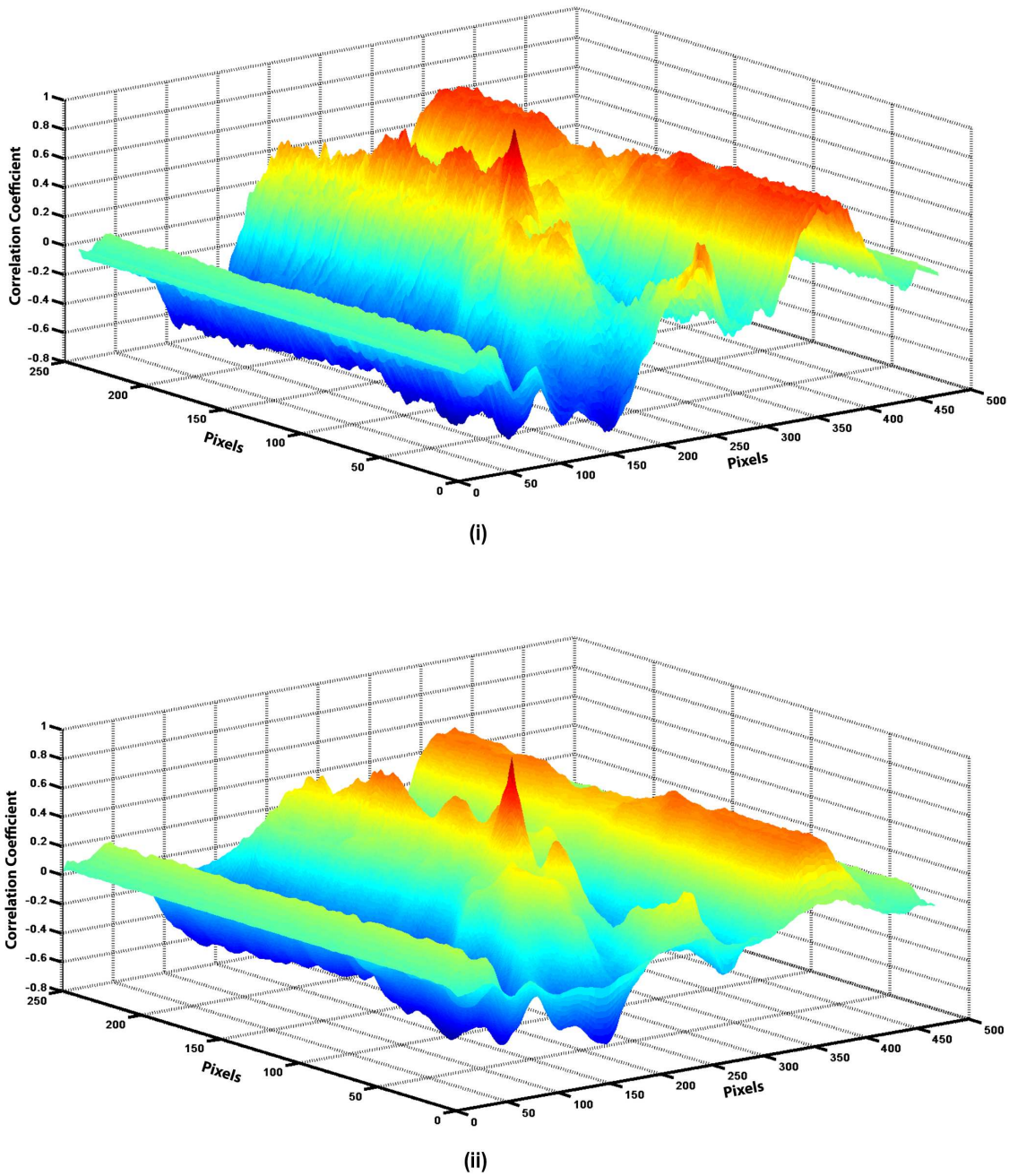

Figure 2.9: Comparison of correlation peaks obtained for (i) 1 line and (ii) 9 line patches from the same region of a template image. A more defined, less noisy peak is obtained in (ii) when more data is used for matching.

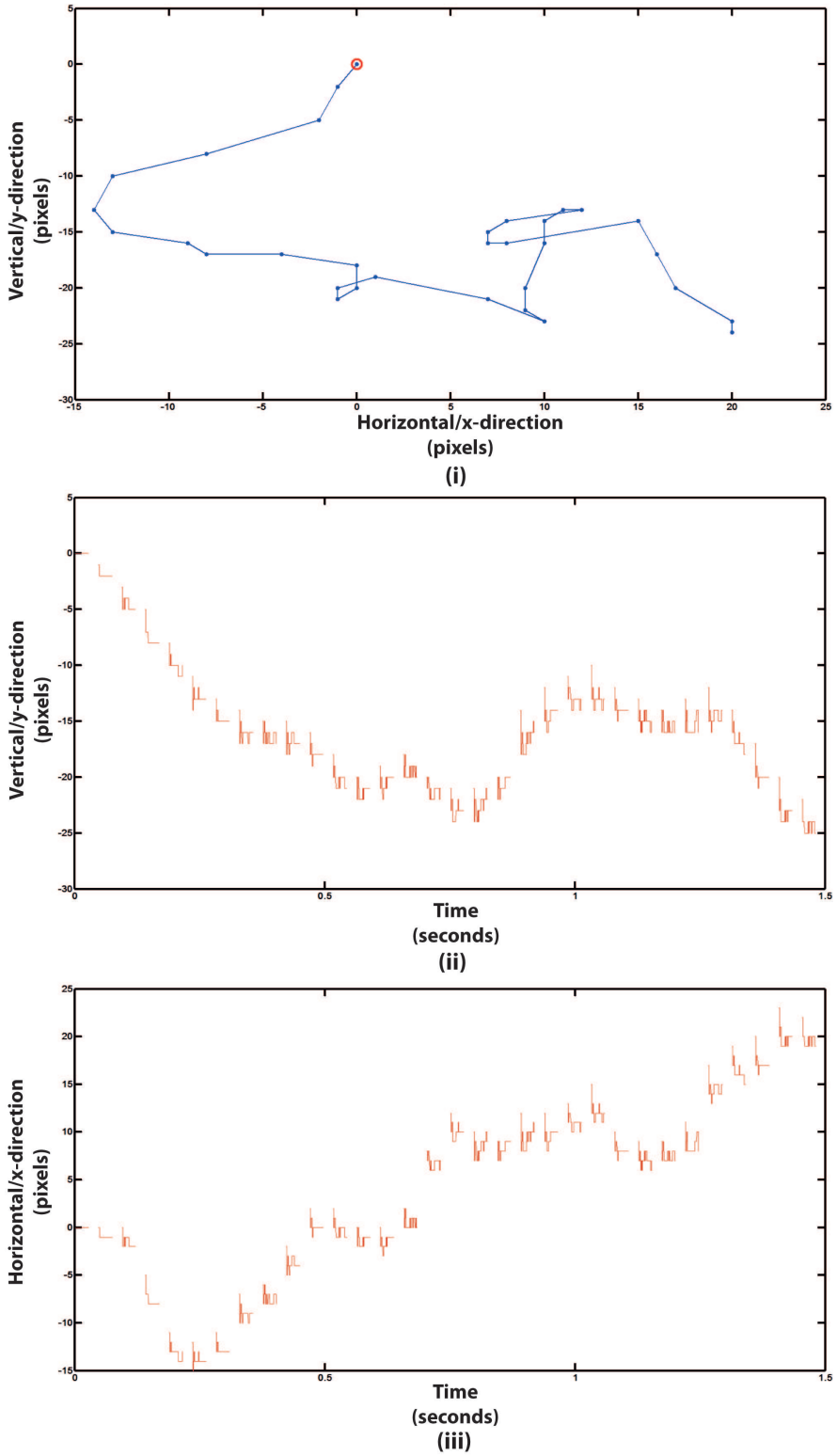

Figure 2.10: Shift Estimates. (i) depicts the inter-frame eye motion estimates that were obtained for a typical sequence, where no images were discarded. The red circle indicates the starting position, (0,0). (ii) and (iii) show the x- and y- motion estimates plotted individually against time, with the intra-frame motion estimates included. Negative values in the x- and y-directions represent movement to the left and upwards with respect to the reference.

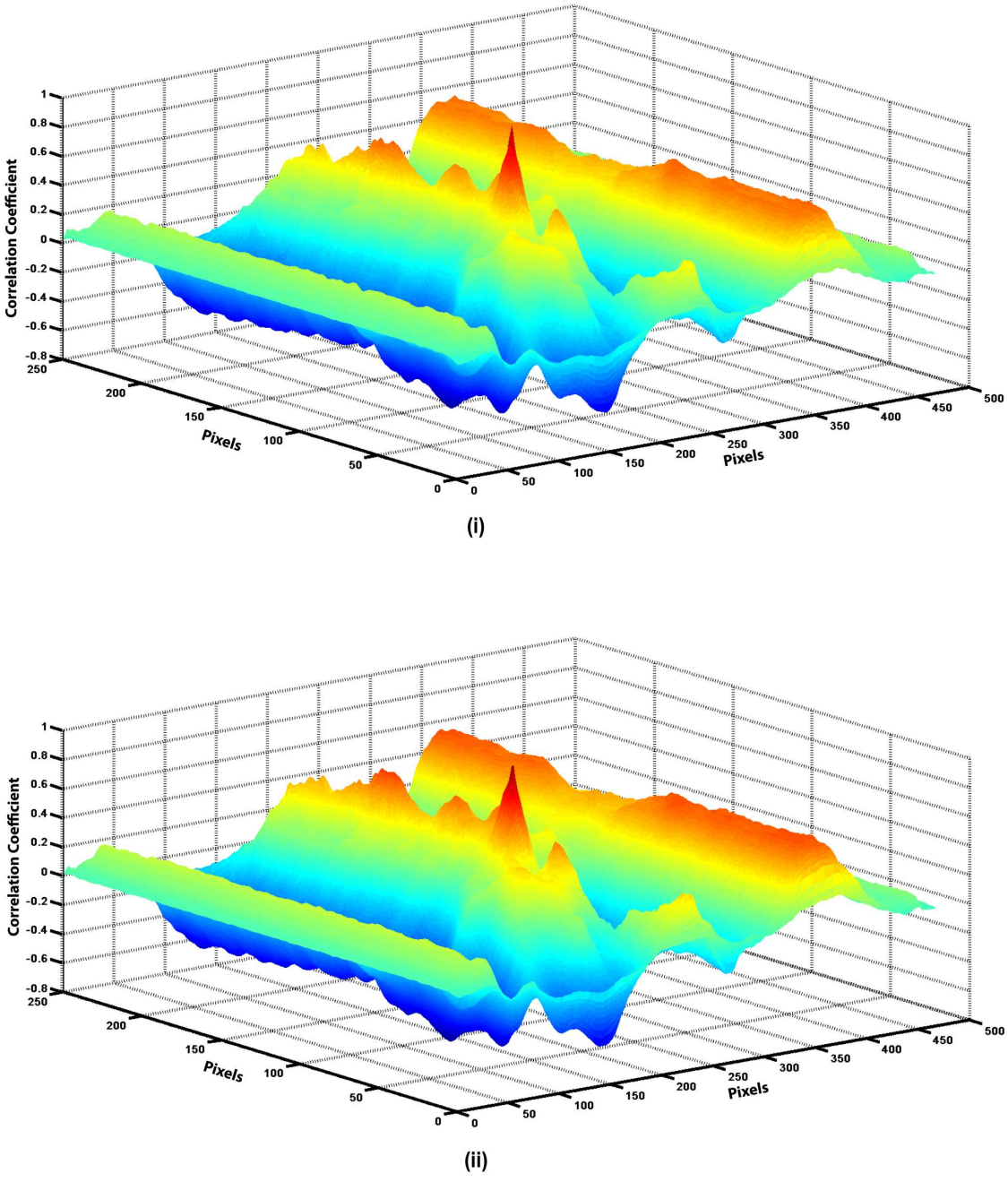

Figure 2.11: Correlation peaks obtained for a 9 line patch from (i) image 5 and (ii) image 27 of the registered, cropped sequence. A well defined peak is obtained for image 5 which has not moved with respect to the reference. A similarly distinct peak is still obtained for image 27 which has undergone considerable translation with respect to the reference.

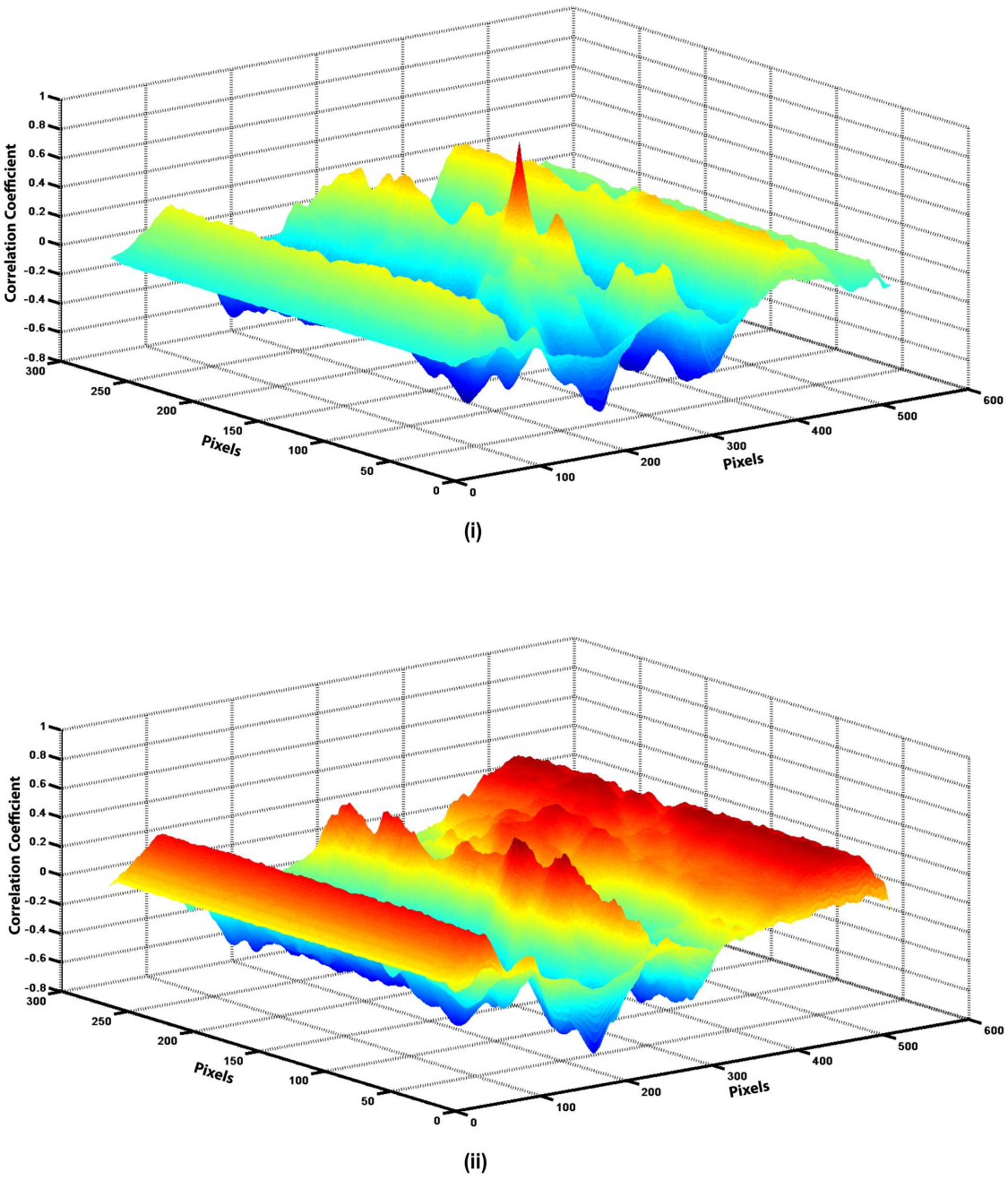

Figure 2.12: Correlation peaks obtained for a 9 line patch from (i) image 5 and (ii) image 27 of the desinusoided sequence. As in Figure 2.11 (i), a well defined peak is obtained for image 5, which has not moved with respect to the reference. However, as the template image moves further from the reference image the peak becomes increasingly diminished. A distinct peak can no longer be discerned for image 27, which has translated considerably with respect to the reference image.

2.4 Image Averaging

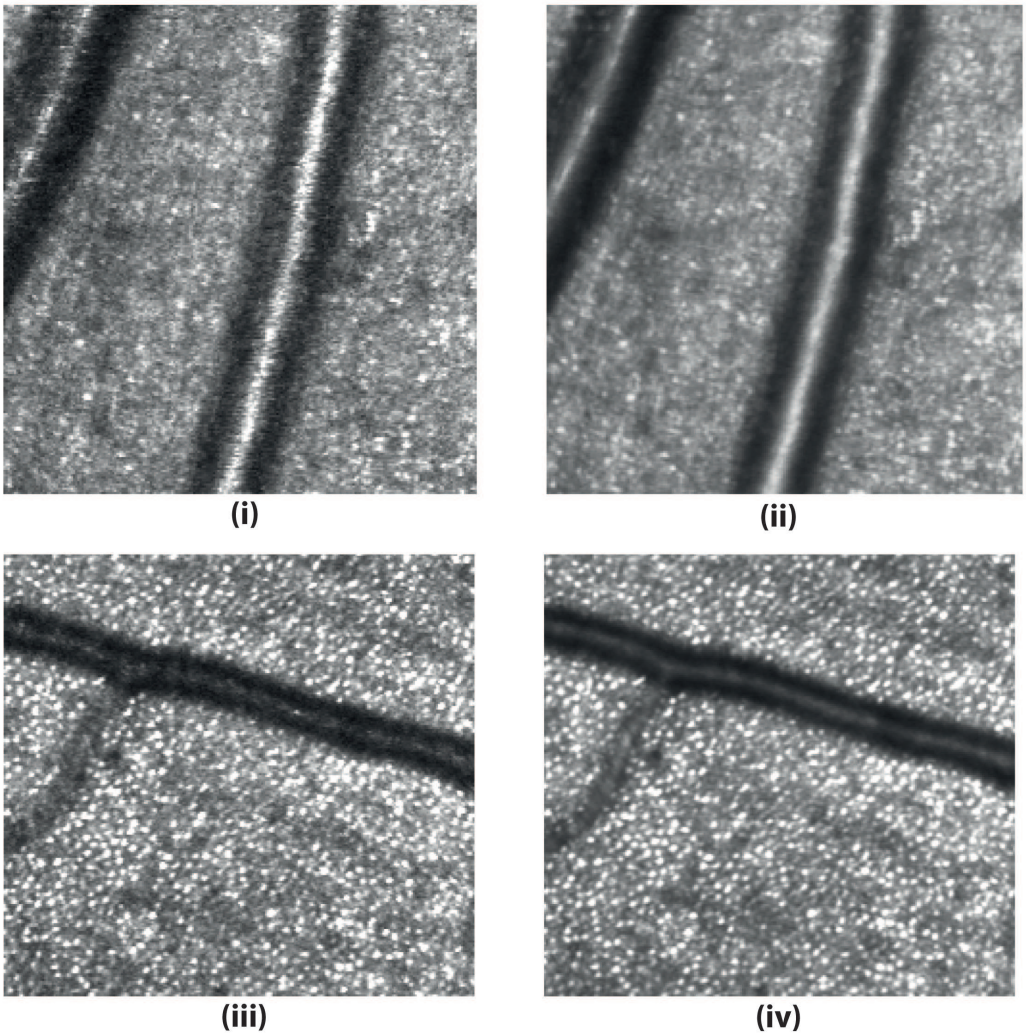

Figure 2.13: Left: (i) and (iii) are single frames of image sequences obtained from the modified HRT-classic. Right: (ii) and (iv) are the temporal averages of the image sequences after registration. In both of these examples all 32 frames of the image sequences were retained after image registration and used in the image averaging step.

Once the images have been registered, high-signal-to-noise images can be obtained by averaging the sequence of images. Image averaging works on the assumption that the noise in the images is uncorrelated. Consider a noisy image $I(x,y)$, it has a stable signal component $f(x,y)$ (the "true" image) and a random noise component $\eta(x,y)$:

$$I(x,y) = f(x,y) + \eta(x,y) \tag{2.14}$$

In a registered sequence of images, the stable signal component stays the same but the

noise component $\eta(x,y)$ differs from one frame to the next. Due to the noise being random, at every pair of coordinates (x,y) the average value is zero. The average image $\bar{I}(x,y)$ of N noisy images is calculated by summing the intensity values for each pixel and dividing by the number of images N:

$$\bar{I}(x,y) = \frac{1}{N}\sum_{i=1}^{N} I_i(x,y) \tag{2.15}$$

The result is that as N increases, $\bar{I}(x,y)$ approaches $f(x,y)$ as the noise component is reduced by a factor equal to the square root of the number of images averaged.

Figure 2.13 shows single frames and temporal averages of registered sequences. An improvement in signal-to-noise in the average image Figure 2.13 (ii) compared to the single image Figure 2.13 (i), is evidence of the registration accuracy. In Figure 2.13 (iii) noise was not as prevalent and individual photoreceptors can be distinguished, the corresponding average image Figure 2.13 (iv) shows no loss of detail, which would occur if the images were not accurately registered.

2.5 Vessel Tracking and Diameter Measurement

A semi-automated vessel tracking and diameter measurement method was implemented. This method is based on the assumption that an arteriole can be considered a curved cylinder consisting of a linkage of many small, straight cylinders.

The algorithm commenced by importing an averaged image. A lowpass Gaussian filter was applied to the average image to reduce sharp transitions in background luminance. The smoothed image was then displayed and the user selected n seed points, sp_n, at the centre of the vessel describing the path of the vessel as can be seen in Figure 2.14. The seed points were selected such that the section of vessel between two successive seed points was approximately straight. Using these seed points the vessel was then divided into $n-1$ segments, where $segment_n$ consisted of the interval $[sp_n, sp_{n+1}]$. The direction of each segment, α_n, was calculated. Estimated centre points, cp, were calculated along the segment. Estimated centre points were calculated to be 2 pixels apart in the segment direction α_n. A cross-section line was calculated at each centre point perpendicular to the segment direction and centred at the centre point, as described in the diagram in Figure 2.15. Figure 2.16 shows a vessel with the cross-section lines plotted at each of the estimated centre points. The vessel profile was then extracted at each cross-section line.

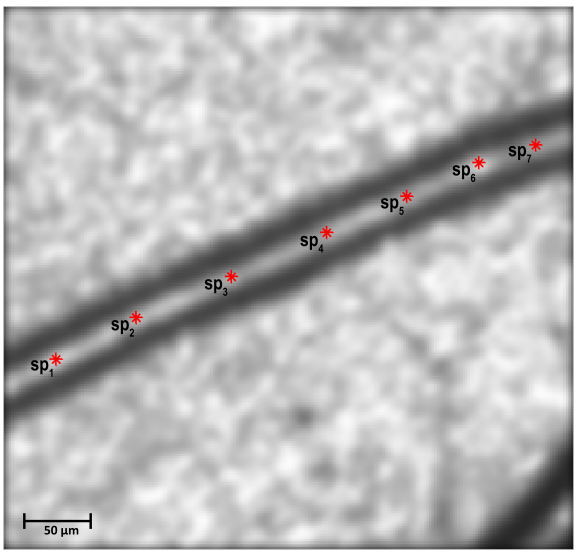

Figure 2.14: The user selected n seed points, sp_n, at the centre of the vessel, describing the path of the vessel. The seed points were selected such that the section of vessel between two successive seed points was approximately straight.

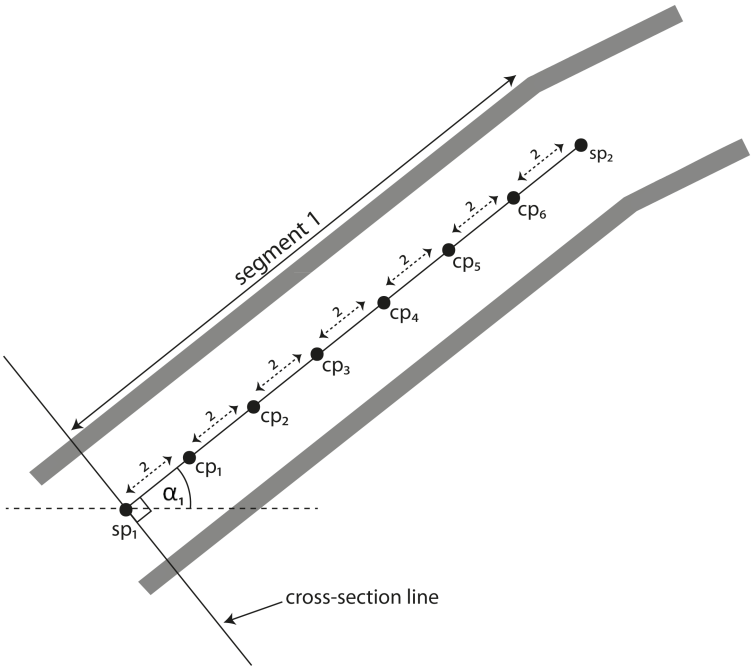

Figure 2.15: Using the seed points selected by the user, the vessel was divided into n - 1 segments, where segment$_1$, which is depicted in this diagram, consisted of the interval between sp_1 and sp_2. The direction of the segment, α_1, was calculated. Estimated centre points, cp, were calculated along the length of the segment. Estimated centre points were calculated to be 2 pixels apart in the segment direction.

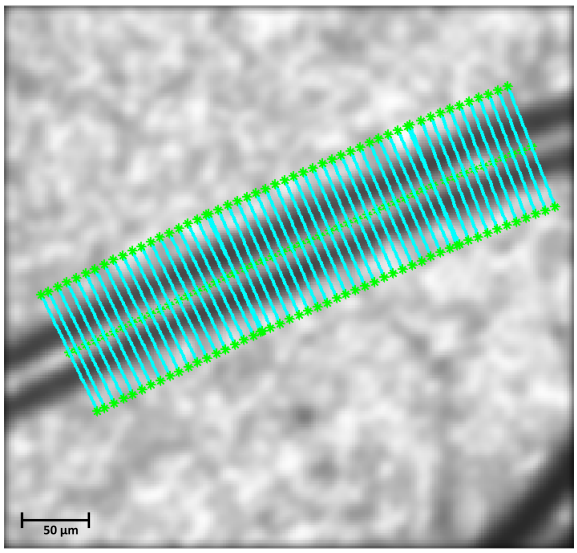

Figure 2.16: A cross-section line was calculated at each estimated centre point, perpendicular to the segment direction and centred at the estimated centre point. This image shows a vessel with its estimated centre points and corresponding cross-section lines plotted.

The vessel edges and centre positions were identified using a sliding linear regression filter method proposed by N. Chapman et al. [87]. This technique is based on fitting a best fit line by linear regression relating image intensity against distance along the profile within a sliding window filter. The window of W points centred on the i^{th} point, was progressively moved point-by-point along the profile, as demonstrated in Figure 2.17 (i). At each point, a straight line was fit to the intensity values within the window using the least squares method. The gradient of the straight line was recorded at each point, m_i. Figure 2.17 (ii) shows the corresponding gradient data of the vessel profile. The edge points were determined from this gradient data. The left edge was taken as the minimum slope obtained from the left half of the profile. The right edge was taken as the maximum slope obtained for the right half of the profile. The actual centre points of the vessel were found by taking the central portion of the vessel profile and locating the point at which the gradient changed from positive to negative. This process is demonstrated in Figure 2.17. Vessel diameters were then set as the distance between corresponding left and right edges, giving a diameter value for each centre point. The median of these vessel widths was taken as the vessel diameter.

In this method one needs to consider the window size W. Large window sizes reduce the occurence of vessel edges being incorrectly located at random bright/dark spots in the background. While short windows provide better edge resolution, especially for small vessels, but at the expense of reduced noise rejection. For this reason,

this technique tracked the vessel twice to incorporate adaptation of the size of the filter window to the approximate size of the vessel. During the first time of tracking, an estimate of the vessel edges, centre points and diameters was calculated using a large cross section line $(100\ pixels)$ and a long window length $(10\ pixels)$. For the second time of tracking, the length of the cross-section line was set to be only slightly greater than the median diameter that was estimated in the first run and a shorter filter was applied (approx. 10% of the length of the cross-section line). Therefore, during the second run, despite the reduced noise rejection due to the shorter filter length, the edge points were rarely identified at random points in the background. This was because little background intensity was included in the extracted profile due to the cross-section line being adapted to an estimate of the vessel diameter, so there were few random bright/dark spots which could mistakenly have been determined as edge points. The diameter of the arteriole was set as the median diameter calculated from the second time of tracking.

Figure 2.18 (i) shows the centre and edge points calculated using this technique. In Figure 2.18 (ii) the edge points displayed were calculated from the resulting arteriole diameter, centred at the calculated centre points and perpendicular to the vessel direction. From this it can be seen that this method delineates the vessel quite well and provides a good estimate of the arteriole diameter.

Arteriole diameter measurements were not converted from pixels to μm using axial length and refractive measurements because relative change was the primary outcome measure desired in this thesis. However, for the 2° FOV, which was used for reactivity measurements, 1 pixel is approximately equal to 2 μm. As diameter measurements were not converted to absolute units they were unsuitable for interindividual comparison. Therefore, results comparing baseline diameters between groups (i.e. smokers vs. nonsmokers, healthy controls vs. hypertensives vs. diabetics) in Chapters 4 and 6, need to be treated with a degree of caution. This limitation does not apply when comparing vessel diameters within groups, i.e. when comparing arteriole diameters across quadrants in Chapter 3 or comparing baseline diameters of the same group of smokers after an abstinence and after smoking a cigarette in Chapter 4.

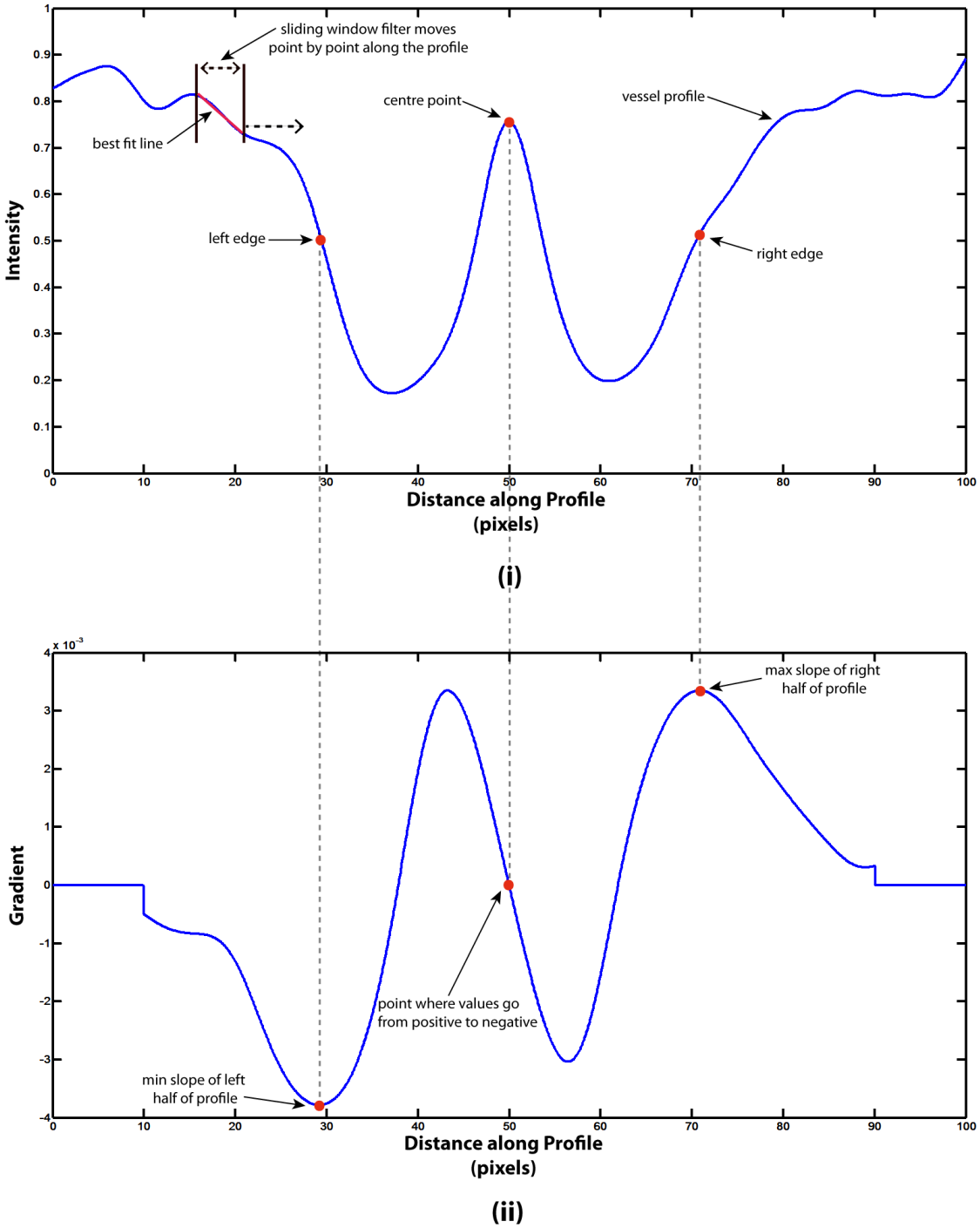

Figure 2.17: A vessel profile (i) was extracted at each cross-section line. The vessel edges and centre positions were identified using a sliding linear regression filter. The window filter was moved point-by-point along the profile. At each point, a straight line was fit to the intensity values within the window using the least squares method, and the gradient of the straight line was recorded (ii). The vessel edges were determined from this gradient data. The left and right edges were taken as the min slope obtained from the left half of the profile and the max slope obtained for the right half of the profile respectively. The centre points were found by taking the central portion of the vessel profile and locating the point at which the gradient changed from positive to negative.

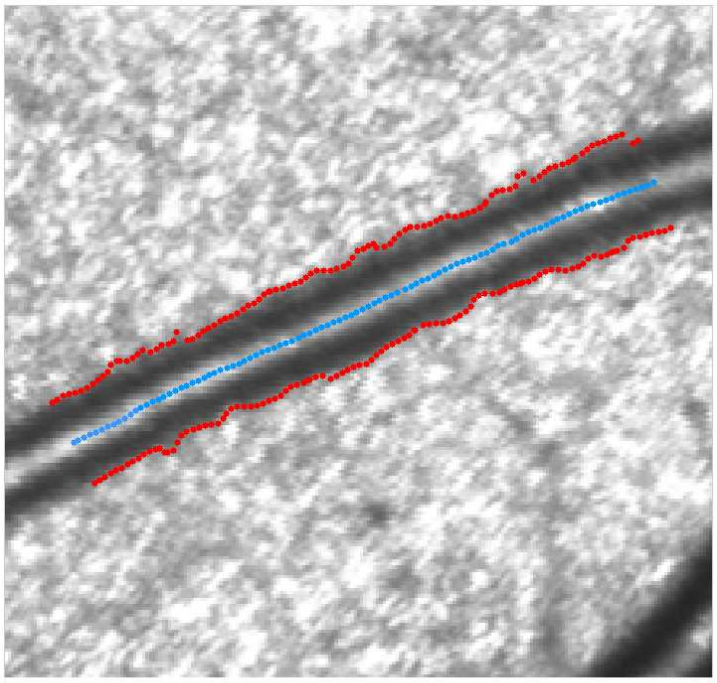

(i)

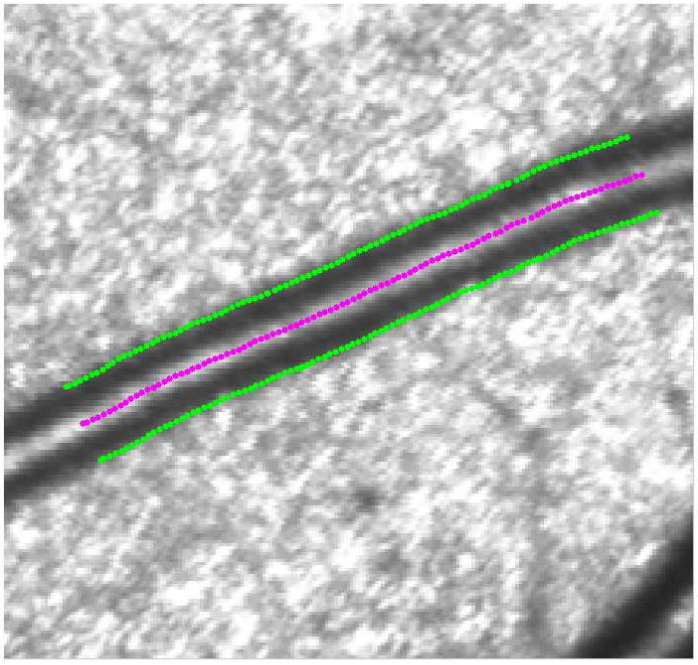

(ii)

Figure 2.18: (i) Vessel centre points and edges calculated at each estimated centre point using the sliding linear regression filter technique. A diameter value was assigned to each centre point by calculating the distance between the corresponding left and right edges. The median of these vessel widths was taken as the vessel diameter. The edge points in (ii) are calculated from this resulting vessel diameter, centred at the calculated centre points and perpendicular to the vessel direction. This illustrates that this method provides a good estimate of the vessel diameter.

2.6 Flow Visualisation

As described in Chapter 1 (Section 1.4, page 10), retinal blood flow is regulated in accordance with the needs of the tissue, by modulating retinal vascular tone. Also, the volumetric blood flow is determined from the cross sectional area of the vessel and the mean velocity of the blood (Section 1.3). Therefore a velocity measurement is also ideally obtained, simultaneous to the vessel diameter measurement, so that the alteration of volumetric blood flow due to hyperoxic provocation can be calculated. However, we did not have a Laser Doppler system to obtain velocity measurements. We therefore attempted to apply previously reported video processing techniques to extract velocity information from our image sequences.

Flow visualisation techniques are based on the idea that the intensity of each pixel in the vessel region will vary frame by frame due to blood flow, while the intensity in the background pixels should remain relatively constant. Such rapid intensity fluctuations along a vessel can be observed in the video - *Fully Cropped Image Sequence*. Variance, range and difference images have previously been applied as techniques to identify active vessels [55, 88, 89]. These approaches alone do not lead to any quantitative measurements of vascular activity, but the calculated images are then used for further analysis to derive velocity information [55, 89, 90].

Variance and Standard Deviation Images

The variance image can be obtained by calculating the temporal variance of intensity values at a given pixel. For N frames the variance image, $V(x,y)$, can be calculated as:

$$V(x,y) = \frac{1}{N}\sum_{i=1}^{N}[I_i(x,y) - \bar{I}(x,y)]^2 \tag{2.16}$$

where $\bar{I}(x,y)$ is the average image, which is calculated as in Section 2.4, page 47.
The stationary background pixels exhibit low temporal variance and appear blue in the variance image. The vessel pixels which exhibit blood flow have a high temporal variance and appear yellow and red in the variance image.
The standard deviation image, $SD(x,y) = \sqrt{V(x,y)}$

Range Image

The range image is the difference between the maximum and minimum intensity values at a given pixel over the sequence of images. The range image, $R(x,y)$ can be

calculated as:

$$R(x,y) = Max(x,y) - Min(x,y) \tag{2.17}$$

where

$$Max(x,y) = Maximum\left[I_i(x,y)\right], \quad i = 1,\ldots,N$$

$$Min(x,y) = Minimum\left[I_i(x,y)\right], \quad i = 1,\ldots,N$$

In a range image the vessel pixels will show a large difference between the maximum and minimum values for a given pixel, thereby giving a large range. Meanwhile the background pixels, which should not exhibit a large variation in intensity should have a similar max and min for a given pixel, giving a small range. Therefore the vessels with a large range should appear red and yellow in the range image, while the background which would have a small range should appear blue. However, as the range image is calculated from only 2 intensity samples at each pixel, it is highly susceptible to noise.

Difference Image

The difference image is the cumulative sum of the squared intensity differences at each pixel between consecutive images in a sequence of N images. The difference image $D(x,y)$ can be determined as:

$$D(x,y) = \frac{1}{N-1}\sum_{i=2}^{N}\left[I_i(x,y) - I_{i-1}(x,y)\right]^2 \tag{2.18}$$

As the intensity differences at each vessel pixel between consecutive images will be larger than at the background pixels, the difference image suppresses the background pixels while emphasising the vessel pixels.

Examples of the average, variance, standard deviation, range and difference image which were calculated for an image sequence can be seen in Figure 2.19. The images have been scaled such that the image data scales to the full range of the colourmap. Median filtering was applied before and after the calculation of each of these images. It can be seen that vessel pixels appear red and yellow, indicating intensity fluctuation in this region, while background pixels appear blue indicating comparatively stable pixel intensity in this region. While the examples in Figure 2.19 illustrate these techniques working quite well, they proved to be very unreliable. In many cases the intensity variation in vessel pixels was similar to the intensity variation of the

background pixels and these techniques failed entirely to distinguish between vessels and the background. Tam et al. [91] also encountered this problem and developed a slightly different approach - Division Standard Deviation Images.

Division Standard Deviation Image

First, for a sequence of N images, a division image is calculated from each pair of consecutive images:

$$D_i = \frac{I_i(x,y)}{I_{i+1}(x,y)}, \quad i = 1,\ldots,N-1 \tag{2.19}$$

Then consecutive division images are averaged to create a "multiframe division image" [91]:

$$M_i(x,y) = \frac{[D_i(x,y) + D_{i+1}(x,y)]}{2}, \quad i = 1,\ldots,N-2 \tag{2.20}$$

The standard deviation image of this sequence of N multiframe division images is then calculated:

$$SD(x,y) = \sqrt{\frac{1}{N}\sum_{i=1}^{N}[M_i(x,y) - \bar{M}(x,y)]^2}, \quad i = 1,\ldots,N \tag{2.21}$$

where $\bar{M}(x,y)$ is the average image calculated from the multiframe division images.

An example of a division standard deviation image can also be seen in Figure 2.19. Median filtering was applied before and after calculation of the division standard deviation image. Again, while this example demonstrates the technique working quite well we found it to be unreliable and failed for many sequences. Due to the unreliability of these flow visualisation techniques to identify vessels we decided not to pursue this avenue of investigation.

It has repeatedly been demonstrated that retinal blood velocity decreased in subjects during oxygen breathing [12, 22, 46, 51, 52, 75, 92, 93]. Also, in a study by Lorentz et al. [94] the change in vessel diameter and blood velocity in response to hypoxia and hyperoxia was investigated in rats. They found that blood velocity increased when vessels dilated and decreased when vessels constricted. In response to hypoxia they measured an increase of approximately 25% in arterial diameters together with an increase of 19% in blood velocity. While they found that arterial diameter and blood velocity decreased by 25% and 17% respectively during hyperoxia. So while we cannot provide a measure of blood flow reduction due to hyperoxic provocation, it

has been proven that blood velocity does not increase to compensate for the decreases in cross sectional area of the vessel and it, in fact, decreases. And, as retinal blood flow is regulated by altering arteriole diameter we use the magnitude of diameter constriction to study retinal arteriole reactivity.

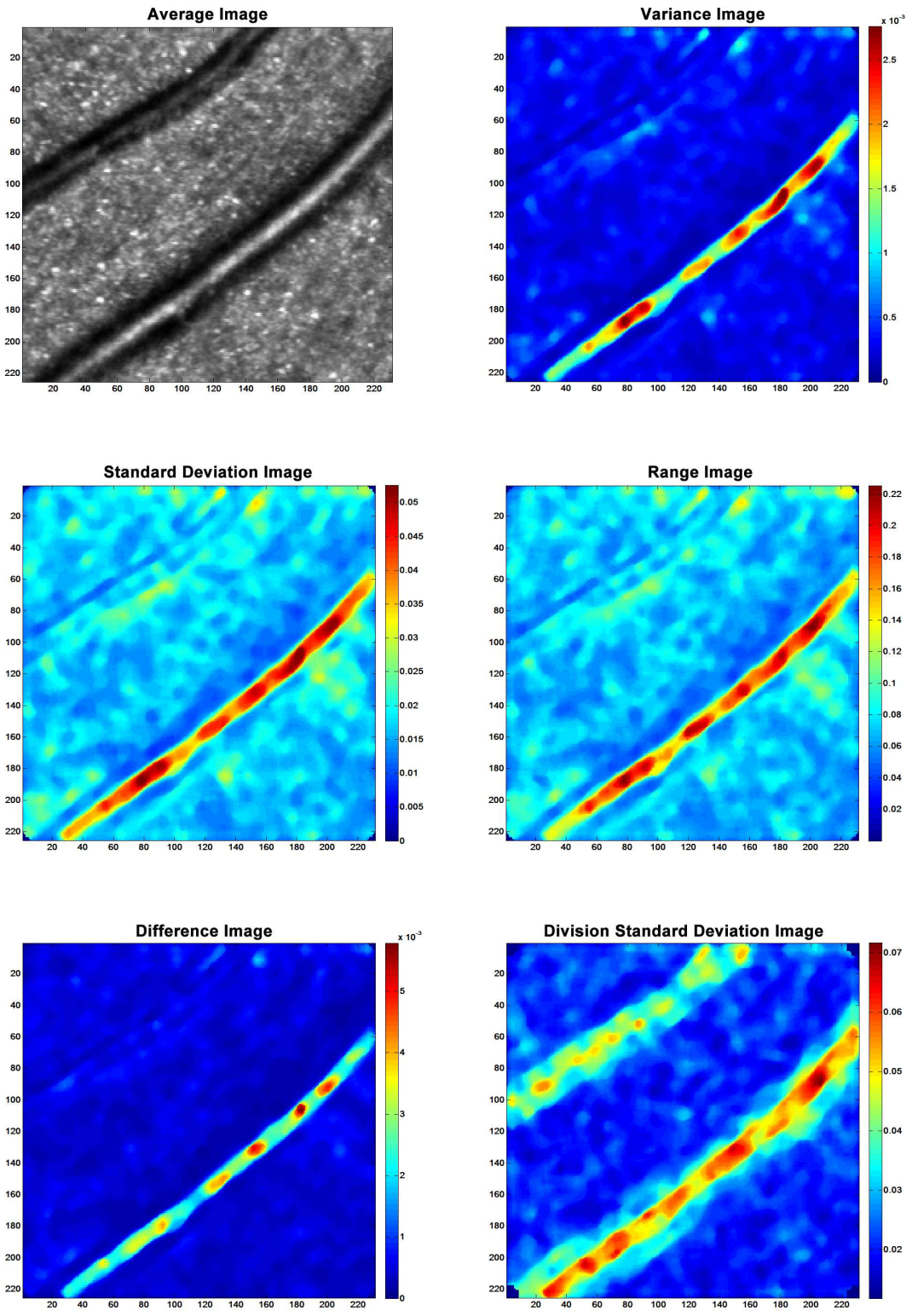

Figure 2.19: The average, variance, standard deviation, range, difference and division standard deviation image calculated for an image sequence. In vessel regions pixels appear red/yellow, indicating intensity fluctuation, while background pixels appear blue indicating comparatively stable intensity in this region.

Chapter 3

Reactivity in Young, Healthy Subjects

3.1 Introduction

Regulation of retinal blood flow is compromised in a number of sight-threatening vascular diseases such as diabetic retinopathy and hypertensive retinopathy. A comprehensive understanding of retinal reactivity in healthy, young subjects is therefore needed to study disturbances in pathology. It is imperative to understand whether the reactivity response to oxygen breathing is independent of arteriolar size and retinal region in order to know if it is possible to draw conclusions about the reactivity of the whole of the retinal vasculature from a single, arbitrary measurement site. It is also important to know the reaction time of the arterioles, so that measurements taken during the hyperoxic phase do not commence before the arterioles are maximally constricted. The following experiments were therefore performed to address these issues.

3.2 Materials and Methods

3.2.1 Sample

Seventeen (4 women and 13 men) healthy, normal volunteers (mean age $\pm$ SD, 21.9 $\pm$ 2.6 years) participated in this study. Each subject signed a written consent after the nature of the study and experiment protocol were explained in detail. All procedures conformed to the tenets of the Declaration of Helsinki and were reviewed and approved by the National University of Ireland Galway Ethics Committee. Exclusion criteria included ages less than 18 or greater than 40 years, smoking, unclear optic media, pregnant or breastfeeding women, any cardiovascular or respiratory disorders, taking medication with known effects on blood flow (e.g. muscle relaxants), taking any chronic medication.

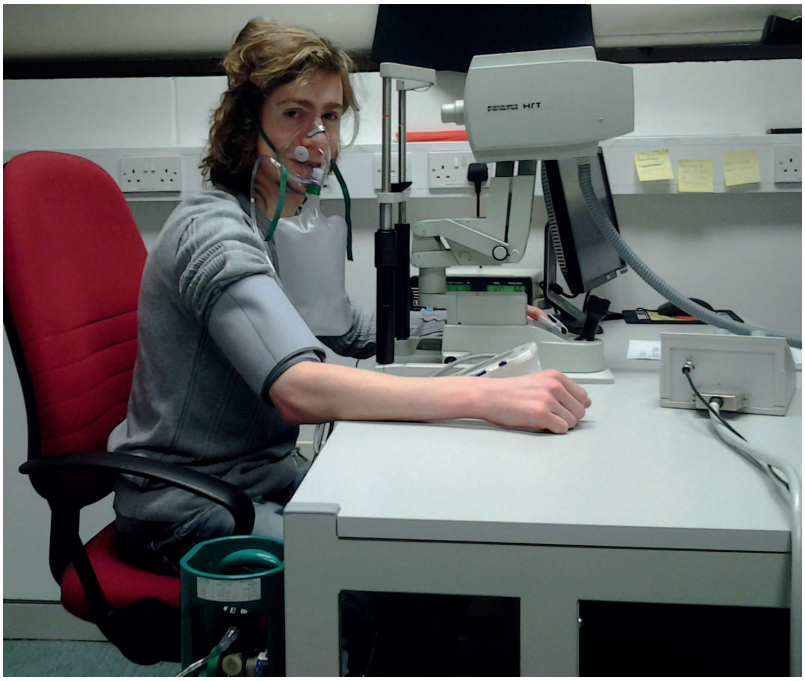

Figure 3.1: Experimental setup.

3.2.2 Visits

Volunteers attended for three visits. The first visit was to determine eligibility, to familiarise the subjects with the measurement technique and to obtain some large field of view (FOV) images. One eye from each subject was selected and approximately

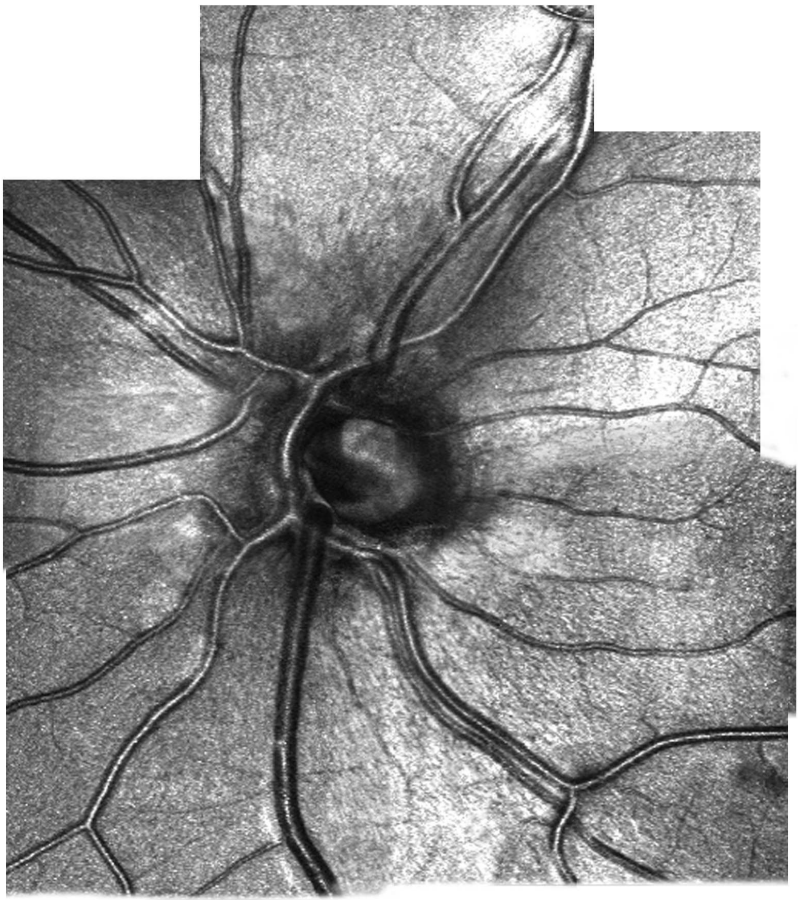

Figure 3.2: A typical mosaic, composed of nine 10° FOV images.

nine 10° FOV (the largest FOV of the HRT classic) were obtained. These images were used to create a mosaic of the retina. The mosaic was used in the second and third visits to define suitable measurement sites (relatively straight arteriole segments with good contrast to the background) and to aid the investigator in navigating the retina at a small FOV. At small FOVs it can be difficult to locate vessels of interest and to repeatedly return to them for multiple measurements. Having the mosaic essentially provided the investigator with a map of the retinal vasculature, greatly increasing the speed and efficiency of imaging at high resolution. The mosaic of the 10° images was generated by first desinusoiding the images and then combining overlapping images using Adobe® Photoshop®. An example of one such mosaic can be seen in Figure 3.2.

The magnitude of retinal vascular reactivity in response to the hyperoxic stimulus was measured during the second and third visits, with intervals of 1–17 days between these visits.

3.2.3 Oxygen Delivery System

Subjects were administered 100% oxygen via a non-rebreathing system at a flow rate of 12 L/min at atmospheric pressure for approximately 20 minutes. The non-rebreathing system consists of an oxygen cylinder, regulator and flowmeter (which adjust the oxygen flow) and a non-rebreathing mask. The non-rebreathing mask with an oxygen reservoir bag can deliver a high concentration of oxygen to subjects. A one-way valve located between the reservoir bag and the base of the mask allows oxygen from the reservoir bag to enter the mask on inhalation but prevents gas in the mask from flowing back into the reservoir bag during exhalation and lowering the oxygen concentration of the bag. One-way valves at the exhalation ports, located at the cheek areas of the mask, prevent room air from entering the mask during inhalation. They also allow the subject's exhaled gases to exit the mask on exhalation. These three one-way valves, along with the high flow of oxygen, result in a minimal intake of room air and an inspired oxygen concentration of 80-90%. The subjects were instructed to report any noticed effect of oxygen inhalation; none of the volunteers noted any reaction to the oxygen.

3.2.4 Experimental Protocol

Subjects were asked to abstain from alcohol and caffeine for 12 hours before the study visits. Subjects rested for at least 5 minutes before the start of each experiment to stabilise baseline cardiovascular and respiratory parameters. All testing was performed in a quiet laboratory, at normal room temperature and at sea level atmospheric pressure.

Visit 2 was to assess the reaction and recovery times of arterioles and visit 3 was to ascertain if regional differences in retinal vascular reactivity exist. Therefore, the experimental protocol was slightly different for visit 2 (protocol A) and 3 (protocol B).

- **Protocol A:** The test protocol was divided into three consecutive phases in which the subject breathed (1) room air for approximately 10 minutes, (2) 100% oxygen for approximately 15-20 minutes via the non-rebreather mask, and (3) room air for approximately 15 minutes. These phases were considered baseline, oxygen breathing, and recovery phases respectively. 2° FOV image sequences of a suitable arteriolar segment were obtained every 30–60 seconds during this session.
- **Protocol B:** The test protocol was divided into two consecutive phases in which the subject breathed (1) room air for approximatly 20 minutes, and (2) 100% oxy-

gen for approximately 20 minutes. These phases were considered baseline and oxygen breathing respectively. A suitable arteriole was selected in each quadrant, one of them being the arteriole imaged in visit 2. Figure 3.3 depicts the retinal quadrants on the retinal mosaic of a left eye. Approximately six 2° FOV image sequences of each of the arterioles were obtained at baseline. Subjects breathed oxygen for 5 minutes before imaging recommenced as they continued to breathe oxygen. The same arterioles imaged at baseline were reimaged, approximately 6 image sequences were captured.

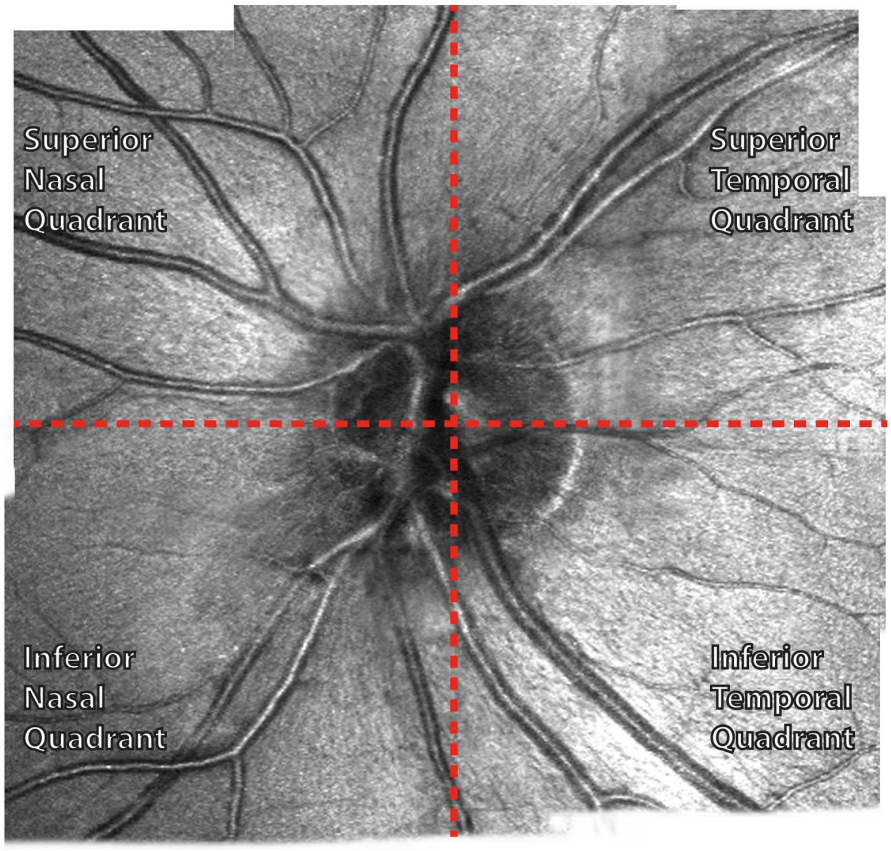

Figure 3.3: Mosaic of a left eye depicting the retinal quadrants. Quadrants are delineated by the dashed red lines.

To assess the relationship between the magnitude of the reactivity response to hyperoxia and vessel calibre, data from image sequences which contained both a large and small arteriole were collated. Arterioles with diameters greater than 30 pixels (approximately 60 μm) were categorised as large, while those with diameters less than 30 pixels were classed as small.

Blood pressure was measured during visits 2 and 3. Three measurments were taken

during each phase. Systolic and diastolic blood pressure were measured on the upper arm by an automated oscillometric device (Omron M10-IT; Omron Healthcare Europe BV, Hoofddorp, The Netherlands). Mean brachial artery blood pressure, BP_m was calculated by

$$BP_m = BP_d + \frac{1}{3}(BP_s - BP_d) \tag{3.1}$$

where BP_d and BP_s were the diastolic and systolic brachial arterial blood pressures respectively. Pulse rate (PR) and oxygen saturation (SpO_2) were also recorded during both visits. Three readings were taken during each phase from a finger pulse oximetric device (Ohmeda Biox 3700e; Datex-Ohmeda, Inc., Madison WI, USA). All measurements were made by the same investigator.

Image sequences were processed as described in Chapter 2, with arteriolar diameters being calculated in pixels as detailed in Section 2.5, page 48.

As described in Section 1.3, page 8, a change in IOP causes a change in perfusion pressure. Previous studies have measured IOP at baseline and during oxygen breathing and found that IOP does not change significantly during hyperoxia [46, 75–77]. Consequently, IOP was not recorded during our experiments.

Previous studies have demonstrated that the magnitude of retinal arteriolar reactivity is independent of gender [21,45,76,95] and left/right eye [45,95], we therefore did not investigate reactivity as a function of these parameters.

3.2.5 Data Analysis

Statistical analysis was performed using Minitab® software package (Release 16; Minitab Inc., PA, USA). Each dataset was group-averaged across subjects as a function of phase (i.e. baseline, hyperoxia, recovery). The response of arteriole diameters to hyperoxia is expressed as a percentage change as compared to baseline. Datasets were assessed to determine if they were normally distributed using the Anderson-Darling test. To investigate the influence of oxygen breathing on parameters two-tailed paired t-tests were performed between baseline values and hyperoxic values. To compare the effect of hyperoxia between 2 different groups (e.g. two different retinal regions, or large versus small arterioles) a two-tailed independent samples t-test was used. A comparison of more than two groups (e.g. comparing across retinal quadrants) was performed using one-way analysis of variance (ANOVA). Variability of measurements was assessed by calculating the standard error and by comparing the results obtained between visits 2 and 3. All data is presented as mean $\pm$ standard error (SE).

The level of significance was set to $p < 0.05$.

3.3 Results

3.3.1 Systemic Haemodynamics

The group-averaged values for each systemic variable for each phase of visit 2 are presented in Table 3.1, and the values obtained for each phase of Visit 3 are presented in Table 3.2.

The group-averaged SpO_2 increased from a baseline of 97.4 $\pm$ 0.3% to 99.6 $\pm$ 0.2% during hyperoxia in visit 2. The baseline and response values did not differ between the two visits. During the recovery phase in visit 2 the SpO_2 returned to its prehyperoxia value.

The baseline value for the group-averaged pulse rate, PR, was 75.0 $\pm$ 2.9 beats per minute (bpm) in visit 2. A small decrease to 70.7 $\pm$ 2.4 bpm was observed during hyperoxia ($p = 0.011$). The baseline ($p = 0.769$) and response values ($p = 0.990$) did not differ between visits 2 and 3. PR returned to its baseline value in the recovery phase of visit 2 ($p = 0.763$).

BP_s was 107.4 $\pm$ 3.7 mm Hg during the baseline phase of visit 2, which did not differ to the baseline value in visit 3 ($p = 0.908$). BP_s did not change significantly during any phase of either visit. In visit 3, the BP_d group mean baseline value was 62.8 $\pm$ 1.2 mm Hg increasing slightly during oxygen breathing to 66.1 $\pm$ 1.6 mm Hg. This result was reflected in the BP_m value which underwent a small increase from 77.9 $\pm$ 1.7 to 79.9 $\pm$ 1.8 mm Hg during the hyperoxic phase. There was no significant difference in the baseline values of BP_d ($p = 0.626$) and BP_m ($p = 0.779$) between the two trial days, however, while these parameters increased slightly during visit 3 they did not alter throughout the experiment during visit 2.

Parameter (n = 16)	Baseline	Hyperoxia	p-value (hyperoxia vs. baseline)	Recovery	p-value (recovery vs. baseline)
SpO_2 (%)	97.4 ± 0.3	99.6 ± 0.2	-	97.8 ± 0.3	-
PR (bpm)	75.0 ± 2.9	70.7 ± 2.4	0.011	74.5 ± 2.7	0.763
BP_s (mm Hg)	107.4 ± 3.7	107.4 ± 3.7	0.934	108.6 ± 3.4	0.529
BP_d (mm Hg)	64.0 ± 2.2	65.0 ± 1.9	0.302	66.4 ± 2.0	0.152
BP_m (mm Hg)	78.5 ± 2.5	79.1 ± 2.2	0.377	80.1 ± 2.3	0.352

Table 3.1: Systemic haemodynamics obtained throughout visit 2. Data are presented as mean ± SE. t-tests were not performed on SpO_2 data as it was not found to be normally distributed.

Parameter (n = 18)	Baseline	Hyperoxia	p-value (hyperoxia vs. baseline)
SpO_2 (%)	97.8 ± 0.3	99.8 ± 0.1	-
PR (bpm)	73.9 ± 2.4	70.7 ± 2.0	0.002
BP_s (mm Hg)	108.0 ± 3.5	107.6 ± 3.0	0.692
BP_d (mm Hg)	62.8 ± 1.2	66.1 ± 1.6	0.001
BP_m (mm Hg)	77.9 ± 1.7	79.9 ± 1.8	0.010

Table 3.2: Systemic haemodynamics obtained throughout visit 3. Data are presented as mean ± SE. t-tests were not performed on SpO_2 data as it was not found to be normally distributed.

3.3.2 Reaction and Recovery Time of Arterioles Under Hyperoxic Provocation

The time course of the response of an arteriole diameter of a single, typical participant to hyperoxic provocation as a function of time is shown in Figure 3.4. The vertical lines in the plot represent the points at which oxygen breathing started and stopped. It can be seen that vasoconstriction occured during the first five minutes of oxygen breathing; thereafter the diameters remained stable for the remaining 15 minutes of oxygen breathing. Upon cessation of the hyperoxic phase, the arteriolar diameter began to increase back to baseline. It is apparent from the plot that the reaction of the arteriole diameter to the hyperoxic stimulus is faster than the recovery back to baseline. After approximately 15 minutes breathing room air, at the end of the oxygen breathing phase, the arteriole had returned to its prehyperoxia testing diameter.

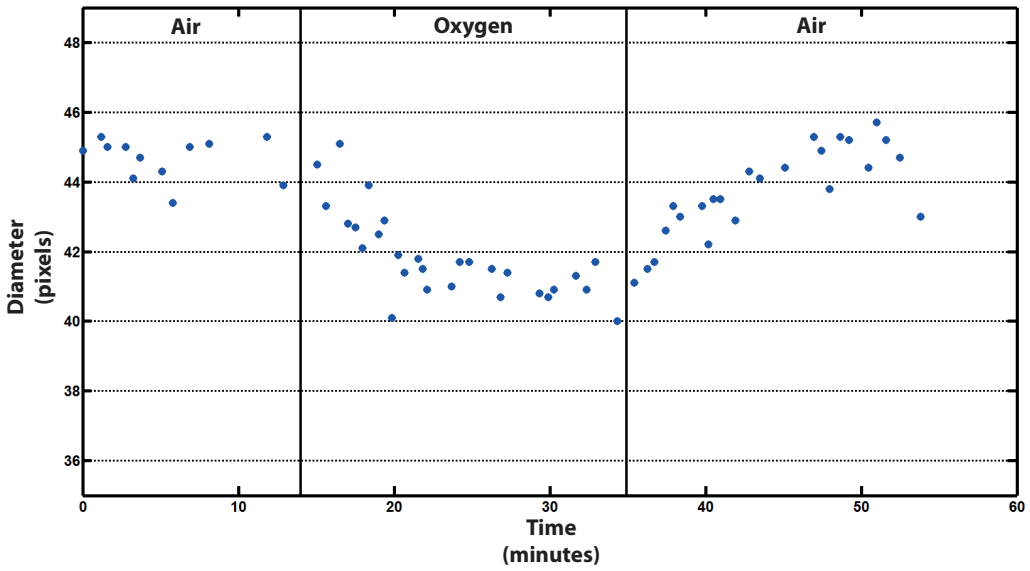

Figure 3.4: Change in the retinal arteriole diameter of a single, typical participant induced by hyperoxia as a function of time. Vertical lines represent the points at which oxygen breathing started and stopped. A pixel subtends approximately 2 μm. The arteriole diameter decreases during the first 5 minutes of oxygen breathing, plateaus, and remains stable for the rest of the oxygen breathing phase. The arteriole diameter increases during the air breathing, recovery phase and has returned to baseline after approximately 15 minutes.

The group mean retinal arteriole diameter was 39.6 $\pm$ 1.5 pixels at baseline. This decreased significantly to 36.5 $\pm$ 1.3 pixels during hyperoxic provocation (p = 0.001) and recovered to 39.1 $\pm$ 1.6 pixels during the recovery phase of room-air breathing. The group mean percentage change in arteriolar diameter during hyperoxic provocation was -9.7 $\pm$ 1.0%.

3.3.3 Regional Differences in Retinal Vascular Reactivity

Figure 3.5 presents a comparison of the group mean, baseline arteriolar diameters in the superior temporal (ST), inferior temporal (IT), superior nasal (SN) and inferior nasal (IN) retinal quadrants. Table 3.3 details the group-averaged arteriole diameter values across quadrants and hemiretina (i.e. temporal, nasal, superior, inferior). It is apparent that the temporal arterioles are larger than the nasal arterioles (p = 0.008), while superior arterioles do not differ from inferior arterioles (p = 0.725). It is also evident that significant vasoconstriction occured in all retinal regions.

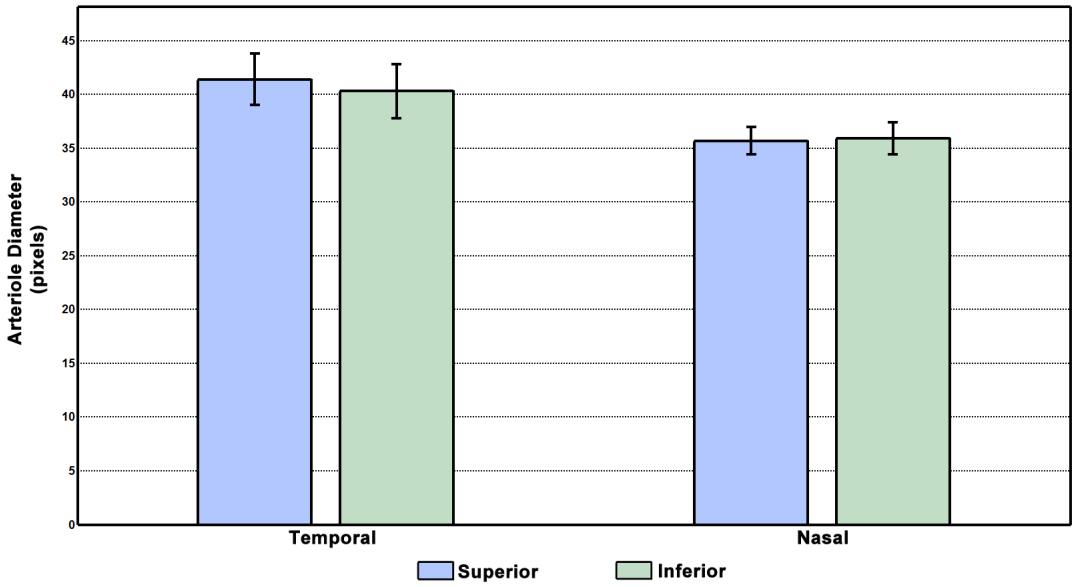

Figure 3.5: Baseline, group mean arteriolar diameters in the retinal quadrants. A pixel subtends approximately 2 μm. Data are presented as mean $\pm$ SE.

Retinal Region	Baseline Diameter (pixels)	Hyperoxic Diameter (pixels)	p-value (hyperoxic vs. baseline)
ST (n = 14)	41.4 $\pm$ 2.4	37.5 $\pm$ 2.3	0.000
IT (n = 16)	40.3 $\pm$ 2.5	36.6 $\pm$ 2.1	0.000
SN (n = 16)	34.9 $\pm$ 1.3	31.0 $\pm$ 1.1	0.000
IN (n = 16)	36.8 $\pm$ 1.4	32.8 $\pm$ 1.2	0.000
Temporal (n = 30)	40.9 $\pm$ 1.7	37.0 $\pm$ 1.5	0.000
Nasal (n = 32)	35.8 $\pm$ 0.9	31.9 $\pm$ 0.8	0.000
Superior (n = 30)	38.2 $\pm$ 1.4	34.0 $\pm$ 1.3	0.000
Inferior (n = 32)	38.3 $\pm$ 1.4	34.7 $\pm$ 1.2	0.000

Table 3.3: Comparing arteriole diameters across retinal regions, before and during hyperoxic provocation. Data are presented as mean $\pm$ SE.

Figure 3.6 presents a comparison of the group-averaged percentage change of the arteriole diameters, relative to baseline, across the retinal quadrants during hyperoxia. Table 3.4 details the percentage change in diameter obtained for each retinal region. The data indicates that systemic hyperoxia induced a group-averaged arteriole constriction of -9.2 $\pm$ 0.9% (ST), -9.0 $\pm$ 0.9% (IT), -11.0 $\pm$ 1.2% (SN) and -10.6 $\pm$ 0.9% (IN). The degree of constriction did not vary across the quadrants (p = 0.372, ANOVA). A comparison of the magnitude of arteriolar constriction in the hemiretinal regions, i.e.

temporal versus nasal and superior versus inferior, revealed that the arterioles in the temporal retina appeared to constrict slightly less than those nasally, but this was not significant (p = 0.080), and the arterioles in the superior retina responded to the same degree as the those in the inferior retina (p = 0.725).

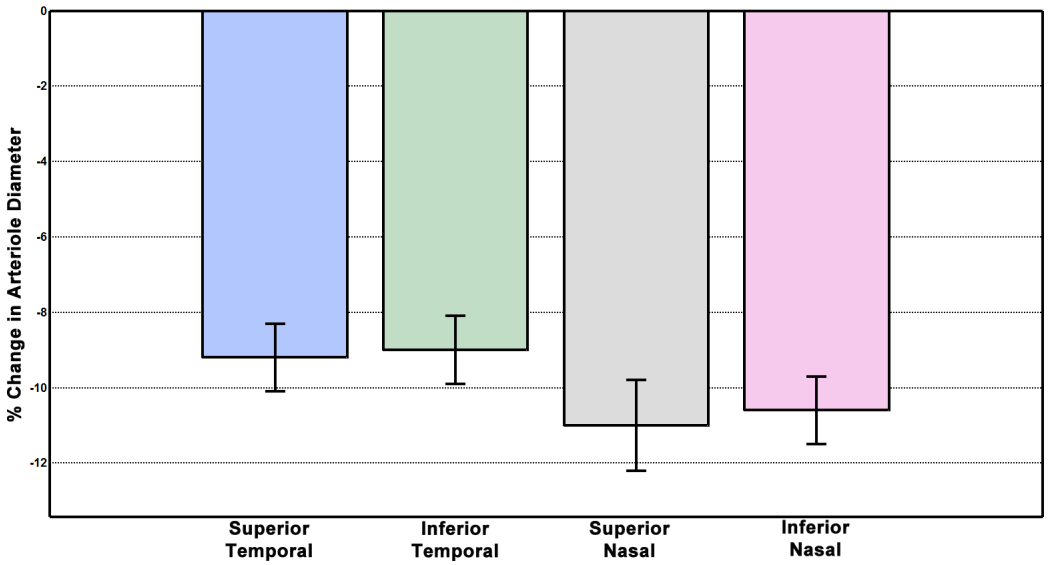

Figure 3.6: Comparing the percentage change in arteriolar diameter from baseline, across retinal quadrants. Data are presented as mean ± SE.

Retinal Region	% Difference
ST (n = 14)	-9.2 ± 0.9
IT (n = 16)	-9.0 ± 0.9
SN (n = 16)	-11.0 ± 1.2
IN (n = 16)	-10.6 ± 0.9
Temporal (n = 30)	-9.1 ± 0.6
Nasal (n = 32)	-10.8 ± 0.7
Superior (n = 30)	-10.1 ± 0.8
Inferior (n = 32)	-9.8 ± 0.6

Table 3.4: Comparing the percentage difference of arteriole diameters due to hyperoxia, compared to baseline, across retinal regions. Data are presented as mean ± SE.

3.3.4 Comparison of Vascular Reactivity in Arterioles of Different Size

The group mean baseline diameter for the narrow arteriolar measurement site was 19.2 $\pm$ 0.8 pixels (n = 18), and for the wide measurement site it was 36.1 $\pm$ 0.7 pixels (n = 22).

The group mean diameter constriction of the small arterioles was -1.9 $\pm$ 0.2 pixels and for the large arterioles it was -3.4 $\pm$ 0.2 pixels. There was a significant difference in the absolute change in diameter between large and small arterioles (p = 0.000).

The group-averaged percentage change in diameter of the small arterioles was -9.8 $\pm$ 0.8% and for large arterioles it was -9.2 $\pm$ 0.6%. There was no difference in the percentage constriction between the large and small vessels (p = 0.538). Figure 3.7 presents a comparison of the group-averaged percentage change of the large and small arterioles due to oxygen breathing. Figure 3.8 shows how the arteriole diameters of a large and small vessel change as a function of time, due to a hyperoxic provocation. From this it can be seen that the large and small vessels react and recovery similarly.

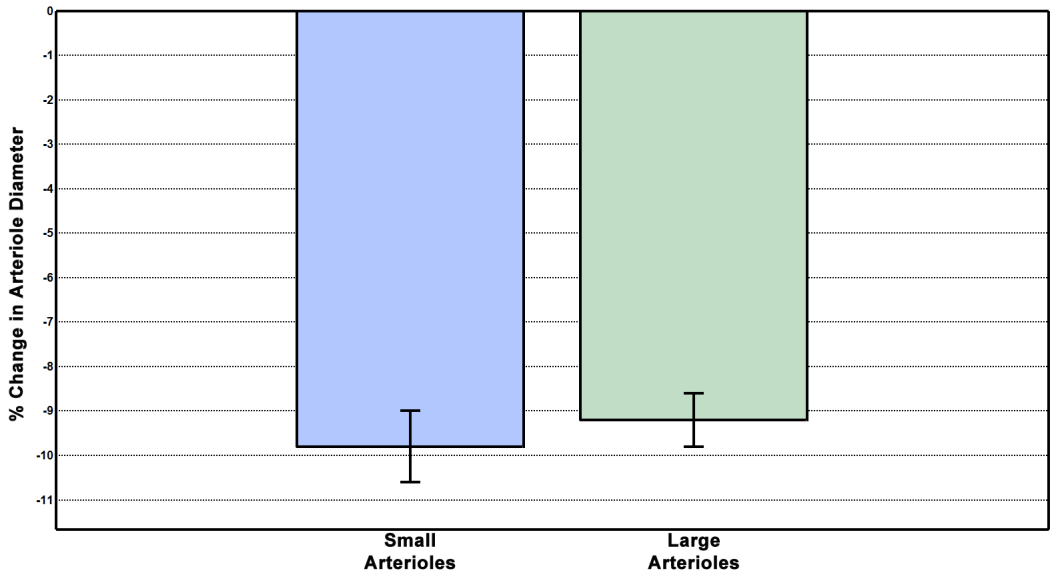

Figure 3.7: Comparison of the percentage change in arteriole diameter between large and small arterioles in response to hyperoxia. Data are presented as mean $\pm$ SE.

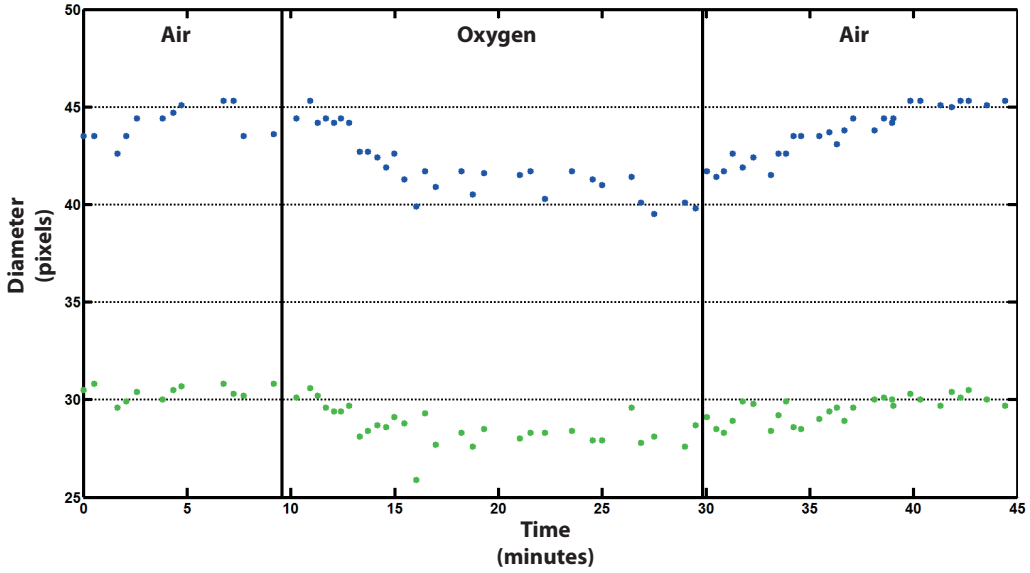

Figure 3.8: Change in diameter of a large and small arteriole, from a single participant, as a function of time.

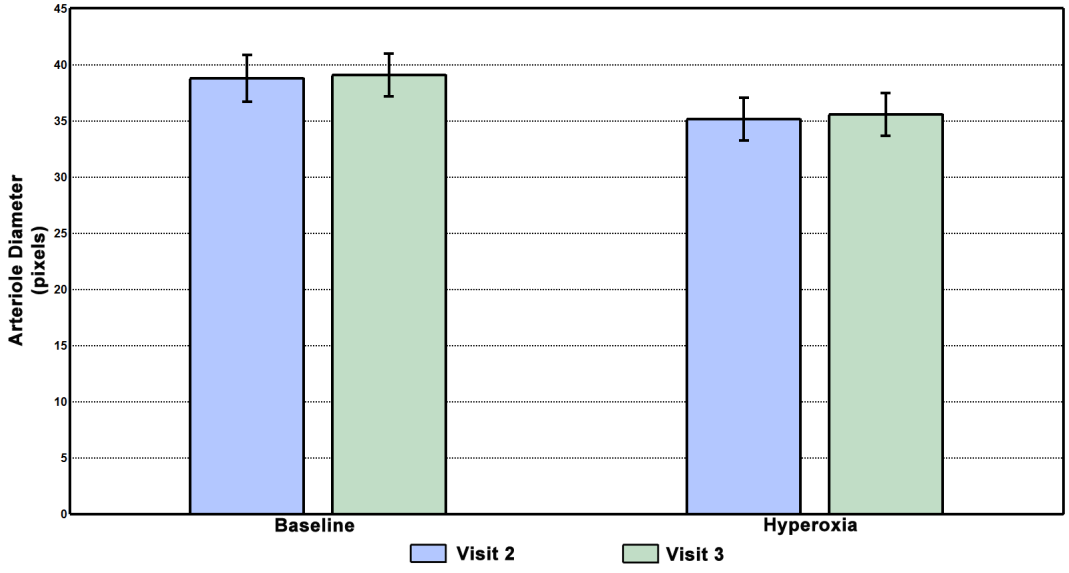

Figure 3.9: Comparing baseline and hyperoxic arteriole diameters, obtained during different visits. Data are presented as mean $\pm$ SE.

3.3.5 Reliability

The arteriole imaged during visit 2, to study the reaction and recovery time, was also chosen as one of the four vessels imaged in visit 3, to study regional differences in

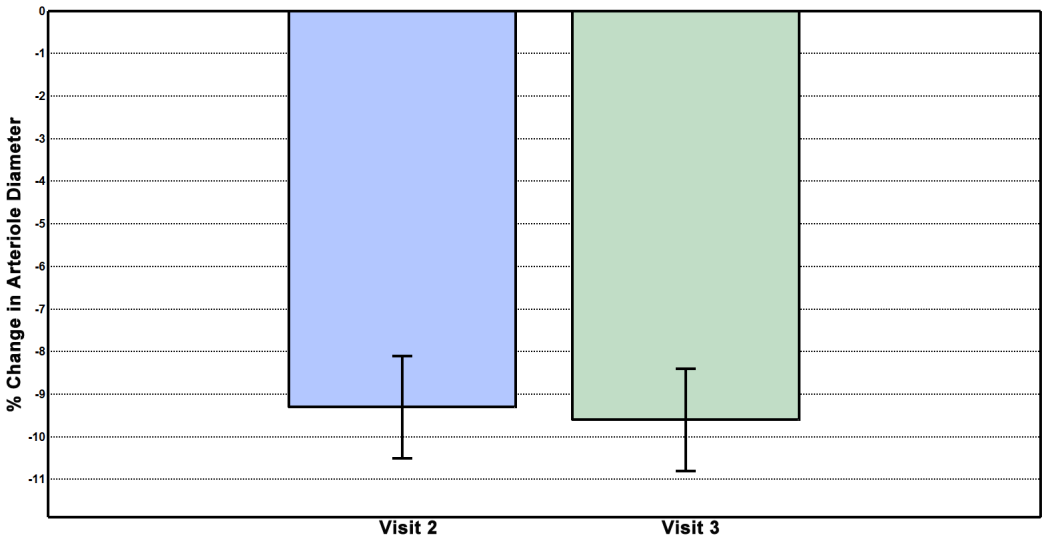

Figure 3.10: Comparison of the magnitude of reactivity observed during the two visits. Data are presented as mean ± SE.

reactivity. To assess the reliability of our measurements we are comparing the values obtained for these arterioles during the two visits.

Figure 3.9 compares the group mean arteriole diameters obtained for the baseline and oxygen breathing phases of the two visits. The data indicates that the group mean baseline diameter of the arterioles in visit 2 was 38.1 ± 2.1 pixels and in visit 3 it was found to be 39.1 ± 1.9 pixels. There was no difference in the baseline diameters between visits (p = 0.907). During the hyperoxic phase of visit 2, the arterioles decreased to 35.2 ± 1.9 pixels, and in visit 3, they decreased to 35.6 ± 1.9 pixels. There was no difference, between the two visits, in the hyperoxic diameters measured (p = 0.888).

Figure 3.10 compares the percentage constriction attained by the arterioles in each visit. The group-averaged constriction reached in visit 2 was -9.3 ± 1.2% and in visit 3 it was found to be -9.6 ± 1.2%. There was no difference in the magnitude of vasoconstriction between the visits (p = 0.871). While the mean difference in the percentage change of diameter between visits was 0.3 ± 0.8% (mean ± SE).

3.4 Discussion

3.4.1 Systemic Haemodynamics

The increased level of SpO_2 during the oxygen breathing phase suggests that systemic hyperoxia was achieved.

Although a small decrease in pulse rate (PR) due to hyperoxia has been previously reported by other investigators [22, 53, 78, 96], consistent with our results, it is not the prevalent finding. The majority of previous studies reported no change in PR during hyperoxic provocation [21, 46, 51, 52, 75, 77, 93]. However, we obtained visit-averaged percentage changes in arteriolar diameter of -9.7 $\pm$ 1.0% and -10.0 $\pm$ 0.5% for visits 2 and 3 respectively, very much in line with previously reported results (which are quoted in Section 3.4.2). Gilmore et al. [22] (the only investigator to observe a decrease in PR to also measure arteriole diameter) also obtained a constriction of -10.6%, consistent with those obtained by other investigators. Therefore, it is believed that this small decrease had little effect on our outcome measure.

BP_m and BP_d were found not to vary throughout visit 3, and BP_s did not alter during any phase of either visit. These observations are consistent with previous studies that observed no alteration in blood pressure due to oxygen breathing [12, 21, 22, 25, 46, 52, 53, 75–78, 93, 96]. However, a small increase in BP_m, resulting from a small increase in BP_d, due to hyperoxia was observed in visit 3. As shown in Section 3.3.5 the arteriolar response, to the same hyperoxic provocation, was found not to differ between the 2 visits. It is therefore concluded that the small increase in BP_m observed in visit 3 did not effect the magnitude of reactivity measured.

In addition, Jeppesen et al. [43], Dumskyj et al. [23] and Robinson et al. [44] investigated the degree of vasoconstriction attained by retinal arterioles due to an increase in perfusion pressure (PP), caused by an elevation of BP_m induced by isometric exercise. They observed increases in BP_m of 21.8 mm Hg [43], 16.7 mm Hg [23] and 33.4 mm Hg [44], along with increased heart rate [44], causing increases in PP of 31.3%, 32.7% and 55%. IOP is unaltered by isometric exercise [23, 24]. This elevation of PP caused mean percentage constrictions of just 2.5%, 3.4% and 0.2% respectively. Considering that large increases in PP induced such small constrictions, it is safe to conclude that the small changes in PR and BP_m observed in our study, which would barely alter PP, contributed little or nothing to the vasoconstriction observed in our study. (See Section 1.3, page 8, for description of the relationship between BP_m, IOP and PP).

3.4.2 Reaction and Recovery Time of Arterioles Under Hyperoxia Provocation

Our results indicate that vasoconstriction occurs during the first 5 minutes in reponse to hyperoxia, after which time the arterioles are maximally constricted and remain stable for the remainder of the oxygen breathing phase. The rate of vasoconstriction was found to be greater than the rate of recovery. Arteriole diameters had recovered to their prehyperoxia, baseline values after approximately 15 minutes of breathing room air in the recovery phase. Our results are in line with previously published data [21, 46, 51, 52, 54]. As vasoconstriction was complete 5 minutes after oxygen breathing commenced, this was set as the standard time subjects breathed oxygen before measurements for the hyperoxic phase commenced, for all subsequent experiments.

The group mean percentage change in arteriolar diameter during hyperoxic provocation was -9.7 $\pm$ 1.0%. This result compares well with those in other studies that used 100% oxygen to investigate retinal arteriolar reactivity. In these studies, investigators recorded reductions of arteriole diameter of -7.8% [25], -9.2% [21], -12.1% [46], -15.0% [52], -9.0% [97], -12.0% [51], -11.5% [76], and -8.7% [98].

3.4.3 Regional Differences in Retinal Vascular Reactivity

Previously published data have consistently reported that blood flow [92,99,100], velocity [92] and vessel diameter [21, 92] are greater in the temporal retina versus the nasal retina. These parameters, however, do not differ when comparing the superior retina to the inferior retina [21, 76, 99, 100]. Only Chung et al. [96], who measured blood flow using a confocal scanning laser Doppler flowmeter (cSLDF), found that blood flow in the inferior retina was greater than that in the superior retina. Our results indicate that temporal arteriolar diameters are larger than those in the nasal retina; while they do not differ between the superior and inferior retina. As described in Section 1.3, page 8, blood flow is a function of r^4, where r denotes the vessel radius. Therefore, we can conclude that our results are in direct agreement with [21, 92], and although we did not measure blood flow, we can also conclude that our results are in agreement with the studies that asessed blood flow [92, 99, 100]. It has been hypothesised that blood flow is greater to the temporal hemiretina as it is 20-25% larger than the nasal hemiretina [13, 92] and it contains the highly metabolic macula.

To our knowledge only a handful of studies have investigated whether regional varia-

tions in the degree of reactivity exist [21,51,76,92,96]; only two of these made measurements in all retinal quadrants [21, 51]; and the results of these studies have not been entirely decisive. Jean-Louis et al. [21] and Kiss et al. [51], both used a retinal vessel analyser (RVA) to study the arteriolar response to a hyperoxic stimulus. Jean-Louis et al. found that vasoconstriction was uniform across all quadrants (% constriction: superior temporal = 8.7%, superior nasal = 9.0%, inferior temporal = 8.9%, inferior nasal = 10.0%), while Kiss et al. reported a more pronounced response from the temporal than the nasal arterioles (% decrease in arterioles: temporal = 13 $\pm$ 2%; nasal = 11 $\pm$ 2%). Rassam et al. [92], measured the arteriolar diameter and blood flow velocity responses to hyperoxia using a Zeiss fundus camera and a bidirectional laser Doppler system. They found no difference in the reduction of arteriolar diameter (% decrease: temporal = 10.4 $\pm$ 1.2%, nasal = 7.7 $\pm$ 1.5%), velocity (% decrease: temporal = 27.1 $\pm$ 3.9%, nasal = 27.4 $\pm$ 5.5%) and volumetric blood flow (% decrease: temporal = 41.2 $\pm$ 3.6%, nasal = 38.0 $\pm$ 5.1%) between the temporal and nasal regions . Sehi et al. [76], used a Canon Laser Blood Flowmeter (CLBF) to compare the percentage decrease in diameter, velocity and blood flow between the superior and inferior temporal regions and found no difference between the regions (Change in arteriolar diameter: superior temporal (ST) = -13.0 $\pm$ 3.7 μm, inferior temporal (IT) = -12.6 $\pm$ 8.0 μm. Change in velocity: ST = -9.5 $\pm$ 6.2 mm/s, IT = -10.5 $\pm$ 4.3 mm/s. Change in flow: ST = -4.1 $\pm$ 2.1 μL/min, IT = -4.9 $\pm$ 2.1 μL/min). Meanwhile, Chung et al. [96], using a cSLDF system, reported that the inferior temporal quadrant was more responsive to vasoconstriction induced by hyperoxia than the superior temporal quadrant (mean flow in arbitrary units (au): Inferior - baseline = 386 $\pm$ 83 au, hyperoxia = 332 $\pm$ 40 au; Superior - baseline = 350 $\pm$ 55 au, hyperoxia = 361 $\pm$132 au) but less responsive to dilation induced by hypercapnia (mean flow in arbitrary units (au): Inferior - baseline = 361 $\pm$ 85 au, hypercapnia = 391 $\pm$ 109 au; Superior - baseline = 330 $\pm$ 69 au, hypercapnia = 400 $\pm$ 108 au). Our results indicated that there was no difference in the percentage change across all the quadrants. Also when comparing the hemiretinal areas (i.e. temporal versus nasal and superior versus inferior), no significant difference in vasoconstriction was found. Our results are in keeping with the majority of the small number of studies in this area [21, 76, 92]. Therefore, while it has been postulated that a differential autoregulatory response may exist between the temporal and nasal regions, the results lead us to conclude that the reactivity response is independent of retinal region.

3.4.4 Comparison of Vascular Reactivity in Arterioles of Different Size

It is known that smaller (resistance) arteries demonstrate a much greater ability to modulate diameter, in order to regulate blood flow in response to a change in blood pressure or an alteration of the metabolic needs of a tissue, than large (conducting) arteries [5,9,101]. Some studies have obtained results which suggest that even within the small range of vessel diameters present in the retina, a dependency exists between the magnitude of reactivity of a vessel and its initial calibre. Kiss et al. [51], studied the retinal arteriolar response to hyperoxia using an RVA system. The size of arterioles they studied ranged from approx. 90 μm to approx. 160 μm. They observed an inverse relationship between the arteriole diameter and the percentage constriction reached. Jeppesen et al. [43] also used an RVA system to study arteriolar diameters in the range 104.8 $\pm$ 6.4 au to 132.1 $\pm$ 7.1 au (arbitrary units) and found a smaller percentage diameter response to isometric exercise in larger arterioles.

Our study found that the change in diameter was greater for large than for small arterioles, while the percentage difference from baseline was the same between vessels of different calibre. Tayyari et al. [7,12] investigated the total vascular reactivity capacity (decrease in blood flow due to hyperoxia and increase in blood flow due to hypercapnia) in large (group mean baseline diameter = 116.7 $\pm$ 12.7 μm) and narrow arterioles (group mean baseline diameter = 92.4 $\pm$ 13.6 μm) using a CLBF system. They also found that the absolute change in flow was greater for the large (Δ flow = 6.6 $\pm$ 3.5 μL/min) than the small arterioles (Δ flow = 3.0 $\pm$ 0.9 μL/min), but that the percentage change did not differ between the measurement sites (% change: large arterioles = 61%; small arterioles = 67%). A number of other studies also found that the percentage change in vessel diameter from baseline due to a stimulus was not dependent on vessel size [41,45,48,49].

At the level of the retina, all arteries have an arteriolar structure [13], so it is of little surprise that our observations are in line with the majority of retinal studies comparing the magnitude of reactivity between large and small vessels. We therefore conclude that the magnitude of the percentage change in retinal arterioles is independent of baseline arteriole diameter.

3.4.5 Reliability

The baseline and hyperoxic diameters and the percentage constriction obtained for the arterioles were found not to differ between visits. Also, the mean difference in

the percentage change of diameters between visits was $0.3 \pm 0.8\%$ (mean $\pm$ SE). This suggests that the method has a high reproducibility.

3.4.6 Conclusions

From our results we can conclude that the vasoconstriction observed in our study is due to metabolic regulation. The retinal arterioles constrict during the first five minutes of oxygen breathing, after which they are maximally constricted and diameters remain stable for the remaining oxygen breathing phase. The reaction of arteriole diameters to hyperoxia is faster than their recovery to baseline. Blood flow to the temporal retina is higher than to the nasal retina, while flow to the superior and inferior retinae does not differ. A differential reactivity response across the retinal regions does not exist. The percentage change in diameter of retinal arterioles is the same irrespective of calibre. Therefore, as the degree of vasoconstriction was independent of retinal region and vessel size, a reactivity measurement taken from a single, arbitrary site can be considered as representative of the reactivity response of the retinal vasculature as a whole.

Chapter 4

Effect of Cigarette Smoking on Reactivity in Young, Healthy Subjects

4.1 Introduction

Tobacco smoke is composed of more than 4,000 chemicals, more than 250 of which are known to be toxic and more than 50 are carcinogenic [102, 103]. They include nicotine, carbon monoxide, tars, hydrogen cyanide, formaldehyde, carbon dioxide, aluminium, lead, mercury and cadmium [103, 104]. Cigarette smoking is a major preventable cause of morbidity and mortality, killing almost 6 million people annually, a number which is estimated to rise to over 8 million by 2030 as tobacco consumption is increasing globally [102]. Smoking is a major independent risk factor for cardiovascular disease, including atheroma, myocardial infarction, sudden cardiac death and stroke [39, 105]. The effects of smoking on the circulation are based on various mechanisms. Cigarette smoking causes increased carbon monoxide levels in the blood, reducing haemoglobin's oxygen carrying capacity [61, 103, 106–108]. Nicotine stimulates the sympathetic nervous system leading to an increase of heart

rate and inducing vasoconstriction [4,61,103,109]. This raises blood pressure and has been shown to reduce coronary [4], cutaneous [110–112] and placental [113] blood flow. Normally functioning vascular endothelium protects against the development of atheroma, which is the most common cause of death and morbidity in the Western World [4]. Endothelial dysfunction is reported to be one of the earliest pathophysiological effects in the development of atheroma, preceding morphological changes in the vessel wall [39, 105]. In vitro and in vivo studies have demonstrated that cigarette smoking diminished endothelial-dependent reactivity in the cerebral [114], coronary [115], brachial [116–120] and digital [121] vasculature. The nature and progression of smoking induced endothelial dysfunction has not been fully elucidated, but oxidative stress and reduced nitric oxide availability are believed to be important mechanisms [4,39,105]. The effect of smoking on the ocular vasculature has not been established as the handful of studies performed produced an inconsistent picture. The following experiments were performed to determine the chronic and acute effects of cigarette smoking on retinal vascular endothelial function by assessing the response of retinal arterioles to hyperoxia.

4.2 Materials and Methods

4.2.1 Sample

Twelve (2 women and 10 men) otherwise healthy, smokers (mean age $\pm$ SD, 22.4 $\pm$ 5.1 years) volunteered to participate in this study. Each subject signed a written consent after the nature of the study and experiment protocol were explained in detail. All procedures conformed to the tenets of the Declaration of Helsinki and were reviewed and approved by the National University of Ireland Galway Ethics Committee. Exclusion criteria included ages less than 18 or greater than 40 years, unclear optic media, pregnant or breastfeeding women, any cardiovascular or respiratory disorders, taking medication with known effects on blood flow (e.g. muscle relaxants), taking any chronic medication. Smoking was identified by self-report. The average number of cigarettes smoked per day ranged from 3 to 20 (mean $\pm$ SD, 10.9 $\pm$ 6.3 cigarettes), and the duration of smoking varied from 1 to 20 years (mean $\pm$ SD, 6.1 $\pm$ 5.7 years).

4.2.2 Visits

Volunteers attended for three visits. The first visit was to determine eligibility, to familiarise the subjects with the measurement technique and to obtain some large field of view (FOV) images. One eye from each subject was selected and approximately nine 10° FOV (the largest FOV of the HRT classic) were obtained. These images were used to create a mosaic of the retina, as described in Section 3.2.2, page 60. The mosaic was used to define a suitable measurement site (relatively straight arteriole segment with good contrast to the background, in any retinal region) and to aid the investigator in navigating the retina at a small FOV during the second and third visits.

The magnitude of retinal vascular reactivity in response to the hyperoxic stimulus was measured during the second and third visits, with intervals of 1–16 days between these visits.

4.2.3 Experimental Protocol

Subjects were asked to abstain from alcohol, caffeine and cigarette smoking for 12 hours before the study visits. Subjects rested for at least 5 minutes before the start of each experiment to stabilise baseline cardiovascular and respiratory parameters. All testing was performed in a quiet laboratory, at normal room temperature and at sea level atmospheric pressure.

Visit 2 was performed to assess the long-term effect of smoking on the magnitude of constriction of arterioles in response to hyperoxia and visit 3 was to investigate the acute effect of smoking on the reactivity response. For visit 2, the experimental protocol was performed after a 12 hour abstinence from cigarette smoking. Volunteers also refrained from smoking for 12 hours before visit 3, however, they were asked to smoke a single cigarette just before the start of the experiment. The test protocol was otherwise identical for both visits. The test protocol was divided into three consecutive phases in which the subject breathed (1) room air for approximately 10 minutes, (2) 100% oxygen for approximately 15-20 minutes via a non-rebreather mask (the oxygen delivery system is detailed in Section 3.2.3, page 62), and (3) room air for approximately 15 minutes. These phases were considered baseline, oxygen breathing, and recovery phases respectively. 2° FOV image sequences of a suitable arteriolar segment were obtained every 30–60 seconds throughout these three phases.

Blood pressure was measured during visits 2 and 3. Three measurments were taken during each phase. Systolic (BP_s) and diastolic (BP_d) blood pressure were measured

on the upper arm by an automated oscillometric device (Omron M10-IT; Omron Healthcare Europe BV, Hoofddorp, The Netherlands). Mean brachial artery blood pressure, BP_m was calculated using Equation 3.1. Pulse rate (PR) and oxygen saturation (SpO_2) were also recorded during both visits. Three readings were taken during each phase from a finger pulse oximetric device (Ohmeda Biox 3700e; Datex-Ohmeda, Inc., Madison WI, USA). All measurements were made by the same investigator.

Image sequences were processed as described in Chapter 2, with arteriolar diameters being calculated in pixels as detailed in Section 2.5, page 48.

To assess the effect of smoking on the parameters measured, data is compared to the data obtained for non-smokers in Chapter 3. As there was no difference between any parameters obtained for non-smokers between visits 2 and 3, the non-smoker data was averaged across both visits.

As described in Section 1.3, page 8, a change in IOP causes a change in perfusion pressure. Previous studies have investigated the effect of cigarette smoking on IOP. IOP was measured before and after cigarette smoking and it was found to be unaltered due to acute smoking [63,64,122–124]. It was also established that there was no difference in IOP values when comparing smokers to non-smokers [47,95,123]. Also, as previously explained in Section 3.2.4, page 62, IOP does not change significantly during hyperoxia. Consequently, IOP was not recorded during our experiments.

4.2.4 Data Analysis

Statistical analysis was performed using Minitab® software package (Release 16; Minitab Inc., PA, USA). Each dataset was group-averaged across subjects as a function of phase (i.e. baseline, hyperoxia, recovery). The response of arteriole diameters to hyperoxia is expressed as a percentage change as compared to baseline. Datasets were assessed to determine if they were normally distributed using the Anderson-Darling test. To investigate the influence of oxygen breathing on parameters two-tailed paired t-tests were performed between baseline values and hyperoxic values. To compare the effect of hyperoxia between 2 different groups (e.g. smokers(no cigarette) versus non-smokers) a two-tailed independent samples t-test was used. A comparison of more than two groups (e.g. smokers(no cigarette) versus smokers(post cigarette) versus non-smokers) was performed using one-way analysis of variance (ANOVA). In data that revealed a significant ANOVA result, post hoc testing was undertaken using the Tukey honest significance difference test. All data is presented as mean $\pm$ standard

error (SE). The level of significance was set to $p < 0.05$.

4.3 Results

4.3.1 Systemic Haemodynamics

The group averaged values for each systemic variable for each phase of visit 2 (abstinence from smoking for 12 hours, $\text{smokers}_{[\text{no cig}]}$) are presented in Table 4.1, and the values obtained for each phase of visit 3 (cigarette smoked immediately before commencement of experiment, $\text{smokers}_{[\text{post cig}]}$) are presented in Table 4.2. Table 4.3 details the systemic parameters of the non-smokers averaged over both visits described in Chapter 3.

Parameter (n = 12)	Baseline	Hyperoxia	p-value (hyperoxia vs. baseline)	Recovery	p-value (recovery vs. baseline)
SpO_2 (%)	97.7 ± 0.3	99.6 ± 0.2	-	97.4 ± 0.4	-
PR (bpm)	72.5 ± 3.0	70.1 ± 2.1	0.252	70.3 ± 2.5	0.131
BP_s (mm Hg)	113.8 ± 3.7	109.7 ± 2.3	0.104	108.5 ± 2.3	0.013
BP_d (mm Hg)	69.9 ± 2.1	66.8 ± 1.3	0.043	68.5 ± 1.6	0.351
BP_m (mm Hg)	84.5 ± 2.5	81.1 ± 1.6	0.030	82.5 ± 1.6	0.267

Table 4.1: Systemic haemodynamics obtained throughout visit 2 (no cigarette). Data are presented as mean $\pm$ SE. t-tests were not performed on SpO_2 data as it was not found to be normally distributed.

The group-averaged SpO_2 of $\text{smokers}_{[\text{no cig}]}$ increased from a baseline of $97.7 \pm 0.3\%$ to $99.6 \pm 0.2\%$ during hyperoxia in visit 2. The baseline and response values for $\text{smokers}_{[\text{no cig}]}$ did not differ to the values obtained for $\text{smokers}_{[\text{post cig}]}$. During the recovery phase the SpO_2 values for $\text{smokers}_{[\text{no cig}]}$ and $\text{smokers}_{[\text{post cig}]}$ returned to their prehyperoxia values. The SpO_2 values obtained for smokers did not differ from those obtained for non-smokers in any phase of either visit, as can be seen in Figure 4.1.

A comparison of the group-averaged PR recorded at each phase for $\text{smokers}_{[\text{no cig}]}$, $\text{smokers}_{[\text{post cig}]}$ and non-smokers is presented in Figure 4.2. The baseline value observed for $\text{smokers}_{[\text{no cig}]}$ was 72.5 ± 3.0 bpm. This was found not to alter during the hyperoxic ($p = 0.252$) or recovery ($p = 0.131$) phases. The PR values obtained for $\text{smokers}_{[\text{no cig}]}$ were not different to those recorded for non-smokers at baseline

Parameter (n = 12)	Baseline	Hyperoxia	p-value (hyperoxia vs. baseline)	Recovery	p-value (recovery vs. baseline)
SpO_2 (%)	97.7 ± 0.5	99.5 ± 0.2	-	97.4 ± 0.5	-
PR (bpm)	86.3 ± 4.4	78.2 ± 3.3	0.001	79.9 ± 2.0	0.009
BP_s (mm Hg)	118.1 ± 2.0	112.6 ± 2.1	0.001	113.5 ± 2.6	0.016
BP_d (mm Hg)	70.5 ± 1.5	67.7 ± 1.2	0.016	67.8 ± 1.7	0.027
BP_m (mm Hg)	86.4 ± 1.5	82.7 ± 1.2	0.001	83.1 ± 1.8	0.003

Table 4.2: Systemic haemodynamics obtained throughout visit 3 (post cigarette). Data are presented as mean ± SE. t-tests were not performed on SpO_2 data as it was not found to be normally distributed.

Parameter	Baseline (n = 34)	Hyperoxia (n = 34)	p-value (hyperoxia vs. baseline)	Recovery (n = 16)	p-value (recovery vs. baseline)
SpO_2 (%)	97.6 ± 0.2	99.7 ± 0.1	-	97.8 ± 0.3	-
PR (bpm)	74.4 ± 1.8	70.7 ± 1.5	0.000	74.5 ± 2.7	0.763
BP_s (mm Hg)	107.8 ± 2.5	107.5 ± 2.3	0.694	108.6 ± 3.4	0.529
BP_d (mm Hg)	63.4 ± 1.2	65.6 ± 1.2	0.002	66.4 ± 2.0	0.152
BP_m (mm Hg)	78.2 ± 1.4	79.5 ± 1.4	0.009	80.1 ± 2.3	0.352

Table 4.3: Systemic haemodynamics obtained for non-smokers, averaged over both visits described in Chapter 4. Data are presented as mean ± SE. t-tests were not performed on SpO_2 data as it was not found to be normally distributed.

(p = 0.588), hyperoxia (p = 0.848) or recovery (p = 0.289). In visit 3, the baseline PR recorded for $smokers_{[post\ cig]}$ was 86.3 bpm. This was significantly greater than the values obtained for $smokers_{[no\ cig]}$ (p = 0.017) and non-smokers (p = 0.005). PR $smokers_{[post\ cig]}$ decreased to 78.2 ± 3.3 bpm during oxygen breathing and remained at this level for the recovery phase. This reduction brought PR $smokers_{[post\ cig]}$ close to the values obtained for $smokers_{[no\ cig]}$ and non-smokers. However, PR $smokers_{[post\ cig]}$ remained significantly higher than the PR value obtained for non-smokers during hyperoxia (p = 0.025) and for the value obtained for $smokers_{[no\ cig]}$ in the recovery phase (p = 0.023).

Figure 4.3 compares the BP_svalues obtained for $smokers_{[no\ cig]}$, $smokers_{[post\ cig]}$ and non-smokers at each phase. A baseline value of 113.8 ± 3.7 mm Hg was obtained for $smokers_{[no\ cig]}$. This value decreased slightly, but nonsignificantly, during the hyper-

oxic phase (p = 0.104). BP_s $smokers_{[no\ cig]}$ underwent a further small decrease during the recovery phase, making it significantly different to the baseline value (p = 0.013). BP_s values recorded for $smokers_{[no\ cig]}$ did not differ to the values found for non-smokers at baseline (p = 0.205), hyperoxic (p = 0.598) or recovery (p = 0.978) phases. BP_s of $smokers_{[post\ cig]}$ was found to be 118.1 $\pm$ 2.0 mm Hg at baseline. This decreased slightly, but significantly, during the oxygen breathing phase, and remained unaltered in the recovery phase (p = 0.785). The BP_s results of $smokers_{[post\ cig]}$ were not different to those obtained for $smokers_{[no\ cig]}$ at baseline (p = 0.321), hyperoxia (p = 0.350) or recovery (p = 0.161). A significant difference was found when comparing the BP_s value obtained for $smokers_{[post\ cig]}$ with that found for non-smokers at baseline (p = 0.023), but not for the hyperoxic (p = 0.219) or recovery phases (p = 0.296).

The baseline value of BP_d recorded for $smokers_{[no\ cig]}$ was 69.9 $\pm$ 2.1 mm Hg. A small but significant decrease was observed during hyperoxia, while the recovery value was not significantly different to the values obtained in the baseline or hyperoxic phases. There was no difference between the BP_d values obtained for $smokers_{[no\ cig]}$ and $smokers_{[post\ cig]}$ for any phase (baseline, p = 0.811; hyperoxia, p = 0.612, recovery, p = 0.768). The baseline values of BP_d for $smokers_{[no\ cig]}$ and $smokers_{[post\ cig]}$ were significantly greater than that obtained for non-smokers (p = 0.009, $smokers_{[no\ cig]}$; p = 0.002, $smokers_{[post\ cig]}$). The hyperoxic (p = 0.549) and recovery (p = 0.695) values did not differ between the three groups. A comparison of BP_d values obtained from $smokers_{[no\ cig]}$, $smokers_{[post\ cig]}$ and non-smokers is shown in Figure 4.4.

The group mean BP_m decreased slightly from a baseline of 84.5 $\pm$ 2.5 mm Hg to 81.1 $\pm$ 1.6 mm Hg during hyperoxia in $smokers_{[no\ cig]}$. The baseline value was significantly greater than the value obtained for non-smokers (p = 0.030), while it was the same as that observed for $smokers_{[post\ cig]}$ (p =0.539). The hyperoxic (p = 0.387) and recovery (p = 0.523) values did not differ between the three groups. Figure 4.5 compares the BP_m values obtained for each group at each phase of the experimental protocol.

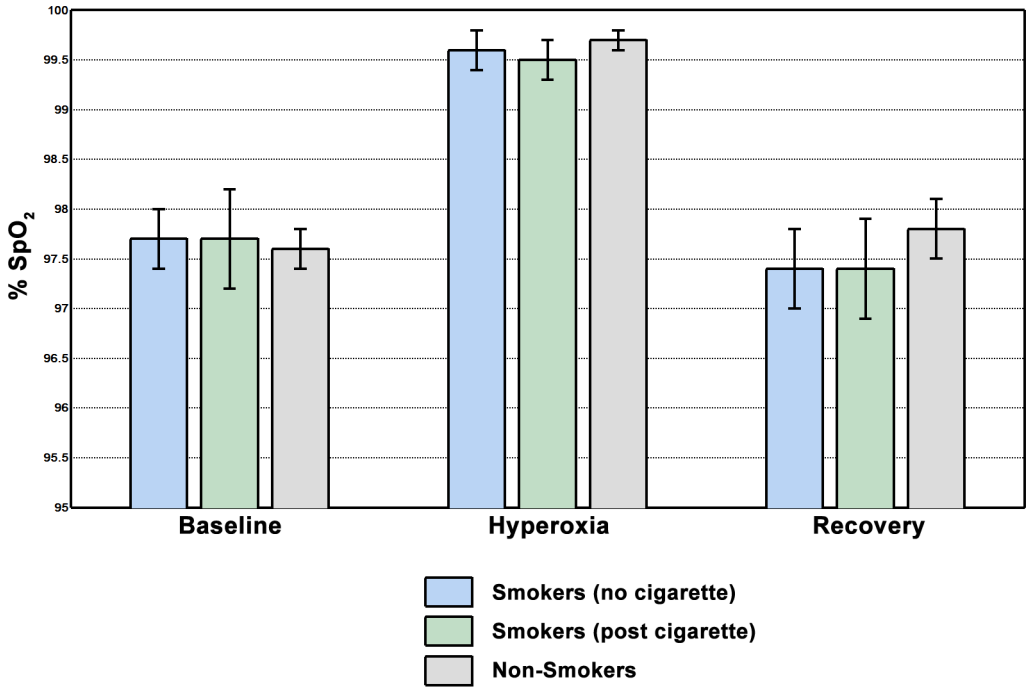

Figure 4.1: Comparison of SpO_2 results for $smokers_{[no\ cig]}$, $smokers_{[post\ cig]}$ and non-smokers. Data are presented as mean $\pm$ SE.

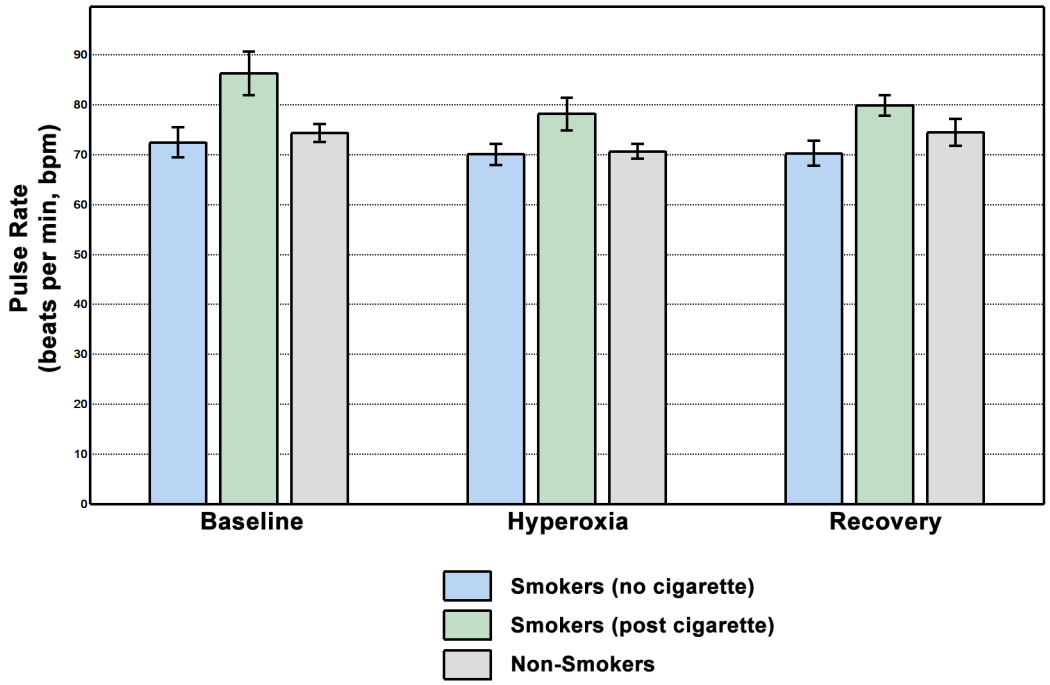

Figure 4.2: Comparison of PR results for $smokers_{[no\ cig]}$, $smokers_{[post\ cig]}$ and non-smokers. Data are presented as mean $\pm$ SE.

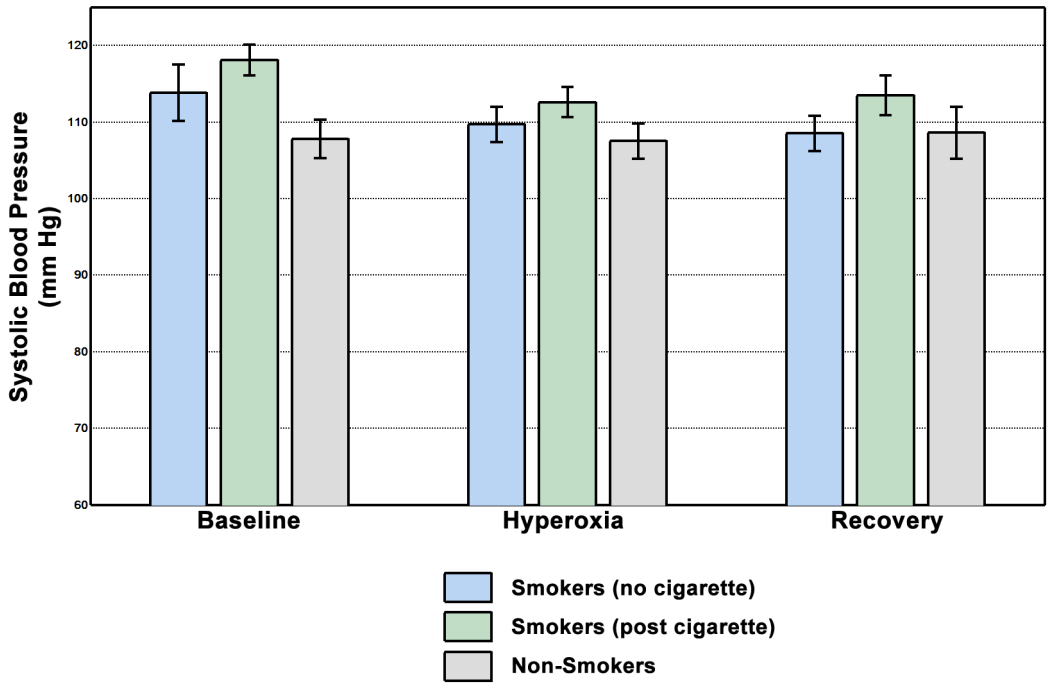

Figure 4.3: Comparison of BP_s results for $smokers_{[no\ cig]}$, $smokers_{[post\ cig]}$ and non-smokers. Data are presented as mean $\pm$ SE.

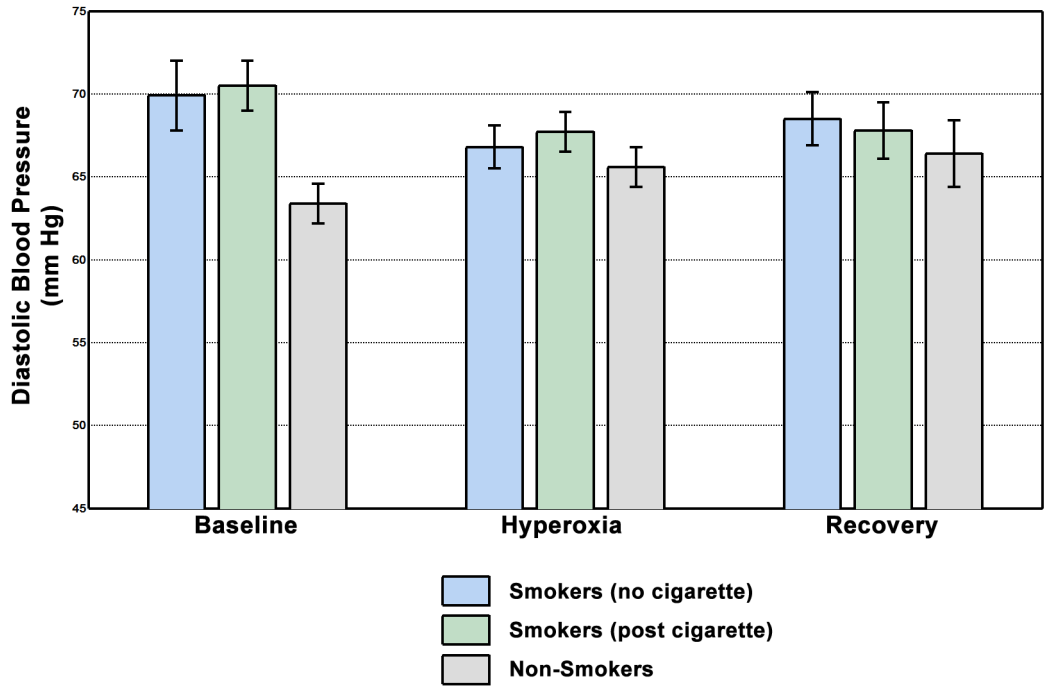

Figure 4.4: Comparison of BP_d results for $smokers_{[no\ cig]}$, $smokers_{[post\ cig]}$ and non-smokers. Data are presented as mean $\pm$ SE.

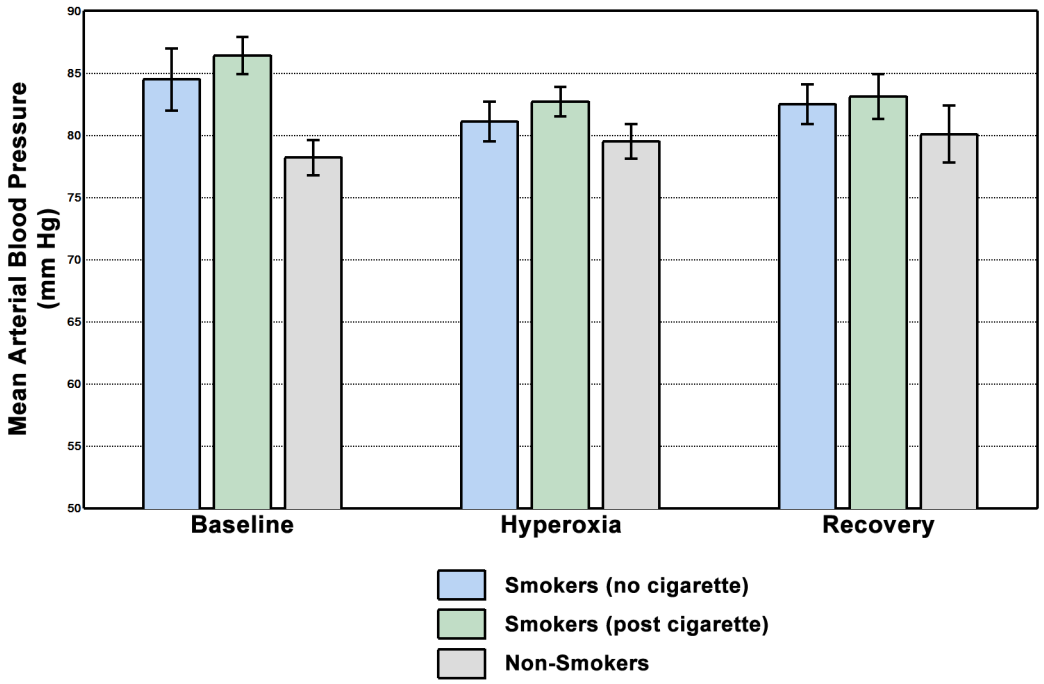

Figure 4.5: Comparison of BP_m results for $smokers_{[no\ cig]}$, $smokers_{[post\ cig]}$ and non-smokers. Data are presented as mean $\pm$ SE.

4.3.2 Vessel Diameter and Reactivity

Table 4.4 details the group-averaged arteriole diameter values across groups (i.e. $smokers_{[no\ cig]}$, $smokers_{[post\ cig]}$ and non-smokers). Figure 4.6 presents a comparison of the group mean, baseline arteriolar diameters in $smokers_{[no\ cig]}$, $smokers_{[post\ cig]}$ and non-smokers. It is evident from Figure 4.6 that the baseline diameters did not differ between $smokers_{[no\ cig]}$ and $smokers_{[post\ cig]}$. While the baseline, group mean arteriole diameters of the non-smoking group appear to be a little larger than those of the smoking group we did not find a significant difference between the groups ($p = 0.186$). It is also apparent, from the data in Table 4.4, that significant vasconstriction occured in all three groups.

Table 4.5 details the percentage change in diameter obtained for each group. Figure 4.7 presents a comparison of the group-averaged percentage change of the arteriole diameters, relative to baseline, attained by $smokers_{[no\ cig]}$, $smokers_{[post\ cig]}$ and non-smokers, during the hyperoxic phase. The data indicates that the degree of vasoconstriction achieved by the smokers was the same when measured after a 12 hour abstinence and immediately after smoking a cigarette ($p = 0.621$). The reactivity of

	Baseline Diameter (pixels)	Hyperoxic Diameter (pixels)	p-value (hyperoxia vs. baseline)	Recovery Diameter (pixels)	p-value (recovery vs. baseline)
$\text{Smokers}_{[\text{no cig}]}$ (n = 17)	35.3 ± 2.6	32.8 ± 2.5	0.000	35.5 ± 2.7	0.498
$\text{Smokers}_{[\text{post cig}]}$ (n = 17)	35.2 ± 2.6	32.8 ± 2.5	0.000	35.4 ± 2.7	0.328
Non-Smokers	38.5 ± 0.8 (n = 82)	34.8 ± 0.8 (n = 78)	0.001	39.1 ± 1.6 (n = 16)	0.766

Table 4.4: Comparing arteriole diameters for each experimental phase (i.e. baseline, hyperoxia and recovery) by smoking status. Data are presented as mean $\pm$ SE.

	% Difference
$\text{Smokers}_{[\text{no cig}]}$ (n = 17)	-7.5 ± 0.7
$\text{Smokers}_{[\text{post cig}]}$ (n = 17)	-7.0 ± 0.7
NonSmokers (n = 78)	-9.9 ± 0.4

Table 4.5: Comparing the percentage difference in arteriole diameters due to hyperoxia, compared to baseline, across smoking status. Data are presented as mean $\pm$ SE.

smokers was, however, significantly less than that of nonsmokers ($\text{smokers}_{[\text{no cig}]}$ versus non-smokers, p = 0.017; $\text{smokers}_{[\text{post cig}]}$ versus non-smokers, p = 0.004). In the recovery phase, the arteriolar diameters of each group returned to their prehyperoxic diameters.

The time course of the response of an arteriole diameter of a single, typical smoker to hyperoxic provocation as a function of time is portrayed in Figure 4.8. The blue dots represent the response of the arteriole diameter to hyperoxia after a 12 hour abstinence from smoking. The green dots describe the response of the diameter of the same arteriole segment to hyperoxia immediately after smoking a cigarette. The vertical lines in the plot mark the points at which oxygen breathing started and stopped. It is evident that smoking a cigarette had no effect on the response of the arteriole diameter to hyperoxia.

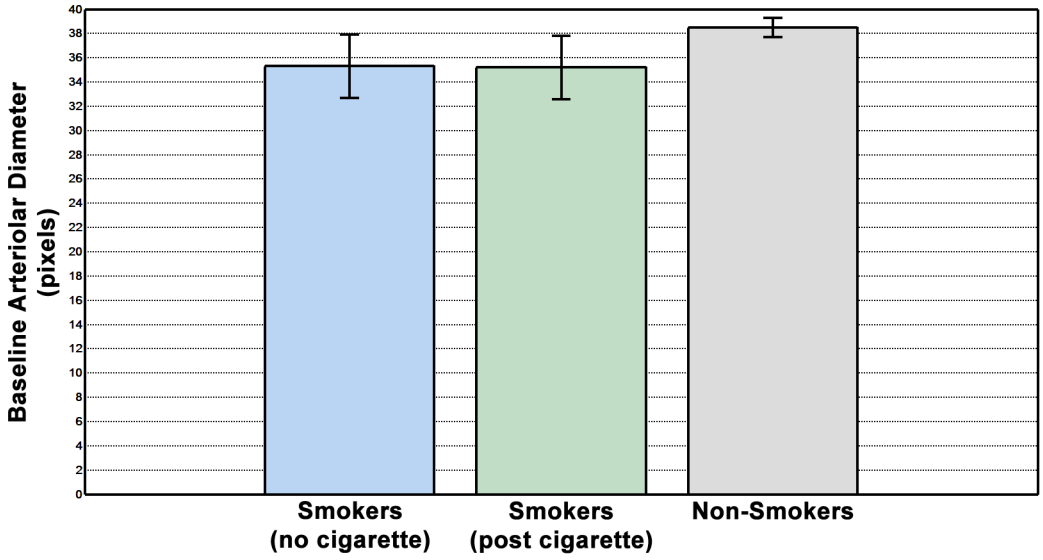

Figure 4.6: Baseline, group mean arteriolar diameters of smokers$_{[\text{no cig}]}$, smokers$_{[\text{post cig}]}$ and non-smokers. Data are presented as mean $\pm$ SE.

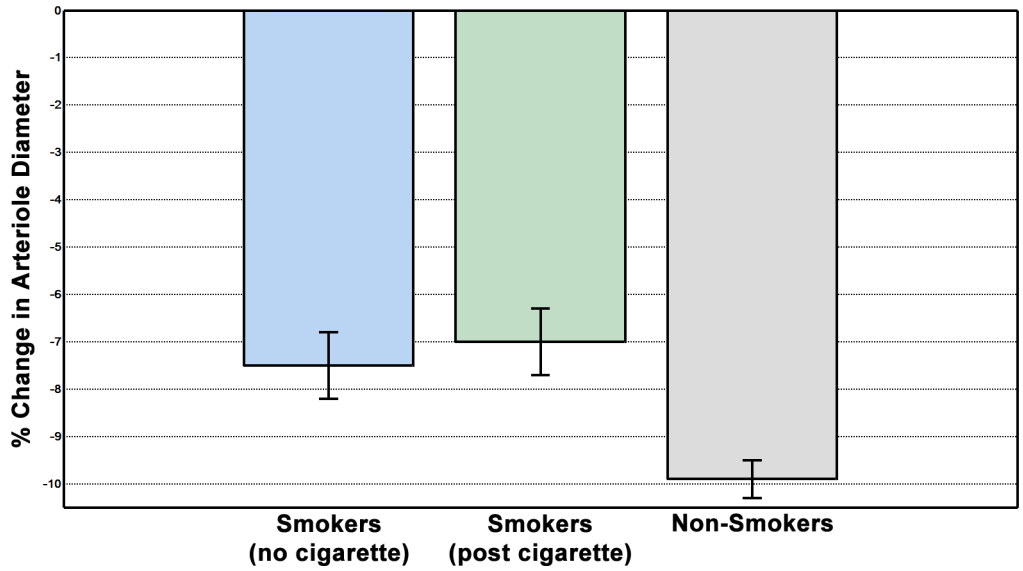

Figure 4.7: Comparing the percentage change in arteriolar diameter from baseline of smokers$_{[\text{no cig}]}$, smokers$_{[\text{post cig}]}$ and non-smokers. Data are presented as mean $\pm$ SE.

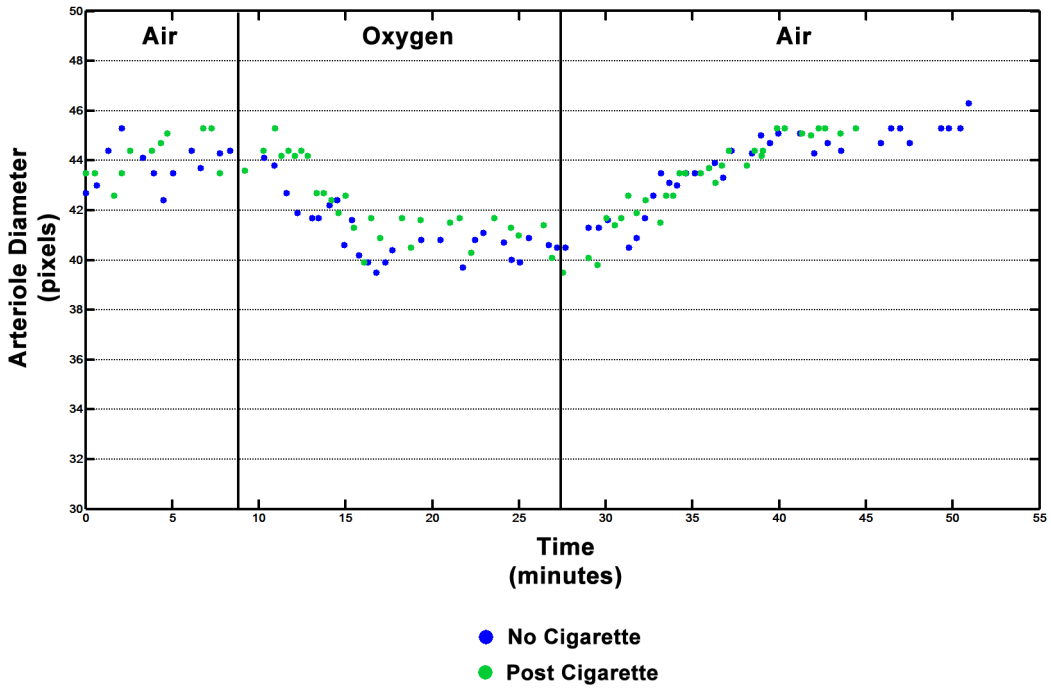

Figure 4.8: Change in the retinal arteriole diameter of a single, typical smoker, induced by hyperoxia as a function of time. The blue dots depict the response of the arteriole diameter to hyperoxia after a 12 hour abstinence from smoking. The green dots delineate the arteriolar diameter response immediately after smoking a cigarette. The vertical lines mark the points at which oxygen breathing started and stopped.

4.4 Discussion

4.4.1 Systemic Haemodynamics

SpO_2 values increased during hyperoxia and returned to their prehyperoxic values during the recovery phase. There was no difference in SpO_2 values between $\text{smokers}_{[\text{no cig}]}$, $\text{smokers}_{[\text{post cig}]}$ and non-smokers at any stage of the experiments. This suggests that systemic hyperoxia was achieved and that smoking had no effect. However, cigarettes contain 1–5% carbon monoxide [108] and haemoglobin has a much greater affinity for carbon monoxide than oxygen. Haemoglobin combined with carbon monoxide is carboxyhaemoglobin. Smokers have increased levels of carboxyhaemoglobin, ranging from 3–15% [108], compared to <1.5% in non-smokers [125]. This results in a reduction in haemoglobin's oxygen carrying capacity. Pulse oximeters cannot distinguish between oxyhaemoglobin and carboxyhaemoglobin, so smokers may have a normal oxygen saturation reading on a pulse oximeter. Wimpissinger et al. [60, 126] analysed blood samples taken from smokers and non-smokers at baseline and during hyperoxia and found no difference in oxygen saturation between the groups at either phase. The reason for this may be that the smoking groups had abstained from smoking for 12 hours before the study and it has been previously shown that even short-term smoking avoidance can reduce carboxyhaemoglobin levels to within the range of non-smokers [61, 127]. No previous studies investigating retinal vascular reactivity in smokers reported oxygen saturation levels before and after smoking a cigarette. However, Armitage et al. [128] measured carboxyhaemoglobin levels in blood samples taken from smokers after an overnight smoking abstinence and again after smoking a cigarette. They reported a two- to three-fold increase in carboxyhaemoglobin levels after smoking. A reduction in oxygen saturation would therefore be expected in $\text{smokers}_{[\text{post cig}]}$. However, systemic hyperoxia was still achieved in $\text{smokers}_{[\text{post cig}]}$ as arterioles constricted and the degree of vasoconstriction did not differ to that of $\text{smokers}_{[\text{no cig}]}$. While we cannot conclude much from our SpO_2 data, we may surmise from the results of previous studies that the oxygen saturation of $\text{smokers}_{[\text{no cig}]}$ did not differ to non-smokers while it is likely that it was reduced in $\text{smokers}_{[\text{post cig}]}$. If oxygen saturation was reduced in $\text{smokers}_{[\text{post cig}]}$ it was not sufficient to effect reactivity results as there was no difference between visit 2 and 3.

PR $\text{smokers}_{[\text{no cig}]}$ did not alter throughout the test protocol and values did not differ to those of non-smokers at any phase. Previous studies also found that the PR of $\text{smokers}_{[\text{no cig}]}$ did not differ to approximately age-matched non-smokers at base-

line [60, 61, 123, 126] and that it did not alter during oxygen breathing [60, 61, 126]. After smoking a cigarette the baseline PR of smokers was found to be elevated. This was significantly greater than the baseline values obtained for smokers$_{[\text{no cig}]}$ and non-smokers. This increase of PR suggest that substantial quantities of nicotine were absorbed [128, 129]. PR smokers$_{[\text{post cig}]}$ decreased significantly during oxygen breathing and remained stable for the rest of the protocol. This reduction brought the PR of smokers$_{[\text{post cig}]}$ close to the values obtained for smokers$_{[\text{no cig}]}$ and non-smokers. Previous investigators have also recorded an increase in PR of smokers after smoking a cigarette [63, 64, 106, 122, 124, 130]. It has been shown that nicotine levels start to decline immediately after the end of smoking or infusion and that as nicotine levels fall so does PR [128, 129]. It is unclear if this explains the drop in PR observed for the hyperoxic phase or if oxygen breathing contributed to the decrease in PR.

The values obtained for BP_m of smokers$_{[\text{no cig}]}$ and smokers$_{[\text{post cig}]}$ did not differ from each other during any phase. BP_m for smokers at baseline was significantly elevated compared to non-smokers. BP_m values of smokers decreased during oxygen breathing and were not different to that of non-smokers during the hyperoxic or recovery phases. The majority of previous studies have found no difference in the BP of smokers$_{[\text{no cig}]}$ and approximately age-matched non-smokers [47, 60, 95, 123, 126] and that hyperoxia had no effect on their BP [61, 126]. An elevated BP has previously been reported in smokers when measured directly after smoking a cigarette [106, 122, 124, 130] due to nicotine absorption. We can not easily explain the discrepancy between our results and those of previous investigators. The BP of smokers$_{[\text{no cig}]}$ and non-smokers were not expected to differ and an elevation of BP was predicted in smokers$_{[\text{post cig}]}$, as considerable amounts of nicotine were absorbed by the smokers, as evidenced by the increase in PR. One suggestion is that in visit 2, the smoking volunteers were somewhat agitated/stressed after a smoking abstinence of at least 12 hours and perhaps required longer than the 5 minutes resting period allocated to stabilise their BP. This slightly elevated BP may then have masked an elevation of BP in visit 3 due to systemic nicotine. Previous studies may not have encountered this problem as they cited much longer resting periods of 15–20 minutes [47, 60, 95, 123, 126].

The differences in PR and BP observed, between smokers and non-smokers and before and after smoking, in these experiments were small. As seen in studies which used isometric exercise to cause a vasoconstriction [23, 43, 44], very large changes in BP of 16.7 – 33.4 mm Hg elicited relatively small reactivity responses of 0.2 – 3.4%. In our study the largest intergroup difference in BP_m was 8.2 mm Hg (between smokers$_{[\text{post cig}]}$ and non-smokers) and the largest drop in BP_m within a group was

3.7 mm Hg (observed in smokers[post cig], going from baseline to hyperoxia). These small differences would have had little or no contribution to the magnitude of vasoconstriction measured.

4.4.2 Vessel Diameter and Reactivity

The bulk of previous studies have found that retinal vessel diameter, blood flow velocity and blood flow of the retina, optic nerve head (ONH) and choroid did not differ between smokers$_{[\text{no cig}]}$ and non-smokers at baseline [47, 60, 61, 95, 123, 126]. Only Wimpissinger et al. [60] found a difference between the groups when measuring choroidal flow with a laser Doppler flowmeter (LDF). They recorded higher blood flow in smokers compared to non-smokers. These findings are in agreement with our results, which suggest that the baseline arteriolar diameters of smokers$_{[\text{no cig}]}$ were the same as those of non-smokers. Studies which measured blood flow velocity in the extraocular vessels (e.g. the ophthalmic artery) using colour Doppler imagers, found blood flow velocities to be diminished in smokers when compared to non-smokers [131, 132]. These investigators do not mention smoking abstinence periods before their experiments, so this attenuation in flow is likely to be due to the effect of nicotine on the sympathetic nervous system causing vasoconstriction. In contrast to these results, however, Kaiser et al. [107] reported enhanced flow velocities in the extraocular vessels of smokers. Investigators studying the effects of smoking on the brachial artery using ultrasonography also found no difference in the vessel size or blood flow when comparing smokers to non-smokers [116–118]. While we are somewhat hesitant to draw conclusions from an intergroup comparison of diameter, as our results are in line with previous findings in the eye as well as the brachial artery, we believe it is very likely that baseline diameters of smokers$_{[\text{no cig}]}$ and non-smokers do not differ.

The results on the acute effects of cigarette smoking on blood flow in the retina have been more controversial. In keeping with our results, which found that arteriolar diameter was unchanged after smoking, Cubbidge et al. [122] observed that acute smoking had no effect on arteriolar or venular diameter using a retinal vessel analyser (RVA). Tamaki et al. [64], using the laser speckle method, discerned no difference in normalised blur (NB) (NB is the term used to describe the measure of tissue blood velocity obtained by the laser speckle method, as described in Section 1.6.4, page 21) measured in the optic nerve head (NB_{ONH}) and found a decrease in NB measured in the choroid-retina ($NB_{ch\text{-}ret}$) (the choroid-retina measurement is obtained halfway

between the macula and ONH in an area with no visible vessels). While the lower $NB_{ch\text{-}ret}$ measured after smoking may appear to be in opposition to our results, it is not. The choroid contributes to $NB_{ch\text{-}ret}$ measurements, and as the choroid is innervated, unlike the retina, it is likely that a decrease in choroidal flow occured, due to the increase in systemic nicotine levels after cigarette smoking, leading to sympathetic activation and vasoconstriction. In contrast to these results, Tamaki et al. [63], in another study also using the laser speckle method, detected enhanced NB_{ONH} and $NB_{ch\text{-}ret}$ after smoking. Robinson et al. [106], using the blue field entoptic phenomenon, also found an increase in macular flow in response to smoking. While, Morgado et al. [124] noted a small decrease in venular diameter in retinal photographs. In other vascular beds, the general consensus is that acute smoking induces vasoconstriction due to stimulation of the sympathetic nervous system [4, 110–113]. Therefore, of the five previous papers reporting on the acute effects of smoking on retinal blood flow, two found no change in flow after smoking, one found a small decrease and two found an increase. However, as discussed in Section 1.6.1, page 19, one needs to be careful when drawing conclusions about retinal blood flow from the blue field entoptic technique, which measured an increase in flow after smoking. From the existing evidence we believe it is most likely that retinal arteriolar diameter is unaffected by acute smoking.

We found the reactivity response of $smokers_{[no\ cig]}$ to be decreased in comparison to non-smokers. Previous studies have been inconsistent with regard their findings for the effect of chronic smoking on the reactivity response to various stimuli. Garhofer et al. [47] observed a diminished response in $smokers_{[no\ cig]}$ to flicker induced vasodilation with an RVA. Langhans et al. [61] measured a reduced response to hyperoxia, using a scanning laser Doppler flowmeter (SLDF), in ONH and choroidal blood flow. In opposition to these findings, an increased arteriolar constriction in response to hyperoxia was recorded by Wimpissinger et al. [126] in $smokers_{[no\ cig]}$ when compared to non-smokers using a RVA, while they observed no difference in the change in venous flow recorded by laser Doppler velocimetry and RVA between the groups. In a separate study, Wimpissinger [123] again observed a greater change in blood flow in $smokers_{[no\ cig]}$. This result was, however, measured in the choroid using a LDF in response to isometric exercise, which induces sympathetic and parasympathetic stimulation [123]. As the choroid is innervated and has been shown to lack a myogenic autoregulatory response (see Section 1.4.1, page 11), its response to isometric exercise is most likely due to extrinsic regulatory mechanisms. In yet another study by Wimpissinger et al. [60] in which they used a LDF, RVA and fundus pulsatility system to compare the responses of $smokers_{[no\ cig]}$ and non-smokers in response to car-

bogen (5% CO_2 and 95% O_2) breathing. They recorded no difference in the arteriolar constriction or ONH blood flow reduction between $\text{smokers}_{[\text{no cig}]}$ and non-smokers, and a diminished change in fundus pulsation amplitude and choroidal blood flow in $\text{smokers}_{[\text{no cig}]}$ in comparison to non-smokers. Endothelium-dependent reactivity has been shown to be impaired in many other vascular beds [114–119, 121]. Despite the contradictory results from the small number of previous investigations of reactivity performed in the eye some did find a diminished response in smokers. These studies are in agreement with our results and the general consensus that endothelium-dependent reactivity is diminished in other vascular beds. We therefore conclude it is likely that retinal vascular endothelial function is impaired due to chronic smoking.

In agreement with our findings for the effect of acute smoking on the reactivity response, Cubbidge et al. [122] and Morgado et al. [124] found no difference in the magnitude of arteriolar constriction when comparing smokers after abstinence and after smoking a cigarette, using a RVA with a flicker stimulus and retinal photography (Zeiss fundus camera) with a hyperoxic stimulus respectively. Morgado did, however, find that the decrease in venular velocity was blunted after smoking. As our results confirm those of both previous studies we conclude that endothelium-dependent reactivity in the retinal vasculature is unaltered by acute smoking. However, results from studies on the effect of acute cigarette smoking on endothelium-dependent vasodilation in the brachial artery, using the flow mediated dilation technique (FMD), imply that dilation is blunted by acute smoking [120, 133–137]. One possible explanation for endothelium-dependent vasodilation being blunted in the brachial artery when this was not found to be the case in the retinal vascular bed is that the brachial artery is innervated. Therefore, with acute smoking, nicotine levels increase, stimulating the sympathetic nervous system and causing vasoconstriction in the brachial artery. Because of the hierarchy of blood flow regulation mechanisms, with extrinsic control mechanisms (including nervous control) being on the top tier (see Section 1.4, page 10), this nicotine-induced stimulation of the sympathetic nerves overrides the endothelium-dependent vasodilation due to FMD, thereby blunting the vasodilatory response. Further research is required to establish if this does explain the diminished response in the brachial artery or if acute smoking affects endothelium-dependent reactivity differentially in different vascular beds, and if so, why?

It is widely reported that cigarette smoking is associated with reduced levels of nitric oxide (NO) [4, 39, 105, 118, 138]. Many studies have also found increased levels of endothelin-1 (ET-1) [39, 126]. Our results do not necessarily fit these observations. Reduced NO availability or increased ET-1 would result in vasoconstriction. We did

not find the baseline arteriolar diameters of smokers$_{[\text{no cig}]}$ to be decreased compared to non-smokers (although, as previously stated, firm conclusions can not be drawn from our inter-group diameter measurement comparisons) and baseline diameters were not reduced in smokers after cigarette smoking. This does not indicate an alteration in the levels of endothelium-secreted vasoactive factors. We can not offer a ready explanation for this discrepancy based on the data available in this study and therefore further work is necessary.

Previous studies have used endothelium-independent vasodilators (e.g. glyceryl trinitrate and nitroglycerin) to establish that endothelium-independent arteriolar dilation was unimpaired [115, 117, 118, 120, 121, 139] in smokers. This implies that the blunted endothelium-dependent responses are indeed due to endothelial dysfunction and not due to degeneration of the vascular smooth muscle cells [118, 139]. We can therefore conclude that the blunted vasoconstriction observed in the smokers in our study was indeed due to endothelial dysfunction.

Methodological differences may go some way to explaining the discrepancies in the results obtained in the retina thus far, as many different measurement devices were used along with a number of different stimuli.

A possible source error in our experiments is that some subjects may have failed to abstain from smoking before the experiments. The importance of abstinence was explained to the volunteers, so it is believed that if some subjects did smoke during the abstinence period, it would have been a very small number that would have done so.

4.4.3 Conclusions

From our results we can conclude that the vasoconstriction observed in this study was due to endothelium-dependent, metabolic autoregulation. Pulse rate increased significantly after smoking a cigarette indicating that substantial amounts of nicotine were inhaled. Baseline arteriolar diameters of smokers, after a short-term abstinence from smoking, did not differ to those of non-smokers. Retinal arteriolar diameters are unchanged by acute cigarette smoking. Our results indicate that the retinal arteriolar response to hyperoxia is blunted in smokers compared to non-smokers, suggesting impaired endothelial function from long-term smoking, while acute smoking had no effect on the magnitude of hyperoxia induced vasoconstriction.

Chapter 5

Effect of Aging on Reactivity in Healthy Subjects

5.1 Introduction

The vascular system degrades with age. The elastic arteries undergo structural changes, including dilation and stiffening. The decline in arterial compliance increases the pulse pressure and cardiac work. These degenerative changes are termed arteriosclerosis [4, 140–142]. Although substantial research has been performed to assess the structural and functional changes in large arteries with age, less is known about age-related alterations in the resistance arteries and arterioles [142,143]. Studies that have been performed in resistance vessels have not found structural changes in arterioles, in contrast to the large elastic arteries [141, 143]. Studies in animal models and in man indicate that blood flow delivery and the ability to adapt blood flow to match metabolic demand are compromised with age [140, 142–145]. Age-related changes in vasoconstrictor and vasodilator responses have been found to be heterogenous, varying between elastic and resistance arteries, between vascular beds and between muscles of different fibre [142–144]. For example, endothelial function in different vascular beds in rats have been found to be differentially effected by aging. Basal nitric oxide (NO) levels were found to be attenuated with age in the aorta and femoral

artery [140, 144], but not in the pulmonary circulation [146]. While aging resulted in a reduction in contractions to endothelin-1 (ET-1) in rat aortas, but not in femoral arteries [144], (The role of NO and ET-1 in the modulation of vascular tone is described in Section 1.4.4, page 13).

In the retina, investigators studying blood flow have reported a decrease in the parameter with aging [147–152]. Studies on retinal vascular reactivity have been more contradictory. Of the ten studies found, six reported that the retinal arteriolar response to stimuli decreased with age [24, 45, 54, 153–155], while four did not find reactivity to be influenced by aging [7, 48, 76, 95]. In order to study retinal autoregulation in diseases such as hypertension and diabetic retinopathy, it is important to have knowledge of as many factors as possible that affect retinal arteriolar reactivity. Taking this into consideration, together with the equivocal nature of previous results of age-related changes in retinal reactivity, it was decided to undertake the following experiments to determine the effects of healthy aging on retinal vascular endothelial function by assessing the response of retinal arterioles to hyperoxia.

5.2 Materials and Methods

5.2.1 Sample

Eleven (4 women and 7 men) healthy, normal volunteers (mean age $\pm$ SD, 48.4 $\pm$ 8.3 years; range, 40–68 years) participated in this study. Each subject signed a written consent after the nature of the study and experiment protocol were explained in detail. All procedures conformed to the tenets of the Declaration of Helsinki and were reviewed and approved by the National University of Ireland Galway Ethics Committee. Exclusion criteria included ages less than 40 years, smoking, unclear optic media, pregnant or breastfeeding women, any cardiovascular or respiratory disorders, taking medication with known effects on blood flow (e.g. muscle relaxants), taking any chronic medication.

5.2.2 Visits

Volunteers attended for two visits. The first visit was to determine eligibility, to familiarise the subjects with the measurement technique and to obtain some large field of view (FOV) images. One eye from each subject was selected and approximately

nine 10° FOV (the largest FOV of the HRT classic) were obtained. These images were used to create a mosaic of the retina, as described in Section 3.2.2, page 60. The mosaic was used to define a suitable measurement site (relatively straight arteriole segment with good contrast to the background, in the temporal hemiretina) and to aid the investigator in navigating the retina at a small FOV during the second visit.

The magnitude of retinal vascular reactivity in response to the hyperoxic stimulus was measured during the second visit.

5.2.3 Experimental Protocol

Subjects were asked to abstain from alcohol and caffeine for 12 hours before the study visit. Subjects rested for at least 5 minutes before the start of the experiment to stabilise baseline cardiovascular and respiratory parameters. All testing was performed in a quiet laboratory, at normal room temperature and at sea level atmospheric pressure.

Visit 2 was performed to assess the magnitude of vasoconstriction due to hyperoxic provocation in healthy subjects 40 years of age or older. The experimental protocol was divided into two consecutive phases in which the subject breathed (1) room air for approximately 15 minutes, and (2) 100% oxygen via a non-rebreather mask (the oxygen delivery system is detailed in Section 3.2.3, page 62) for approximately 15 minutes. These phases were considered baseline and oxygen breathing respectively. Approximately six 2° FOV image sequences of the selected arteriole were obtained at baseline. Subjects breathed oxygen for 5 minutes before imaging recommenced as they continued to breathe oxygen. The arteriolar segment imaged at baseline was reimaged, approximately 6 image sequences were captured.

Blood pressure was measured during visit 2. Three measurments were taken during each phase. Systolic (BP_s) and diastolic (BP_d) blood pressure were measured on the upper arm by an automated oscillometric device (Omron M10-IT; Omron Healthcare Europe BV, Hoofddorp, The Netherlands). Mean brachial artery blood pressure, BP_m was calculated using Equation 3.1. Pulse rate (PR) and oxygen saturation (SpO_2) were also recorded during both visits. Three readings were taken during each phase from a finger pulse oximetric device (Ohmeda Biox 3700e; Datex-Ohmeda, Inc., Madison WI, USA). All measurements were made by the same investigator.

Image sequences were processed as described in Chapter 2, with arteriolar diameters being calculated in pixels as detailed in Section 2.5, page 48.

To assess the effect of aging on the parameters measured, data from the >40 group is compared to the data obtained for the younger subjects (mean age ± SD, 21.9 ±2.6 years; range, 18–28 years) in Chapter 3. As there was no difference between any parameters obtained for the younger group between visits 2 and 3, the <40s data was averaged across both visits.

As described in Section 1.3, page 8, a change in IOP causes a change in perfusion pressure. Previous studies have investigated the effect of aging on IOP. IOP was found to be unaltered by age in a few studies [147, 156], but the majority of previous studies reported an increase in IOP with age [148, 149, 157, 158]. These increases in IOP were, however, quite small, ranging from 0.5 – 1.9 mm Hg. Grunwald et al. [148] recorded the largest increase in IOP. They measured an increase of 1.9 mm Hg in IOP between their younger (15 – 45 years) and older (45 –76 years) subjects. Using the IOP values obtained by Grunwald et al. and the BP_m values we obtained for the >40s and <40s, an increase in PP of just 5.3% in the older subjects is obtained. Previous studies which used isometric exercise to increase PP [23,43,44], found that very large increases in PP of 31.3–55% elicited mean percentage arteriolar constrictions of just 0.2–3.4%. Therefore an increase in PP of 5.3% would have little or no impact on vascular tone. Also, as previously explained in Section 3.2.4, IOP does not change significantly during hyperoxia. Consequently, IOP was not recorded during our experiments.

5.2.4 Data Analysis

Statistical analysis was performed using Minitab® software package (Release 16; Minitab Inc., PA, USA). Each dataset was group-averaged across subjects as a function of phase (i.e. baseline, hyperoxia). The response of arteriole diameters to hyperoxia is expressed as a percentage change as compared to baseline. Datasets were assessed to determine if they were normally distributed using the Anderson-Darling test. To investigate the influence of oxygen breathing on parameters two-tailed paired t-tests were performed between baseline values and hyperoxic values. To compare the effect of hyperoxia between 2 different groups (e.g. >40s versus <40s) a two-tailed independent samples t-test was used. All data is presented as mean ± standard error (SE). The level of significance was set to $p < 0.05$.

5.3 Results

5.3.1 Systemic Haemodynamics

The group-averaged values of each systemic variable for each phase of the experiment conducted with the older volunteers are presented in Table 5.1. Table 5.2 details the systemic parameters of the younger volunteers, averaged over both visits detailed in Chapter 3.

The group-averaged SpO_2 of the >40s increased from a baseline 96.6 $\pm$ 0.4% to 99.2 $\pm$ 0.2% during oxygen breathing. These values were very similar to those of the <40 group of volunteers.

The mean baseline value for pulse rate (PR) of the older group was 74.0 $\pm$ 3.1 beats per minute (bpm). A small decrease to 67.8 $\pm$ 2.5 bpm was noted during hyperoxia ($p = 0.000$). The baseline ($p = 0.912$) and hyperoxic ($p = 0.343$) values did not differ between the >40 and <40 groups.

The group-mean BP_s of the older group was 109.5 $\pm$ 3.1 mm Hg during the baseline phase and remained unaltered during the hyperoxic phase ($p = 0.856$). The BP_s values of the older and younger groups did not differ from each other during the baseline ($p = 0.720$) and hyperoxic ($p = 0.763$) phases.

The group-averaged BP_d of the >40s was found to be 71.3 $\pm$ 2.1 mm Hg at baseline, this was significantly greater than the mean baseline value observed in the younger volunteers ($p = 0.002$). The BP_d of the older group did not change during hyperoxia ($p = 0.831$) and remained significantly increased compared to the younger group ($p = 0.012$).

Reflecting the values obtained for BP_s and BP_d, the group-mean baseline value for BP_m was recorded as 84.0 $\pm$ 2.0 mm Hg and remained constant thoughout the experiment in the >40 group ($p = 0.961$). The BP_m of the >40s was found to be slightly increased when compared to the <40s, significantly so at baseline ($p = 0.040$), but the difference was not significant during the oxygen breathing phase ($p = 0.108$).

5.3.2 Vessel Diameter and Reactivity

The group mean retinal arteriole diameter of the >40 group was 49.6 $\pm$ 2.7 pixels at baseline. This decreased significantly to 47.4 $\pm$ 2.7 pixels during hyperoxic provocation ($p = 0.000$). The group-averaged percentage change in arteriolar diameter during

Parameter (n = 11)	Baseline	Hyperoxia	p-value (hyperoxia vs. baseline)
SpO_2 (%)	96.6 ± 0.4	99.2 ± 0.2	-
PR (bpm)	74.0 ± 3.1	67.8 ± 2.5	0.000
BP_s (mm Hg)	109.5 ± 3.1	108.9 ± 4.3	0.856
BP_d (mm Hg)	71.3 ± 2.1	71.7 ± 1.7	0.831
BP_m (mm Hg)	84.0 ± 2.0	84.1 ± 2.4	0.961

Table 5.1: Systemic haemodynamics obtained for the older subjects throughout visit 2. Data are presented as mean ± SE. t-tests were not performed on SpO_2 data as it was not found to be normally distributed.

Parameter (n = 34)	Baseline	Hyperoxia	p-value (hyperoxia vs. baseline)
SpO_2 (%)	97.6 ± 0.2	99.7 ± 0.1	-
PR (bpm)	74.4 ± 1.8	70.7 ± 1.5	0.000
BP_s (mm Hg)	107.7 ± 2.5	107.5 ± 2.3	0.694
BP_d (mm Hg)	63.4 ± 1.2	65.6 ± 1.2	0.002
BP_m (mm Hg)	78.2 ± 1.4	79.5 ± 1.4	0.009

Table 5.2: Systemic haemodynamics obtained for the younger subjects, averaged over both visits described in Chapter 4. Data are presented as mean ± SE. t-tests were not performed on SpO_2 data as it was not found to be normally distributed.

the oxygen breathing phase was -4.9 ± 0.8%. Figure 5.1 presents a comparison of the mean percentage change of arteriole diameters, relative to baseline, attained by the older and younger groups. The data indicates that the degree of vasoconstriction achieved by the >40s was significantly diminished compared to the <40s ($p = 0.000$), whose arterioles constricted by 9.9 ± 0.4% on average.

5.4 Discussion

5.4.1 Systemic Haemodynamics

The increased level of SpO_2 during the oxygen breathing phase suggests that systemic hyperoxia was achieved.

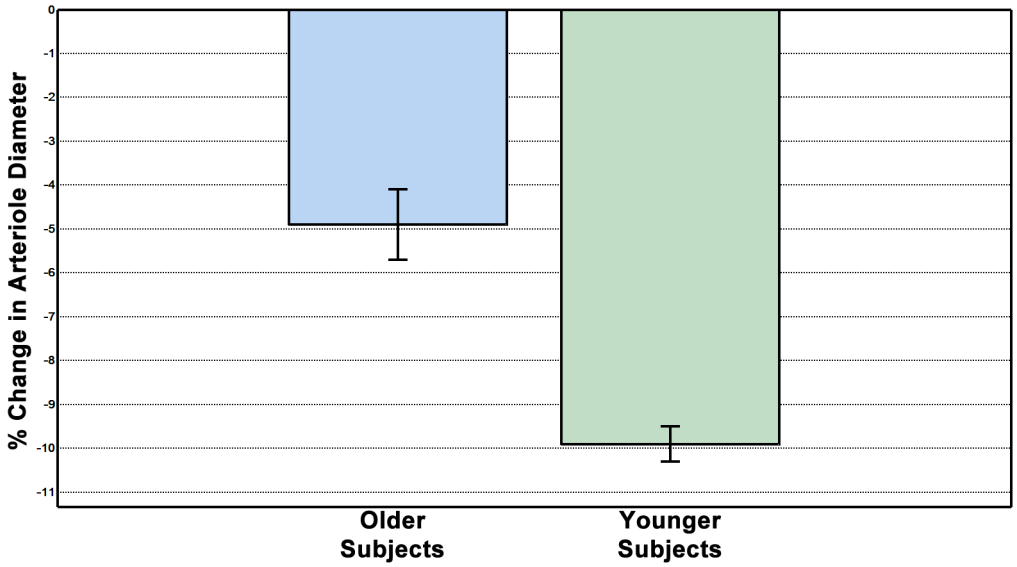

Figure 5.1: Comparing the percentage change in arteriolar diameter from baseline, of the older and younger volunteers. Data are presented as mean $\pm$ SE.

A small decrease in PR was observed during hyperoxia, as it was in the younger group. PR was found not to differ between the younger and older groups during either phase of the experiment. This was in agreement with what was expected, as aging is believed to have little effect on the resting heart rate [4].

BP_m was found to be significantly higher in the older group in comparison to the younger group. This was as expected, as it is widely reported that aging is associated with an increase in blood pressure [4, 147, 148]. BP_m was found not to alter during the oxygen breathing phase. The four studies found which used oxygen breathing to investigate the effects of aging on the reactivity response of retinal arterioles, did not report blood pressure measurements. Our observations are, however, consistent with previous studies on younger cohorts that observed no change in blood pressure during hyperoxia [12,21,22,25,76], and there is no evidence to suggest that this would alter with age.

The difference in BP_m between the older and younger group and the decrease in PR during hyperoxia in these experiments were small. As seen in studies which used isometric exercise to cause vasoconstriction [23, 43, 44], very large changes in blood pressure of 16.7–33.4 mm Hg elicited relatively small vasoconstrictions of 0.2–3.4%. In this study the group-averaged BP_m of the older subjects was just 5.8 mm Hg higher than that of the younger volunteers. This small difference would have had little or no influence on vascular tone.

5.4.2 Vessel Diameter and Reactivity

In this part of our study we did not compare the baseline arteriolar diameters of the older and younger groups for a number of reasons. Firstly, scatter in the eyes of a number of the >40s group was found to be somewhat increased, resulting in a deterioration in image quality; therefore the larger arterioles were generally imaged in this group. While in the <40s group a greater range of vessel calibres was imaged. We could have compared the >40s baseline diameter data to a subgroup of the <40s consisting of only the larger arterioles, however, it would have been difficult to exclude smaller arterioles in an unbiased manner. Therefore, no conclusions could have satisfactorily been drawn from such a comparison. In any case, a comparison of the reactivity response was the primary outcome measure of interest as all previous studies investigating the effect of age on blood flow in the retina have found it to be diminished. Wong et al. [151] measured retinal arterioles of 4,247 individuals, aged 43 to 84 years, from retinal photographs. The arteriolar diameter was found to decrease with increasing age, which implies a decrease in blood flow with advancing years as blood flow is a function of r^4, where r denotes the vessel radius (as described in Section 1.3, page 8). Grunwald et al. [147] obtained results, using the blue field entoptic phenomenon, that suggested that blood flow decreases with increasing age. Using laser Doppler flowmetry Grunwald et al. [148], Boehm et al. [149] and Groh et al. [150] found that retinal blood flow was diminished in older subjects compared to their younger counterparts. Groh et al. did, however, also find that optic nerve head blood flow did not appear to be influenced by age while they observed that blood flow velocity in the central retinal artery decreased with advancing age using pulsed Doppler sonography.

Using a hyperoxic provocation we discovered a significantly smaller vasoconstriction in older subjects compared to their younger counterparts. Tayyari [7], Blum et al. [154], Sieker et al. [54] and Sehi et al. [76] also used oxygen breathing to provoke an arteriolar constriction. Tayyari used a retinal vessel analyser (RVA) and observed no difference in reactivity between their older and younger groups. Sehi et al. also found that the magnitude of vasoconstriction was not associated with age using a Canon Laser Blood Flowmeter (CLBF). However, in this study the reactivity response was measured in young subjects with a small age range (mean $\pm$ SD, 24.4 ± 4.7 years). Such a narrow range of (young) ages is unlikely to be sufficent to detect a decrease in the parameter with age, if it exists. In agreement with our results, Blum et al. and Sieker et al. observed the reduction in arteriole diameter to be less in older subjects using a RVA and fundus camera respectively. From the available evidence we believe

we can conclude that the hyperoxia-induced constriction of the retinal arterioles diminishes with age. As endothelin-1 (ET-1) plays a major role in hyperoxia-induced vasoconstriction [40], this would suggest that aging reduces ET-1 production or diminishes the response to its release in the retina. Another possibility is that, as arterioles narrow with age, they may have a reduced capacity for futher increases in tone in response to a stimulus, such as oxygen breathing. Further studies are needed to confirm the impairment in the vasoconstrictor response with age. Using isometric exercise to induce retinal arteriolar constriction Blum et al. [153] and Jeppesen et al. [24] both used a RVA and both measured a decrease in diameter change with increasing age. Tachibana et al. [45] measured the degree of dilation in arterioles due to a decrease in perfusion pressure (PP) caused by a postural change from a recumbant to erect position. They measured a reduction in the percentage increase in arteriole diameter with advancing age. These results suggest an age-related deterioration in the retinal vasculature's ability to regulate arteriolar tone in response to a change in PP. Nagel et al. [48], Heitmar et al. [95] and Kneser et al. [155] all used RVA systems to assess the retinal arteriolar reaction to a flicker stimulus. As described in Section 1.5.2, page 17, flickering light alters the metabolic demand of the retina eliciting an increase in blood flow through a dilation of the arterioles. Constriction of the vessel diameter to below baseline level occurs upon cessation of the flicker stimulus, before returning to its pre-flicker value. Nagel [48] reported that the overall reactivity response (i.e. taking into account the maximum dilation achieved during flicker and the constriction attained post-flicker) did not decrease significantly with age. Heitmar [95] observed no significant change in vasodilation or constriction with advancing years. Kneser [155], on the other hand, found a significant decrease in overall arteriolar reactivity response. This was due almost entirely to a significant decrease in vasoconstriction with age, while they found the dilatory response to remain almost constant. As flicker-induced dilation is believed to be primarily mediated by NO [36], this would suggest that retinal NO availability is unaffected by aging, but again, further investigation would be needed to confirm this.

5.4.3 Conclusions

From our results we can conclude that the vasoconstriction observed in this study was due to endothelium-dependent, metabolic autoregulation.

Retinal arteriolar constrictions due to oxygen breathing are significantly diminished with advancing age. This should be an important consideration when conducting clinical studies of autoregulation in retinal vascular disease.

Chapter 6

Retinal Arteriolar Reactivity in Pathology

6.1 Introduction

6.1.1 Hypertension

Cardiovascular disease (CVD) is the number one cause of death globally [159]. An estimated 17.3 million people died from CVDs in 2008 (representing approximately 1 in 3 deaths), and this number is projected to increase to 23.3 million by 2030 [159,160]. Hypertension is a major risk factor for CVDs and is the most common chronic disease; it is estimated to effect a billion people worldwide and to cause approximately 7 million deaths per year [4,160]. Systemic arterial hypertension is diagnosed as a resting brachial artery pressure exceeding 140/90 mm Hg [4,161], however the relationship between blood pressure and CVD risk is a continuous one, with risk of CVD rising with blood pressure levels [4,160,162,163]. Although blood pressure lowering has been shown to reduce deaths and enhance quality of life the majority of diagnosed hypertensives are inadequately controlled [160].

In 1898 hypertensive retinopathy was described for the first time by Marcus Gunn [164]. Signs of hypertensive retinopathy include generalised and focal arteriolar nar-

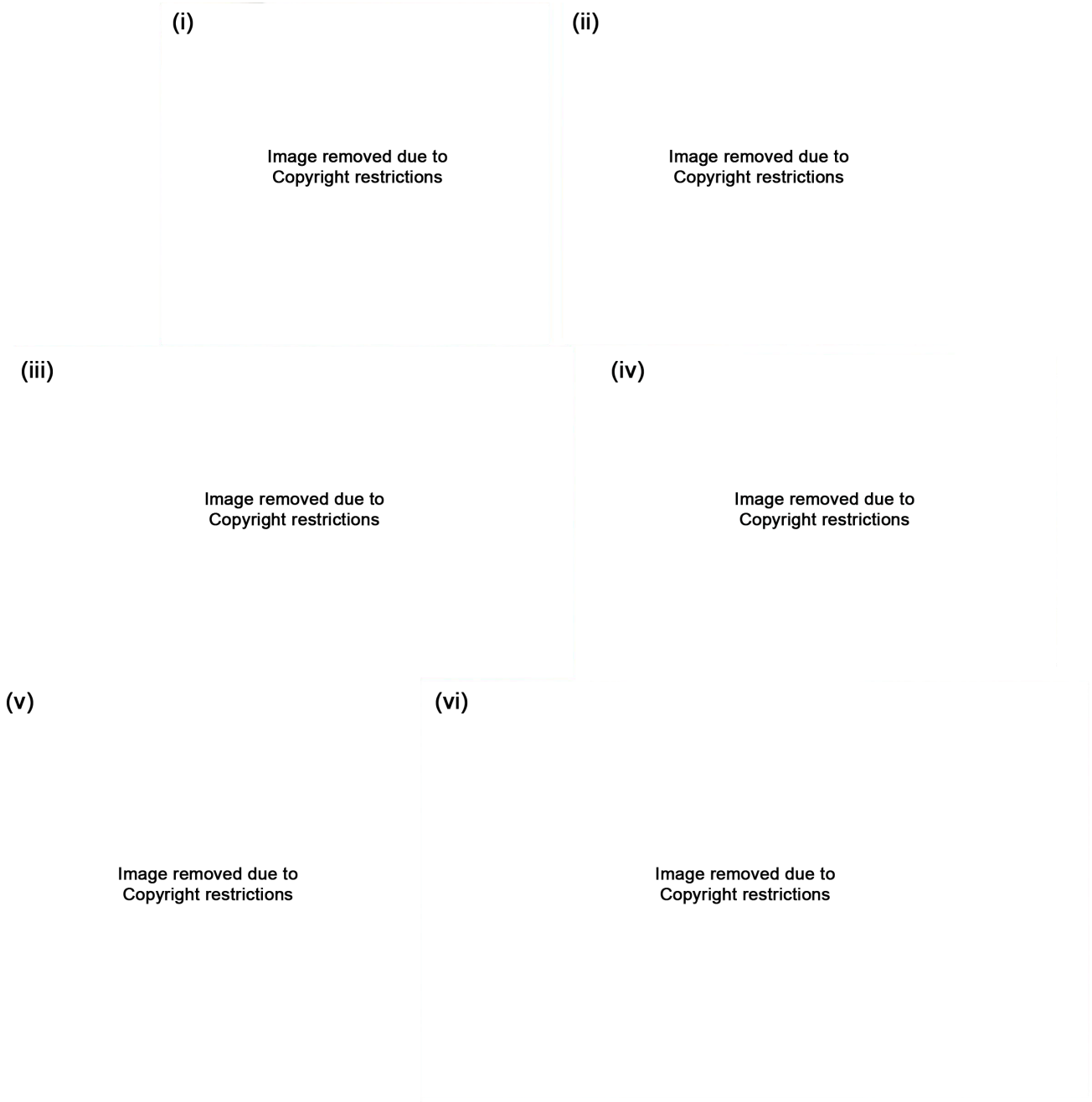

Figure 6.1: Hypertensive Retinopathy. (i) Focal arteriolar narrowing. Image taken from [1]. (ii) Arteriovenous nicking. Image taken from [1]. (iii) Increased arteriolar light reflex (copper or silver wiring). Image taken from [2]. (iv) Flame-shaped haemorrhages. Image taken from (http://goo.gl/wnuZm). (v) Cotton wool spots. Image adapted from (http://goo.gl/36A11). (vi) Optic disc swelling. Image taken from [3].

rowing, arteriovenous nicking, increased arteriolar light reflex (copper or silver wiring), microaneurysms, flame- and blot-shaped haemorrhages, cotton-wool spots, and swelling of the optic disc. Examples of these retinal changes are shown in Figure 6.1. In 1939, Keith et al. [165] demonstrated that increased severity of these hypertension-induced retinal changes was linked to increased mortality. This observation led them to develop a classification system, which categorised these signs into 4 grades of increasing severity. In recent years, however, the usefulness and relevance of this classification system (and subsequent revisions of the scheme), have been called into question [163, 166], due to a dramatic decline in incidence of severe retinopathy as a result of improved methods of blood pressure control [163, 167] and difficulty in determining between mild retinopathy grades [167,168], resulting in poor predictive value [163, 166, 168].

Patients at high risk of CVD are currently identified by physicians using traditional risk factors such as, hypertension, diabetes, age, cigarette smoking, cholesterol and obesity [160, 162], but a large percentage of cardiovascular morbidity and mortality is not explained by these risk factors [169]. For this reason, identification of novel risk factors is of great interest. Arteriolar narrowing has been a focus of much of the research in this area, and endothelial dysfunction is now also emerging as a potential risk factor. While some limited evidence exists that these measures may predict future cardiovascular events [170,171], there needs to be consistent demonstration that their addition to traditional screening methods improves prediction of CVD morbidity and mortality. Substantial work remains in this area.

6.1.2 Diabetes Mellitus

The World Health Organisation (WHO) estimates that 347 million people currently suffer from diabetes mellitus [172]. Diabetes is a leading cause of morbidity and mortality; it increases the risk of heart disease and stroke and it is a leading cause of kidney failure [10, 172, 173]. It is estimated that 3.4 million people died in 2004 from the consequences of hyperglycaemia (high fasting blood sugar levels), and it is projected that diabetes deaths will double by 2030 [172]. Diabetes mellitus is a chronic condition in which either the body does not produce enough insulin (type 1 diabetes; previosuly known as insulin-dependent or juvenile/childhood-onset) or because cells fail to respond properly to the insulin it produces (type 2 diabetes; previously known as insulin-independent or adult onset) [172, 174]. Insulin is a hormone that is produced in the pancreas, which is necessary to regulate blood sugar levels [172, 174]. 90% to

95% of diabetics have type 2 diabetes [172,175].

Diabetic retinopathy is the leading cause of new cases of blindness in the working-age population of most developed countries; it is characterised by microvascular occlusion and leakage [175–177]. The earliest stage of diabetic retinopathy is called non-proliferative diabetic retinopathy and the earliest visible manifestations include microaneurysms, which can be seen in Figure 6.2, and haemorrhages [15,175–177]. Non-proliferative retinopathy progresses with the presence of cotton-wool spots, hard exudates, intraretinal microvascular abnormalities (IRMA), venous beading and looping, and retinal thickening (oedema), including macular oedema [33,168,175–177], which can be seen in Figure 6.4. The more advanced stage is called proliferative diabetic retinopathy, the primary feature of which is neovascularisation, which can occur at the optic disc and elsewhere in the retina, this is an attempt to revascularise hypoxic retina [15, 175–177]. These new vessels are weak and prone to leaking, which can result in vitreous haemorrhage [175–177]. Fibrosis associated with these new vessels can even result in retinal detachment [175–177]. Examples of features of diabetic retinopathy can be seen in Figure 6.3. The main causes of visual impairment in diabetic retinopathy include macular oedema, vitreous haemorrhage and retinal detachment [15,33,175–177].

Although a greater proportion of type 1 diabetics develop diabetic retinopathy and they are more prone to developing more severe complications, than type 2 diabetics, as they comprise only 5 to 10% of the total number of diabetics, the majority of people with diabetes-induced visual impairment are type 2 diabetics [175]. Twenty years after the development of diabetes, the majority of patients will have retinopathy [25, 168, 175–177]. The primary risk factors for developing diabetic retinopathy are duration of disease and poor blood glucose control [175,177], with hypertension, which is very common in persons with type 2 diabetes, being another important factor [168,175–178]. The exact underlying mechanisms linking diabetes to the development of diabetic retinopathy remain unclear. Many believe that endothelial dysfunction may play a role in the aetiology of diabetic reinopathy [178–182]. While some small cross-sectional studies have demonstrated that vascular reactivity is diminished in people with diabetes [25,42,54,183–185] and those at high risk of diabetes (e.g. people with impaired glucose tolerance and first-degee relatives of diabetics) [186–189], this needs to be confirmed with consistent results from large, prospective studies. It is also necessary to elucidate if this diminution of vascular reactivity is due to pericyte and smooth muscle cell damage or functional damage of the endothelial cells, or possibly a combination of both. Should this be confirmed, it may lead to the devel-

opment of new treatment strategies, which could help prevent the development and progression of diabetic retinopathy.

Application of a high resolution imaging system to the measurement of arteriolar diameters and endothelial function may afford greater insight in future studies of these diseases. The participants in our studies thus far were students and lecturers studying and working in the university. These subjects were generally young, healthy, and very cooperative. We recognised that using our experimental set-up in a clinical setting may be more challenging. To assess the difficulties of obtaining our measurements in patients and to obtain some pilot data in hypertensives and diabetics, the following experiments were undertaken.

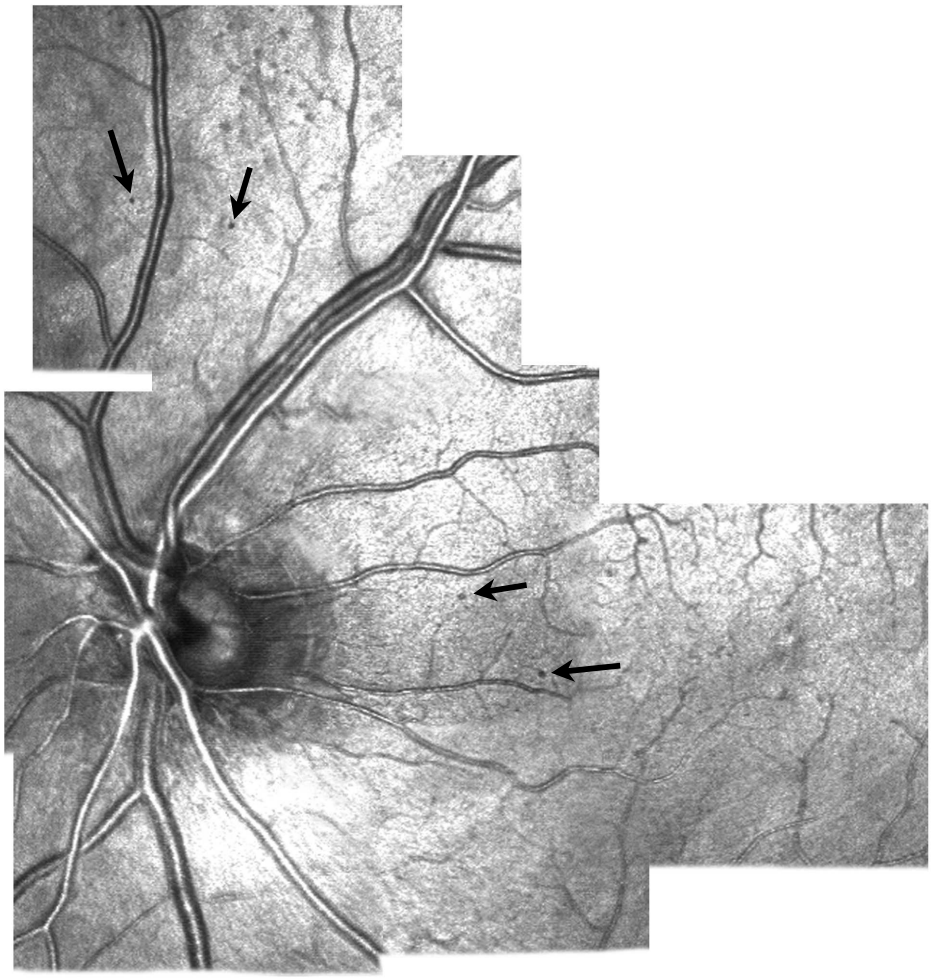

Figure 6.2: Nonproliferative diabetic retinopathy, showing microaneurysms.

(i)

Image removed due to Copyright restrictions

(ii)

Image removed due to Copyright restrictions

(iv)

Image removed due to Copyright restrictions

(v)

Image removed due to Copyright restrictions

Figure 6.3: Diabetic Retinopathy. (i) Hard Exudates. Image taken from (http://goo.gl/A7gyn). (ii) Venous beading. Image adapted from (http://goo.gl/ZEZ8S). (iii) Neovascularisation. Image taken from (http://goo.gl/C4yrz). (iv) Vitreous haemorrhage. Image taken from (http://goo.gl/D7K9r). (v) Retinal detachment. Image taken from (http://goo.gl/ZZdFp).

Figure 6.4: Diabetic Macular Oedema.

Figure 6.5: Patient's-eye view of a beach with normal vision and a patient with diabetic retinopathy-induced visual impairment.

6.2 Materials and Methods

6.2.1 Sample

A total of twenty-two (8 women and 14 men) individuals, composing two groups, participated in this study. The first group included fifteen (6 women and 9 men) subjects with hypertension (mean age $\pm$ SD, 73.5 $\pm$ 9.8 years; range, 44–84 years), and the second group comprised seven (2 women and 5 men) volunteers with type 2 diabetes (mean age $\pm$ SD, 56.3 $\pm$ 8.6 years; range, 46–68 years). Each subject signed a written consent after the nature of the study and experiment protocol were explained in detail. All procedures conformed to the tenets of the Declaration of Helsinki and were reviewed and approved by Galway University Hospital's Research Ethics Committee. Exclusion criteria included ages less than 18 years, smoking, unclear optic media, pregnant or breastfeeding women, any respiratory disorders, taking medication with known effects on blood flow (e.g. muscle relaxants), epilepsy.

Hypertension and diabetes were identified from medical records by an opthalmologist during routine clinical assessment. All the hypertensive subjects were receiving various antihypertensive treatment, with varying degrees of blood pressure control. The diabetic subjects were being treated with insulin or glycemic agents. Three of the diabetic subjects had concurrent hypertension, one of who did not have well-controlled blood pressure.

6.2.2 Experimental Protocol

In this study all experimental procedures were conducted during one visit by the volunteers. Participants underwent opthalmological examination before inclusion in the study. Subjects had abstained from alcohol for 12 hours and caffeine for at least 3 hours before the study visit. Subjects rested for at least 5 minutes before the start of the experiment to stabilise baseline cardiovascular and respiratory parameters. All testing was performed in a quiet room, at normal room temperature and at sea level atmospheric pressure.

The study period for each participant was divided into two stages. The first stage was performed to familiarise the subjects with the measurement technique and to obtain some large field of view (FOV) images. One eye from each subject was selected and approximately six 10° FOV (the largest FOV of the HRT classic) were obtained. These images were used to define a suitable measurement site (relatively straight arteriole

segment with good contrast to the background, in the temporal hemiretina) and to aid the investigator in navigating the retina at a small FOV during the second stage of the study.

The second stage of the study was performed to assess the magnitude of vasoconstriction due to hyperoxic provocation in subjects (1) with hypertension and (2) with type 2 diabetes. The test protocol was divided into two consecutive phases in which the subject breathed (1) room air for approximately 15 minutes, and (2) 100% oxygen via a non-rebreather mask (the oxygen delivery system is detailed in Section 3.2.3, page 62) for approximately 15 minutes. These phases were considered baseline and oxygen breathing respectively. Approximately six 2° FOV image sequences of the selected arteriole were obtained at baseline. Subjects breathed oxygen for 5 minutes before imaging recommenced as they continued to breathe oxygen. The arteriolar segment imaged at baseline was reimaged, approximately 6 image sequences were captured.

Blood pressure was measured during the experiment. Three measurments were taken during each phase. Systolic (BP_s) and diastolic (BP_d) blood pressure were measured on the upper arm by an automated oscillometric device (Omron M10-IT; Omron Healthcare Europe BV, Hoofddorp, The Netherlands). Mean brachial artery blood pressure, BP_m was calculated using Equation 3.1. Pulse rate (PR) and oxygen saturation (SpO_2) were also recorded during the second stage of the experiment protocol. Three readings were taken during each phase from a finger pulse oximetric device (Ohmeda Biox 3700e; Datex-Ohmeda, Inc., Madison WI, USA). All measurements were made by the same investigator.

Image sequences were processed as described in Chapter 2, with arteriolar diameters being calculated in pixels as detailed in Section 2.5, page 48.

To assess the effect of hypertension and diabetes on the parameters measured, data from these groups were compared to the data obtained for the healthy subjects over 40 years of age (mean age $\pm$ SD, 48.4 $\pm$ 8.3 years; range, 40–69 years) described in Chapter 5. Thus, the subjects described in Chapter 5 acted as our healthy, control subjects in this section of our study.

As described in Section 1.3, page 8, a change in IOP causes a change in perfusion pressure. Previous studies reported that the IOPs measured in hypertensives [42] and diabetics [42, 180, 182, 190–193] did not differ to those of the control groups. Also, as previously explained in Section 3.2.4, IOP does not change significantly during hyperoxia. Consequently, IOP was not recorded during our experiments.

6.2.3 Data Analysis

Statistical analysis was performed using Minitab® software package (Release 16; Minitab Inc., PA, USA). Each dataset was group-averaged across subjects as a function of phase (i.e. baseline, hyperoxia). The response of arteriole diameters to hyperoxia is expressed as a percentage change as compared to baseline. Datasets were assessed to determine if they were normally distributed using the Anderson-Darling test. To investigate the influence of oxygen breathing on parameters two-tailed paired t-tests were performed between baseline values and hyperoxic values. To compare the effect of hyperoxia between 2 different groups (e.g. controls versus hypertensives) a two-tailed independent samples t-test was used. All data is presented as mean $\pm$ standard error (SE). The level of significance was set to $p < 0.05$.

6.3 Results

6.3.1 Systemic Haemodynamics

The group-averaged values for each systemic variable for each phase of the experiment conducted with the hypertensive subjects are presented in Table 6.1 and the values obtained for each phase of the experiment conducted with the diabetics are presented in Table 6.2. Table 6.3 details the systemic parameters of the healthy control subjects described in Chapter 5.

The group-mean baseline value for SpO_2 of the hypertensives was 94.9 $\pm$ 0.5% and increased to 98.4 $\pm$ 0.3% during the hyperoxic phase. The group-averaged SpO_2 of diabetics increased from a baseline of 96.2 $\pm$ 0.5% to 98.4 $\pm$ 0.2% during hyperoxia. These values were similar to those obtained for the control group.

The group-mean pulse rate (PR) of the hypertensives was 68.6 $\pm$ 2.7 beats per minute (bpm) at baseline and decreased slightly but significantly to 65.9 $\pm$ 2.4 bpm during oxygen breathing. These values did not differ significantly to the values obtained for the controls at any phase of the experiment (baseline, $p = 0.206$; hyperoxia, $p = 0.601$). The PR recorded for diabetics at baseline was 72.4 $\pm$ 6.5 bpm. This value decreased slightly to 68.8 $\pm$ 7.2 bpm during oxygen breathing, however this small reduction in PR was not found to be significant. The diabetic PR values were also not significantly different from the controls during the baseline ($p = 0.803$) or hyperoxic ($p = 0.866$) phases.

The group-averaged BP_s of the hypertensive group was found to be 135.9 $\pm$ 5.7 mm Hg during the baseline phase and remained unaltered during the hyperoxic phase of the experiment. The BP_s values of the hypertensives were significantly higher than those of the controls throughout the experiment (baseline, p = 0.001; hyperoxia, p = 0.002). The baseline group-mean value of BP_s of the diabetic group was 128.4 $\pm$ 6.8 mm Hg. This value increased to 134.6 $\pm$ 5.8 mm Hg during oxygen breathing. The baseline BP_s value of the diabetics was significantly higher than that of the control group (p = 0.010) and remained so during hyperoxia (p = 0.004).

The group-mean hypertensive and diabetic BP_d baseline values were 79.7 $\pm$ 3.4 mm Hg and 74.6 $\pm$ 2.9 mm Hg respectively. These values did not change during hyperoxia in either group. The BP_d values of both groups were found not to differ significantly from those of the healthy control group during baseline (hypertensives, p =0.068; diabetics, p =0.389) or hyperoxia (hypertensives, p = 0.167; diabetics, p = 0.094).

Reflecting the values obtained for BP_s, the group-mean baseline value for BP_m was recorded as 98.5 $\pm$ 3.9 mm Hg in the hypertensive group at baseline and this value remained unchanged throughout the experimental protocol. The group-averaged BP_m of the diabetic group increased from a baseline of 92.5 $\pm$ 3.2 mm Hg to 96.5 $\pm$ 2.7 mm Hg during oxygen breathing. The BP_m values of both groups were found to be significantly higher than those of the healthy, control group during both the baseline (hypertensives, p = 0.007; diabetics, p = 0.034) and hyperoxic phases (hypertensives, p = 0.015; diabetics, p = 0.008).

Parameter (n = 15)	Baseline	Hyperoxia	p-value (hyperoxia vs. baseline)
SpO_2 (%)	94.9 $\pm$ 0.5	98.4 $\pm$ 0.3	-
PR (bpm)	68.6 $\pm$ 2.7	65.9 $\pm$ 2.4	0.002
BP_s (mm Hg)	135.9 $\pm$ 5.7	136.1 $\pm$ 5.9	0.870
BP_d (mm Hg)	79.7 $\pm$ 3.4	78.1 $\pm$ 3.6	0.368
BP_m (mm Hg)	98.5 $\pm$ 3.9	97.5 $\pm$ 4.0	0.401

Table 6.1: Systemic haemodynamics obtained for the hypertensive subjects. Data are presented as mean $\pm$ SE. t-tests were not performed on SpO_2 data as it was not found to be normally distributed.

Parameter (n = 7)	Baseline	Hyperoxia	p-value (hyperoxia vs. baseline)
SpO_2 (%)	96.2 ± 0.5	98.4 ± 0.2	-
PR (bpm)	72.4 ± 6.5	68.8 ± 7.2	0.070
BP_s (mm Hg)	128.4 ± 6.8	134.6 ± 5.8	0.045
BP_d (mm Hg)	74.6 ± 2.9	77.4 ± 2.9	0.135
BP_m (mm Hg)	92.5 ± 3.2	96.5 ± 2.7	0.041

Table 6.2: Systemic haemodynamics obtained for diabetic subjects. Data are presented as mean $\pm$ SE. t-tests were not performed on SpO_2 data as it was not found to be normally distributed.

Parameter (n = 11)	Baseline	Hyperoxia	p-value (hyperoxia vs. baseline)
SpO_2 (%)	96.6 ± 0.4	99.2 ± 0.2	-
PR (bpm)	74.0 ± 3.1	67.8 ± 2.5	0.000
BP_s (mm Hg)	109.5 ± 3.1	108.9 ± 4.3	0.856
BP_d (mm Hg)	71.3 ± 2.1	71.7 ± 1.7	0.831
BP_m (mm Hg)	84.0 ± 2.0	84.1 ± 2.4	0.961

Table 6.3: Systemic haemodynamics obtained for the healthy control subjects described in Chapter 6. Data are presented as mean $\pm$ SE. t-tests were not performed on SpO_2 data as it was not found to be normally distributed.

6.3.2 Vessel Diameter and Reactivity

Table 6.4 details the group-averaged arteriole diameter values, during the baseline and hyperoxic phases, across groups (i.e. hypertensives, diabetics, healthy controls). Figure 6.6 presents a comparison of the group-mean baseline diameters of the hypertensive, diabetic and control subjects. It is evident from Figure 6.6 that the baseline diameters did not differ between the hypertensive and control groups ($p = 0.732$). The baseline, group-mean arteriole diameters of the diabetic group appear to be a little smaller than those of the healthy controls, but a significant difference was not found between the groups ($p = 0.187$). It is also apparent, from the data in Table 6.4, that the arterioles underwent a significant constriction in the hypertensive and control groups, however, this was not the case for the diabetics for whom a significant vasoconstriction was not observed.

	Baseline Diameter (pixels)	Hyperoxic Diameter (pixels)	p-value (hyperoxia vs. baseline)
Hypertensives (n = 16)	50.6 $\pm$ 1.1	49.7 $\pm$ 1.1	0.036
Diabetics (n = 7)	43.8 $\pm$ 1.8	42.5 $\pm$ 1.7	0.210
Healthy Controls (n = 16)	49.6 $\pm$ 2.7	47.4 $\pm$ 2.7	0.000

Table 6.4: Comparing arteriole diameters across pathological status, before and during hyperoxic provocation. Data are presented as mean $\pm$ SE. NOTE: While the hypertensive group consisted of 15 subjects, the reactivity response of an arteriole in each eye of one of the volunteers was measured, giving 2 reactivity measurements for this volunteer. Therefore n = 16 for the hypertensive group. Similarly for the healthy controls, while the reactivity response of 11 volunteers was measured, the magnitude of arteriolar constriction was measured at 2 sites in 5 subjects. Therefore n = 16 for the healthy controls.

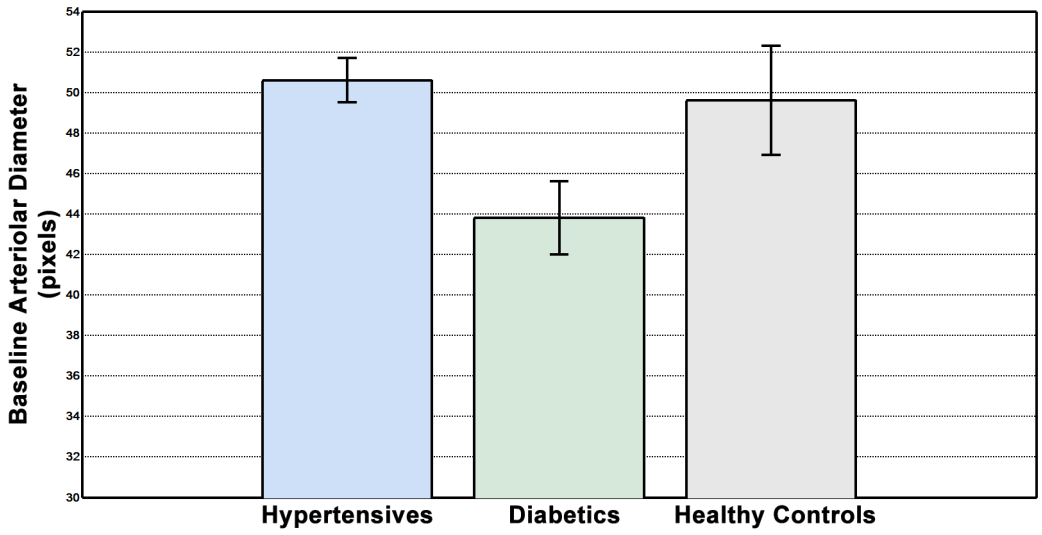

Figure 6.6: Baseline, group-mean arteriolar diameters of the hypertensive, diabetic and control groups. Data are presented as mean $\pm$ SE.

Table 6.5 details the percentage change in arteriolar diameter obtained for each group. Figure 6.7 presents a comparison of the group-averaged percentage change of the arteriole diameters, relative to baseline, attained by the hypertensives, diabetics and controls, during the hyperoxic phase. The data indicates that the degree of vasoconstriction achieved by the hypertensives was significantly less than that of the healthy control group (p = 0.004). The group-mean reactivity response of the diabetics is

somewhat more difficult to interpret due to the large standard error associated with it. The mean percentage change in arteriole diameter from baseline was found not to be significantly different to the control group (p = 0.200), however, performing a 1-sample t-test to assess whether the percentage constriction differed significantly from 0% resulted in a p-value of 0.219, implying that no significant constriction occurred in the diabetic group.

	% Difference
Hypertensives (n = 16)	-1.7 ± 0.7
Diabetics (n = 7)	-2.6 ± 1.9
Healthy Controls (n = 16)	-4.9 ± 0.8

Table 6.5: Comparing the percentage difference in arteriole diameters due to hyperoxia, compared to baseline, across pathological status. Data are presented as mean $\pm$ SE. Comparing arteriole diameters across pathological status, before and during hyperoxic provocation. Data are presented as mean $\pm$ SE. NOTE: While the hypertensive group consisted of 15 subjects, the reactivity response of an arteriole in each eye of one of the volunteers was measured, giving 2 reactivity measurements for this volunteer. Therefore n = 16 for the hypertensive group. Similarly for the healthy controls, while the reactivity response of 11 volunteers was measured, the magnitude of arteriolar constriction was measured at 2 sites in 5 subjects. Therefore n = 16 for the healthy controls.

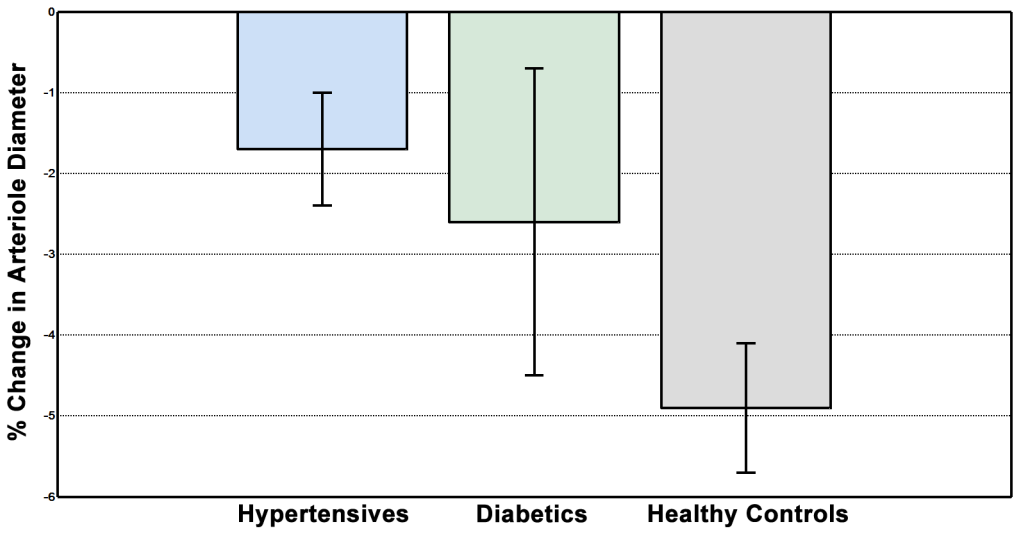

Figure 6.7: Comparing the percentage change in arteriolar diameter from baseline of the hypertensive, diabetic and control groups. Data are presented as mean $\pm$ SE.

6.4 Discussion

6.4.1 Systemic Haemodynamics

The increased level of SpO_2 in the hypertensive and the diabetic subjects, during the oxygen breathing phase, suggests that systemic hyperoxia was achieved in both groups.

In the hypertensive group, a small decrease in PR was observed during hyperoxia, as it was in the healthy control group. PR was found not to differ between the hypertensive and control group during either phase of the experiment. A previous study also found that PR of hypertensives did not differ from that of a healthy control group [28]. This is in agreement with what was expected, as cardiac output is believed to be normal or slightly reduced in hypertension [4,194]. In the diabetic group PR remained stable throughout the experiment and was found not to differ to that of the controls. This is in agreement with previous studies which also found that PR was not altered in diabetes [184] and that the PR of diabetics was unaffected by oxygen breathing [184,185].

BP_m of the hypertensive subjects was found not to alter throughout the experimental protocol. BP_m was found to be significantly higher in the hypertensive group in comparison to the healthy control group, in spite of antihypertensive therapy. This is not surprising as our exclusion criteria did not include sub-optimal blood pressure control and as a result the hypertension group included subjects with a range of blood pressure control. In the diabetic group BP_m underwent a small but significant increase during hyperoxia and was significantly higher than that of the normal control group. It is not surprising that BP_m was elevated in this diabetic group as 3 of the 7 participants also had hypertension, one of who was poorly controlled. Previous studies investigating hyperoxia-induced vasconstriction did not observe a change in BP_m in diabetics during oxygen breathing [25,184,185]. As discussed in Section 3.4.1, page 73, however, a small increase in BP_m, like the 4 mm Hg we observed in our diabetics, would have little or no effect on vascular tone. For example in the study by Bek at al. [192], an increase in BP_m of 20 mm Hg, induced by isometric exercise induced an non-significant vasoconstriction in normals and diabetics, while Jensen et al. [195] measured vasoconstrictions of just $\sim$2.5% and less than 1%, in response to isometric exercise-induced increases in BP_m of approximately 19 mm Hg and 20 mm Hg, in normals and diabetics respectively.

6.4.2 Vessel Diameter and Reactivity

A core feature of hypertension is narrowing of proximal resistance arteries and arterioles [4]. A number of large, population-based studies report narrowing of the retinal arterioles in people with hypertension [196–200] and also that a decreased arteriolar calibre in normotensives is predictive of future hypertension [201–204]. Our results, however, show that the baseline diameters of the hypertensive group did not differ to those of the control group; this was not the expected result. Upon comparing our result to those of other small studies investigating the reactivity response in hypertensive patients, we discovered that they too found baseline arteriolar diameters and blood flow to be comparable between hypertensives and controls. Pemp et al. [42] and Chapman et. al [98] measured retinal arteriolar diameters using a Retinal Vessel Analyser (RVA) and fundus camera respectively and both found the baseline diameters to be similar in hypertensives and normotensives. Delles et al. [205] measured blood flow velocity in retinal capillaries and the central retinal artery (CRA) using a scanning laser Doppler flowmeter (SLDF) and a pulsed Doppler sonograph respectively. They found blood flow velocity in the CRA and retinal capillary flow to be similar in normotensives and hypertensives. Studies investigating reactivity in the forearm of hypertensives also found basal forearm blood flow to be similar in hypertensives and controls [28, 30]. What could be the source of the discrepancy between our obtained result and the result we expected? There are a number of possibilities:

- In our and other small studies, where the total number of subjects ranged from 12 to a maximum of 110, there may have been an insufficient number of participants for the decrease in diameter of the retinal arterioles in hypertensives to reach significance and the large population-based studies, where the number of subjects ranged from 1,900 to 9,300, are required for this.

- Our subjects had been receiving anithypertensive therapy for a number of years. It has been reported in a number of studies that some therapies (angiotensin converting enzyme (ACE) inhibitors and angiotensin receptor blockers) may at least partially resolve the hypertension-induced structural changes in the vessel wall and normalise vessel calibre [206]. In studies by Hughes et al. [207] and Nagel et al. [208] arteriolar diameters were measured in untreated hypertensive patients using a fundus camera and RVA respectively. They then began antihypertensive treatment and were subsequently remeasured 52 weeks [207] and 24 months [208] later. In the study by Nagel they received 'various' antihypertensive therapies and in the Hughes study the therapy given was either

a calcium-channel-blocker or an ACE-inhibitor regimen. Both studies reported that therapy resulted in blood pressure reduction and an increase in the arteriolar diameter, with Nagel citing an increase of approximately 3.7 μm per 10 mm Hg reduction in BP_m. However, in a large population-based study conducted by Wong et al. [196], results suggest that well controlled blood pressure with antihypertensive therapy widened arteriolar diameters to some extent (persons with well-controlled hypertension had larger arterioles than those with untreated or poorly controlled hypertension), but that arterioles were still narrowed compared to normotensives. Many studies have also found arteriolar narrowing to be related to blood pressure levels measured 3-8 years previously, independent of concurrent BP [167, 169, 198, 200], suggesting that it is a persistent effect of elevated blood pressure. Also, in the other small studies, who did not find the arteriolar diameters of hypertensives to be decreased compared to normotensives, the hypertensive patients were untreated [42, 98, 205], so this would not explain the discrepancy in their cases.

- Some of the large studies have reported that the degree of arteriolar narrowing due to high blood pressure was greater in younger subjects [196, 199]. Wong et al. [196] reported that retinal arteriolar diameters were narrower by 7.0 μm in persons aged 43 to 54 years and by 2.5 μm in persons aged 75 to 80 years for each 10 mm Hg increase in BP_m; while Ikram et al. [199] found that hypertension-induced narrowing became insignificant in hypertensives aged 80 years or more. As our group of hypertensives did not consist of younger individuals, with only one person being under 65 years and ten of the fifteen subjects being over 70 years of age, the degree of narrowing may be expected to be less. However, as arterioles also narrow with increasing age [196,197], our hypertensives may still be expected to have smaller vessel calibre as they were considerable older than the control group. The other small studies were approximately age-matched and included younger patients, in their thirties, forties and fifties, in the cohort [28, 30, 42, 98, 205], so this would not explain why they did not observe reduced arteriolar diameters in their hypertensive patients.

The unexpected result we obtained (baseline arteriolar diameters similar in hypertensives and normotensives) may have been as a result of any, or a combination, of the above reasons. No satisfactory conclusions can therefore be drawn from the baseline arteriolar diameters of our hypertensive group at this time, and further work is necessary to determine if narrowing caused by elevated blood pressure can be observed in small studies, if antihypertensive treatment restores normal vessel calibre, and to

confirm if the influence of elevated blood pressure on arteriolar narrowing diminishes with increasing age.

Using a hyperoxic provocation we discovered a significantly smaller vasoconstriction in patients with hypertension compared to their normotensive counterparts. Sieker et al. [54] and Chapman et al. [98] also used oxygen breathing to provoke an arteriolar constriction. They both used a fundus camera to image the arterioles and they both found vasoconstriction to be significantly reduced in hypertensives. Chapman also used hypercapnia to provoke vasodilation and they also found this response to be significantly attenuated in hypertensives. Pemp et al. [42] and Nagel et al. [48] used RVA systems to assess the retinal arteriolar reaction to a flicker stimulus. Both studies found the flicker-induced vasodilation to be reduced in hypertension. Delles et al. [205] also used a flicker stimulus and found that it provoked an increase in blood flow velocity in the CRA in normotensive subjects but that it had no significant effect on blood flow velocity in hypertensive subjects. In the brachial artery [42] and the vasculature of the forearm [28–30, 34] the reactivity response of hypertensive subjects has also been shown to be subtantially diminished compared to normotensive subjects.

It is currently unclear what causes the diminished reactivity response in hypertension. A number of possible causes have been hypothesised including endothelial cell damage, reduced nitric oxide (NO) bioavailability and structural, sclerotic wall changes that render a diameter change impossible. Studies performed by Ghiadoni et al, Panza et al. and Taddei et al. [28–30, 34, 35] demonstrated that the vasodilatory response in the forearm of hypertensives in response to acetylcholine (an endothelium-dependent vasodilator) was significantly reduced compared to normotensives, but that their response to sodium nitroprusside (an endothelium independent vasodilator) was found to be similar to that of the control group. As endothelium-independent dilation was found to be undiminished in hypertensives, this would imply that structural changes in the vessel walls of hypertensives do not impede the reactivity capacity of the arterioles of hypertensives. It is widely accepted that NO is a primary mediator in flicker-induced vasodilation [36], because of this, it is believed that diminished production of NO linked to endothelial cell damage or a reduction in its availability due to excess reactive oxygen species (ROS) (ROS production is believed to be abnormally high in hypertension [206]) could be responsible for the reduced flicker response in hypertension [209]. The results from previous studies appear to bear this out. Delles et al. [205] showed that L-NMMA (L-NMMA inhibits the synthesis of NO) significantly decreased retinal capillary flow in normal control subjects,

but that it had no significant effect on retinal capillary flow in hypertensives. Ghiadoni et al. [35] also observed that L- NMMA caused a significantly greater reduction in forearm blood flow in normotensives compared to hypertensives. In normotensives L-NMMA also increased BP_m and decreased PR, however, in hypertensives it decreased PR but had no significant effect on BP_m [205]. This implies that it increased peripheral resistance in normotensives but not in hypertensives. Panza et al. and Ghiadoni et al. [30, 35] showed that L-NMMA blunted the response of acetylcholine (endothelium-dependent vasodilator) in the forearms of normotensives but did not significantly alter the degree of dilation in hypertensives. The results of these studies indicate that both a basal and stimulated deficit of NO exists in hypertensives and they are therefore unaffected by inhibition of its synthesis by L-NMMA. The cause of the reduced vasoconstrictive response to hyperoxia is currently unknown. One potential cause is that narrowing of the arterioles in hypertension reduces the capacity for further increases in vascular tone in response to oxygen breathing, resulting in the diminished response we observed. The study by Ghiadoni et al. [35] suggests that this is not the case. They observed that the degree vasoconstriction in the forearm of hypertensives in response to norepinephrine (an endothelium-independent vasoconstrictor) was only slightly blunted compared to normotensives; they did not compare this endothelium-independent response to an endothelium-dependent vasoconstriction however. Further studies are required to confirm this finding. Another possibility is a reduced production or availability of endothelin-1, as it is believed to play a primary role in hyperoxia-induced constriction [40], however there is little information pertaining to the effects of elevated blood pressure on endothelin-1 levels. The study of Ghiadoni et al. [35] also observed the effects of TAK-044 (an endothelin-1 receptor antagonist) and they recorded a small degree of vasodilation in normotensives and a more pronounced vasodilation in hypertensives. This result would imply that basal levels of endothelin-1 are actually elevated in hypertension, which would not explain the diminished vasoconstrictive response to a hyperoxic stimulus (which Ghiadoni and co-workers did not measure). Further work is necessary to elucidate the mechanisms involved in endothelial dysfunction in hypertension.

It should be noted that our reactivity results should be interpreted with a certain degree of caution for a couple of reasons. Firstly, all of our hypertensive subjects were receiving antihypertensive treatment, and had been for a number of years, and there is some evidence that some antihypertensive therapies (ACE inhibitors and angiotension receptor blockers) may improve endothelial function in hypertension [209]. The handful of previous studies that have investigated whether antihypertensive therapy restores endothelial function in humans have been somewhat inconsistent. Delles et

al. [205] found that after 7 days of treatment with an angiotensin-receptor-blocker, in previously untreated hypertensives, the retinal capillary flow response to L-NMMA increased, as did the blood flow velocity flicker response in the CRA. Ghiadoni et al. [35,210], also found that ACE inhibitors improved endothelial function in the forearm of patients with previously untreated essential hypertension. In contrast to this this result, Nagel et al. [48] found the flicker response to be unaltered after 24 months of 'various' antihypertensive treatment using an RVA. Panza et al. [34] also found the response to acetylcholine to be unmodified in the forearm by a range of antihypertensive medications, however, as they compared the response of patients while taking medication to the response of the same patients just 2 weeks after withdrawal of the medication, this should probably not be considered as a definitive result. While the effect of antihypertensive treatment remains unresolved, if therapy does restore endothelial function to some degree, we would expect to find the reactivity response to be even more blunted in untreated hypertensives and therefore this does not preclude us from drawing the conclusion that vasoconstriction is blunted by elevated blood pressure. Our second note of caution is that our hypertensive and normotensive subjects were not age-matched, with the hypertensive group being significantly older than the control group (mean age $\pm$ SD: hypertensives - 73.5 $\pm$ 9.8 years; controls - 48.4 $\pm$ 8.3 years). This limitation is of greater concern because the reactivity response diminishes with age, as we saw in Chapter 5, therefore the diminished reactivity response could be at least partially attributable to their greater age. However, the other studies were approximately age-matched and they all found a diminution of reactivity with elevated blood pressure. Therefore we believe that if our subjects had been age-matched, while the difference in vasoconstriction between hypertensives and normotensives may have been less pronounced, we still would have observed a difference. While we would be somewhat reticent to draw conclusions based solely on our results, as all previous (age-matched) studies also found reactivity to be reduced, we believe we can tentatively conclude that reactivity is impaired in hypertension.

Previous studies have reported abnormalities of the haemodynamic parameters measured in diabetics, however, results remain controversial. Some large studies have shown that arteriolar narrowing may be associated with risk of developing type 2 diabetes [173, 211, 212], and with incidence and progression of diabetic retinopathy [180], others have demonstrated that it is an increase in venular calibre that is associated with risk of diabetes and incidence and development of diabetic retinopa-

thy [213–216], while Rogers et al. [217] found that increased arteriolar calibre was associated with incident diabetic retinopathy and Tikellis et al. [215] found that retinal arterioles were significantly larger in diabetics but that risk of retinopathy was associated with venular dilation. Small studies on the other hand, for the most part, observed no difference in vessel calibre with diabetes [25,184,185,191,192,218]. In our diabetic group, the group-mean baseline arteriolar diameter was less than the normal control group, but this difference was not significant. We don't believe we can draw any conclusions about arteriolar diameters in diabetes from our results, due to the small number of diabetics studied, and the numerous limitations of our study (discussed in the next section). Substantial work in the future is required to resolve this issue and high resolution imaging may aid investigators arriving at a definitive result.

We are unable to draw any conclusions about hyperoxia-induced vasoconstriction in diabetics from our data, because while the percentage constriction measured did not differ significantly from 0%, it was also not significantly different to the vasoconstriction observed in our healthy controls. This is due to numerous limitations, including the low number of diabetic subjects measured. However, it has been repeatedly demonstrated in previous studies, that the retinal vascular reactivity response to flickering-light stimulation [42, 179, 181, 183, 185, 191, 192, 195, 219], hyperoxia [25, 54,182,184,185,220] and isometric exercise [195,221] is impaired in diabetes. This impairment has been measured in patients before the appearance of any signs of diabetic retinopathy [42,179,219], and has been demonstrated to increase with increasing levels of retinopathy [179,184,220], leading many to believe that it may be a pathogenic factor in the development of diabetic retinopathy. The cause of this impairment is unknown, but possibilities include functional damage of the endothelial cells and loss of pericytes and smooth muscle cells. Loss of smooth muscle cells in arterioles and pericytes destruction in capillaries appears to be widely accepted [14,15,176,177], and has been observed in studies of dogs with diabetes [222]. However, studies comparing the vasodilatory response to acetylcholine (endothelium-dependent dilator) and sodium nitroprusside or glyceryl trinitrate (endothelium-independent dilators) have been inconsistent with their findings. All the studies observed an impaired response to acetylcholine, but while some studies also found the endothelium-independent dilation to also be diminished [188, 223–225], others did not [189, 226, 227]. It is also reported that NO availability is diminished in diabetes [14, 33] for a number of speculated reasons, including decreased production and decreased bioavailability due to an increase in superoxide generation [10, 14, 33]. Some believe that the production of endothelin-1 is increased in diabetes [10, 33, 180], but as endothelin-1 is believed to play a major role in vasoconstriction in response to oxygen breathing [40], how an in-

crease in endothelin-1 production relates to the diminished response to hyperoxia in diabetics, which has been consistently found in previous studies, remains uncertain. The degree to which these factors play a role in reduced reactivity and the development and progression of diabetic retinopathy remains unknown. Therefore, while it is widely accepted that vasomotor responses are impaired in diabetes, further work is necessary to elucidate the underlying mechanisms.

Limitations of Study

There were a number of limitations associated with this study.

- Firstly, the cohorts were not ideal. While the mean age of the diabetics (56.3 $\pm$ 8.6 years) was not vastly different to that of the normal control group (mean age: 48.4 $\pm$ 8.3 years), the hypertensives (mean age: 73.5 $\pm$ 9.8 years) were significantly older than the control group, making comparisons between them somewhat untenable. As vessel calibre and reactivity response diminish with age, age-matched samples are crucial.

- The patient samples were small (the diabetics in particular), with subjects having different levels of disease severity. The hypertensives had varying degrees of blood pressure control; the diabetics had varying degrees of blood glucose level control, duration of disease, degree of retinopathy and three had concurrent hypertension (one with poor control despite antihypertensive treatment). To draw satisfactory results and to obtain greater insight into these conditions, larger samples sizes are necessary with patients graded according to severity of disease and coexistence of complications (e.g. concurrent hypertension in diabetics).

- All the patients were undergoing some form of treatment, therefore the possibility that medication may have influnced the parameters being measured (e.g. reversing arteriolar narrowing or restoring endothelial function) could not be ruled out. Ideally, baseline measurements would have been made in patients before they commenced treatment and they would have been remeasured some months, or possible years later, to assess the affect of medication on the parameters measured.

- While none of the patients were currently smokers, three of the hypertensives were ex-smokers, having quit 1, 9 and 23 years previous to the study. It is known that chronic smoking blunts the reaction of arterioles to a stimulus, as shown in

Chapter 4, however, it is not known if this is reversed after quitting and if it is, the timeline of this reversal needs to be elucidated. It is also unknown if vascular reactivity continues to decrease as the number of years smoking increases. A greater understanding of the effects of smoking on endothelial function is required.

- Patients abstained from caffeine for a shorter period (at least 3 hours) than the control group (at least 12 hours). This was unavoidable as the full experimental protocol has to be performed in one visit and as suitable participants were identified by an ophthalmologist during routine clinical assessment there was no way to request patients abstained from caffeine prior to the study day.

- As is experienced by all other imaging studies, many potential participants could not be included in the study due to unclear optic media, which would result in poor quality images.

- While the experimental protocol for our study involved fairly simple tasks (fixating steadily on a target) and the time required to perform our measurements was not extensive, taking approximately 20-30 minutes, for older subjects this proved difficult. Imaging at a small field of view (FOV) requires the subject to sit very still and to fixate steadily; many older subjects were just not able to do this for the time required, due to eye fatigue and discomfort from remaining as still as possible. This meant that image acquisition became increasingly difficult as the experiment progressed. This excluded many older participants, who would otherwise have been suitable for inclusion. For this reason, the importance of keeping the protocol time as short as possible cannot be understated.

- The fixation target we used in all of our experiments was a Samsung Galaxy Tab^{TM}, which displayed a red dot that could be altered in size and moved around the screen by the investigator to centre the arteriole of interest in the captured image. Subjects fixated on the target with the opposite eye to the one being imaged. This setup had worked very well in our previous experiments on smokers etc., but difficulties were encountered when imaging some patients. Many of our subjects were pseudophakic, as we found we could obtain the best images from these patients. Some of these participants, however, had one pseudophakic eye (which we imaged) and were awaiting surgery for their fellow eye (which fixated on the target). In these patients if the cataract in their fixating eye was quite cloudy, or if they had any other sight-impairment in this eye, their fixation on the target was more unstable, making image acquisition at the small

FOV more difficult, and impossible in some cases. For this reason, if conducting further work in a clinical setting, I would look into improving the fixation target, to aid measurements in these types of patients. Imaging at a small FOV would, however, remain quite challenging in older subjects, regardless of the target used.

6.4.3 Conclusions

No firm conclusions can be drawn from our results in this study. We did, however, assess the difficulties of using our set-up in a clinical setting, which would be valuable for future experiments, allowing for improvements in the set-up and modification of the protocol.

Chapter 7

Conclusions

In this thesis, we presented a study of the retinal arteriolar reaction to a hyperoxic stimulus. This was achieved using a high resolution confocal scanning laser ophthalmoscope and image processing techniques. To our knowledge, this is the first time a high-resolution imaging technique has been applied to the task of investigating retinal vascular reactivity. This chapter is divided into two sections. Firstly, we will summarise and discuss the findings of our work, including conclusions drawn from the results obtained. We will then discuss topics derived from this work that remained without investigation, but could potentially be addressed by future research.

7.1 Summary of Thesis Work

In Chapter 2, we detailed the image processing techniques applied to our images. The first step was to desinusoid the images to remove the distortion caused by the velocity of the horizontal scanner varying across each scan line. Our image registration algorithm, which was implemented to facilitate image averaging, was then described, followed by our semi-automated vessel tracking and diameter measurement method.

We comprehensively examined the retinal arteriolar response of young, normal subjects to oxygen breathing and came to a number of conclusions. From the results of the systemic parameters measured we were able to conclude that the constriction of arterioles observed during hyperoxic provocation is due to metabolic regulation. We

also observed that, arteriole diameters constrict during the first 5 minutes of oxygen breathing, plateau, and remain stable while hyperoxia is maintained. Arteriole diameters increase back to their baseline values upon cessation of oxygen breathing. The reaction of arteriolar diameters to hyperoxia is faster than their recovery to baseline. We also found that blood flow to the temporal retina is higher than to the nasal retina, while flow to the superior and inferior retinae does not differ. We measured the arteriolar response to hyperoxia in an arteriole in each quadrant of the retina and determined that the magnitude of vasoconstriction does not vary across retinal regions. We compared the percentage constriction of large and small retinal arterioles and concluded that the percentage constriction attained, does not depend of vessel size. The retinal arteriolar reactivity response is independent of retinal region and vessel calibre and therefore a reactivity measurement taken from a single arbitrary site can be considered as representative of the reactivity response of the retinal vasculature as a whole.

The chronic and acute effects of smoking on the reactivity response of retinal arterioles was investigated in otherwise healthy, young subjects. From the results of the systemic parameters measured we were able to conclude that the constriction of arterioles in our group of smokers in response to hyperoxia was due to endothelium-dependent metabolic regulation. From these experiments it was determined that the baseline arteriolar diameters of smokers do not differ to those of non-smokers and are unaltered by acute cigarette smoking. Our results also indicated that the retinal arteriolar response to hyperoxia is diminished in smokers compared to non-smokers, suggesting impaired endothelial function from long-term smoking, while acute smoking had no effect on the magnitude of hyperoxia induced vasoconstriction.

The effect of healthy aging on arteriolar vasoconstriction in response to hyperoxia was also investigated. From the results of the systemic parameters measured we were able to conclude that the constriction of the arterioles observed during hyperoxic provocation was due to endothelium-dependent vasoconstriction. From these experiments it was determined that retinal arteriolar constrictions due to oxygen breathing are significantly diminished with advancing age.

Finally, we obtained some preliminary data in hypertensives and diabetics, which allowed us to assess the difficulties of using the modified HRT-classic and our experimental protocol to obtain measurements in patients. From the systemic parameters measured in these subjects we were able to conclude that systemic hyperoxia was achieved in both patient groups and that the arteriolar responses observed were due to endothelium-dependent metabolic regulation. While we were unable to draw any

firm conclusions from the diameter and reactivity results of this section of our study, many areas of interest for future research were identified and these experiments also exposed the difficulties of conducting our study in patients in a clinical setting, highlighting the importance of a short protocol, a comfortable and relaxed subject and a more versatile target.

7.2 Proposal for Future Research

There is a substantial amount of potential future work in this area. In our case, we would commence by investigating the possibility of introducing a new target within the instrument to allow the eye being imaged to also be the fixating eye. This would provide us a greater ability to image vessels closer to the fovea, and provide greater flexibility when imaging patients; for example, this would alleviate the problem of imaging a patient with one pseudophakic eye and a cataract or other visual impairment in their fellow eye, this issue was described in Section 6.4.2. We would incorporate axial measurements, using a Zeiss IOLMaster®, and velocity measurements, using a birdirectional laser Doppler velocimeter, into the experimental protocol. Axial length measurements would allow us to convert diameter measurements from pixels to μm, which would aid intergroup comparisons of baseline diameters, for example when comparing: smokers vs. non-smokers; older persons vs. younger persons; patients vs. healthy normals. As discussed in Section 1.7, page 22, vessel diameter measurements are a good surrogate marker for blood flow measurements, however, if velocity measurements could also be obtained this would allow us to calculate the volumetric blood flow, which is the ideal outcome measure. We would also investigate the possibility of including other provocations, such as flicking light, into our experiments. This would provide valuable additional information. The vasodilatory response elicited by flicker, in combination with the hyperoxia-induced vasoconstriction data, would give the full reactivity range of the subjects. In some subjects, such as smokers and patients, measuring the response to a number of stimuli which provoke a reaction by activating different pathways, may provide valuable information to help understand the exact mechanisms underlying their endothelial dysfunction. It may allow us to identify the most practical stimulation method to implement in patients, for example, flicker may allow for a shorter experimental protocol.

We would test the above, suggested amendments in the experimental setup and protocol in normal subjects, as this would also facilitate the collection of more normative data, of which there is a lack, and much of that which does exist, is contradictory. For

example, due to the ambiguous nature of the results reported in the handful of previous studies, I would take the opportunity to confirm my findings that the reactivity response is independent of retinal region and vessel size. Also, while we conclusively showed that there was no difference in reactivity response between larger and smaller vessels for the range of vessels measured in our experiments, this conclusion was based on vessels ranging in size from approx. 19 pixels ($\sim$38 μm) to approx. 45 pixels ($\sim$90 μm). Therefore, we cannot rule out the possibility that the largest retinal arterioles react to a different degree to the smallest vessels. We would therefore address this issue, and obtain measurements in the largest and smallest retinal vessels to confirm that reactivity is independent of retinal vessel size.

The effects of smoking on endothelial function remain poorly understood. While we obtained conclusive results from our experiments in young subjects, previous studies have been equivocal with regards the acute effect of smoking on baseline diameters and on the chronic effects of smoking on the reactivity response. We would therefore like to repeat these measurements, with the addition of axial length and velocity measurements to allow calculation of vessel diameters and volumetric blood flow, to confirm our findings and to finally provide a definitive result. It is not known if vascular reactivity continues to diminish as the number of cigarettes smoked per day or the number of years smoking increases. It is also unknown if this impairment is reversed upon cessation of the habit. This needs to be investigated by obtaining measurements in a very large group of smokers, who have been smoking for a wide range of years, and ex-smokers who have quit for a range of years. While a diminution of NO bioavailability has been postulated to be the cause of the impairment of reactivity, this also remains to be clarified. The addition of other provocations, such as flicker stimulation or L-NMMA administration, may help to shed some light on this.

It has been definitively shown that arteriolar response to oxygen breathing is reduced with age, the reason for this reduction is, however, unknown. A study which investigates endothelium-dependent and independent vasoconstriction may help resolve this point in question. As aging has been shown to decrease the arteriolar response to hyperoxia, for this provocation to be used in clinical studies, it is vital that the rate of this decline in reactivity is known. A study needs to be undertaken which investigates the reactivity response in a large number of people with a wide range of ages, to observe how reactivity diminishes with age. It should also be confirmed whether vasodilation in response to a flicker stimulus really is unaltered by aging, which has been suggested by a small number of previous studies. If further investigation supported previous results, this may provide a means of simplifying reactivity

measurements in clinical studies.

A large number of studies have been conducted to investigate vessel calibre and reactivity in hypertension and diabetes; however, substantial work remains to be done in these areas. In hypertension, it is widely accepted that arteriolar narrowing occurs and this has been repeatedly demonstrated in both cross-sectional and prospective, population-based studies [196–200], and is suggested to associated with CVD mortality [171]. Small studies on the other hand, with subject numbers less than $\sim$100, repeatedly fail to find a significant difference in arteriolar calibre between hypertensives and normals [28, 30, 42, 98, 205]. This may suggest that interindividual scatter is just too large to allow this parameter to be used to assess risk in individuals. This needs to be investigated. Endothelial function is also emerging as a possible factor for risk prediction in CVDs. While it has been unequivocally shown that endothelial function is diminished in hypertension [42, 48, 54, 98, 205], there needs to be a demonstration of independent predictive value that substantially adds to traditional risk factors; thus far, this has not been conclusively demonstrated. The source of this dysfunction also remains to be elucidated by further work. Finally, there is a need to evaluate whether any existing medications can restore arteriolar caliber and endothelial function, and, if so, whether this approach will result in improved patient outcomes and a reduced risk of cardiovascular morbidity and mortality. The exact pathogenesis of diabetic retinopathy remains incompletely understood. The effect of diabetes on vessel calibre remains unresolved due to the contradictory nature of previous results. Resolution of this matter may provide insights into the underlying mechanisms of the progression of disease. As with hypertension however, the vast majority of small studies observed no vessel calibre changes in diabetes, which again raises the question of whether calibre measurements will prove useful in differentiating risk at an individual level. There is now a large body of evidence from small, cross-sectional studies of a diminution of the reactivity response in diabetics. Furthermore, reactivity has been shown to be impaired before the incidence of diabetic retinopathy [42, 179, 219]; and that this impairment worsens with increasing retinopathy severity [179,184,220]; for this reason it has been suggested that endothelial function may be a pathogenic factor in the development of diabetic retinopathy. Long-term observational studies are required to determine if endothelial dysfunction does indeed predict incidence and progression of diabetic retinopathy. Future studies are also needed to determine which factors alter endothelial function in diabetes and to assess whether any medications can restore function and whether restoration of function can prevent or at least slow diabetic retinopathy progression.

The good performance of high-resolution imaging in any random subject, in particular one that might be ill-at-ease due to pathology, cannot yet be guaranteed. In spite of this, the utility of high-reolution retinal imaging in the clinical environment needs to be thoroughly investigated, as its use in the measurement of changes in retinal vascular calibre and reactivity, offers great potential to advance our understanding of the early pathophysiological pathways of disease development.

Appendix A: Statistical Methods

The Sampling Distribution and Standard Error

When samples of size n are drawn from a given population, the sample mean will vary from sample to sample [228,229]. If we were able to draw all the possible samples of size n from the population and calculate their means, these means would form a distribution [228, 229]. The distribution of all possible means that can be drawn from a population is called the sampling distribution [229]. The means of our samples are therefore themselves a sample from this sampling distribution. The mean of the sampling distribution equals the mean of the parent distribution, whilst its standard deviation is equal to $\sigma/\sqrt{n}$, where σ is the standard deviation of the population [228, 229]. The standard deviation of the sampling distribution is called the standard error [228, 229]. The sample mean is an estimate of the population mean and the standard error provides a measure of how well the sample mean estimates the population mean [228, 229]. The standard error is inversely proportional to the sample size; therefore as the size of the samples increases, the dispersion of the sample means decreases [228]. In the majority of circumstances we do not know the standard deviation of the population, and it is therefore estimated using the standard deviation of the sample means, s. The standard error is therefore calculated using this estimate: $s/\sqrt{n}$ [229].

The one-sample t-test

We may wish to test whether the mean of certain data is consistent with a given value. If the sample is small (usually taken to mean $n < 30$), and the standard deviation of the data from which the sample is drawn is unknown, a t-test, sometimes known as a t-score, is used:

$$t_{score} = \frac{\bar{x} - \mu}{\frac{s}{\sqrt{n}}}$$

We are determining how many standard errors the sample mean, $\bar{x}$, is from the mean of the null hypothesis, μ. The t-test assumes that the data from which the sample was drawn is approximately normally distributed. The t-distribution depends on the number of degrees of freedom and as n increases the t-distribution becomes more and more like the Normal distribution [229].

The independent samples t-test

If we wish to compare the means of two small samples drawn from independent sets of data, we use the independent samples t-test. This test assumes that the data from which both samples were drawn are approximately normally distributed and have approximately the same variance [229]. The test statistic is calculated as:

$$t_{obs} = \frac{\bar{x}_1 - \bar{x}_2}{\sqrt{\frac{s_p^2}{n_1} + \frac{s_p^2}{n_2}}}$$

where

$$s_p = \sqrt{\frac{(n_1 - 1)s_1^2 + (n_2 - 1)s_2^2}{n_1 + n_2 - 2}}$$

s_p^2 is known as the pooled variance, which is an estimate of the common variance. The number of degrees of freedom, df, are calculated by:

$$df = n_1 + n_2 - 2$$

The paired samples t-test

The independent samples t-test assumes that the populations from which the two samples were drawn are independent. If we wish to compare two samples that are not independent (for example in this thesis we wanted to compare vessel diameters measured before and after causing them to constrict), we use the paired samples t-

test. This test is also commonly called the repeated measures t-test. In this test the differences (the decreases in vessel diameters) are calculated and a one-sample t-test to test the null hypothesis that the mean vessel constriction was zero is performed.

Analysis of variance (ANOVA)

Analysis of variance (ANOVA) compares the means of three or more samples, with the null hypothesis being that all the means are equal. To implement the ANOVA procedure the data must adhere to the following assumptions [229]:

- The samples must be independent
- Each sample must be approximately normally distributed
- The variance of the samples must be approximately equal, to allow for the calculation of a pooled variance

ANOVA of two samples is another way of performing an independent samples t-test [229]. As the ANOVA procedure is somewhat long-winded to calculate by hand, and is now always implemented using software packages such as Minitab®, we will not go into the detail of its calculation here.

The Tukey honest significance difference (HSD) test is a post-hoc test, performed after an ANOVA test. If a difference between samples is found, a Tukey test is performed to determine which means differ from which [229]. The Tukey test is a conservative estimate, meaning that if this test finds a difference between sample means, there almost certainly is one – the chances of committing a type I error are low.

The Anderson-Darling test

Many of the tests described above assumed that the population from which the samples are drawn are normally distributed. Therefore, to assess if our data satisfies this assumption, we first use the Anderson-Darling test. This test measures how well the data follows a particular distribution (the normal distribution in our case). The better the data fits the specified distribution the smaller this statistic is. In Minitab® an associated p-value is also quoted, with the null hypothesis being that the data follows the specified distribution. Therefore, if the p-value is lower than the chosen significance level (usually $\alpha = 0.05$) conclude that the data does not follow the specified distribution.

Bibliography

[1] G. Liew and J. J. Wang. Retinal vascular signs: A window to the heart. *Rev Esp Cardiol*, 64(6):515–21, 2011.

[2] M. L. Baker, P. J. Hand, G. Liew, T. Y. Wong, E. Rochtchina, P. Mitchell, R. I. Lindley, G. J. Hankey, J. J. Wang, and the Multi-centre Retinal Stroke Study Group. Retinal microvascular signs may provide clues to the underlying vasculopathy in patients with deep intracerebral hemorrhage. *Stroke*, 41:618–623, 2010.

[3] Tony Garcia, Ghislain Bonnay, Ayman Tourbah, and Carl Arndt. Optical coherence tomography in neuro-ophthalomology. Online, 2013. Available from: http://www.intechopen.com/books/optical-coherence-tomography/optical-coherence-tomography-in-neuro-ophthalmology.

[4] J. Rodney Levick. *An Introduction to Cardiovascular Physiology*. Hodder Arnold, 2011.

[5] Dee Unglaub Silverthorn. *Human Physiology. An Integrated Approach.* Pearson. Benjamin Cummings., 2004.

[6] C. L. Stanfield and W. J. Germann. *Principles of Human Physiology*. Pearson. Benjamin Cummings., 2009.

[7] F. Tayyari. The relationship between retinal vascular reactivity and arteriolar diameter. Master's thesis, University of Waterloo, Ontario, Canada, 2006.

[8] Paul L. Kaufman and Albert Alm, editors. *Adler's Physiology of the Eye: Clinical Application*. Mosby, tenth edition, 2003. Various Authors.

[9] M. J. Mulvany and C. Aalkjaer. Structure and function of small arteries. *Physiological Reviews*, 70(4):921–961, 1990.

[10] Ivan O. Haefliger, Josef Flammer, Jean-Louis Beny, and Thomas F. Luscher. Endothelium-dependent vasoactive modulation in the ophthalmic circulation. *Progress in Retinal and Eye Research*, 20(2):209 – 225, 2001.

[11] Richard S. Snell and Michael A. Lemp. *Clinical Amatomy of the Eye*. Blackwell Publishing Ltd, second edition, 1998.

[12] Faryan Tayyari, Subha T. Venkataraman, Edward D. Gilmore, Tien Wong, Joseph Fisher, and Chris Hudson. The relationship between retinal vascular reactivity and arteriolar diameter in response to metabolic provocation. *Investigative Ophthalmology & Visual Science*, 50(10):4814–4821, 2009.

[13] Constantin J. Pournaras, Elisabeth Rungger-Brandle, Charles E. Riva, Sveinn H. Hardarson, and Einar Stefansson. Regulation of retinal blood flow in health and disease. *Progress in Retinal and Eye Research*, 27:284–330, 2008.

[14] E. D. Gilmore, C. Hudson, R. K. Nrusimhadevara, P. T. Harvey, M. Mandelcorn, W. C. Lam, and R. G. Devenyi. Retinal arteriolar diameter, blood velocity, and blood flow response to an isocapnic hyperoxic provocation in early sight-threatening diabetic retinopathy. *Investigative Ophthalmology & Visual Science*, 48(4):1744–1750, 2007.

[15] N. Patton, T. Aslam, T. MacGillivray, A. Pattie, I. J. Deary, and B. Dhillon. Retinal vascular image analysis as a potential screening tool for cerebrovascular disease: a rationale based on homology between cerebral and retinal microvasculatures. *Journal of Anatomy*, 206:319–348, 2005.

[16] Alon Harris, Larry Kagemann, and George A. Cioffi. Assessment of human ocular hemodynamics. *Survey of Ophthalmology*, 42(6):509–532, 1998.

[17] L. Schmetterer and M. Wolzt. Ocular blood flow and associated functional deviation in diabetic retinopathy. *Diabetologia*, 42(4):387–405, 1999.

[18] V. A. Alder, E. N. Su, D. Yu, S. Cringle, and P. Yu. Overview of studies on metabolic and vascular regulatory changes in early diabetic retinopathy. *Australian and New Zealand Journal of Ophthalmology*, 26:141–148, 1998.

[19] A Bill and G O Sperber. Control of retinal and choroidal blood flow. *Eye*, 4:319–325, 1990.

[20] H. S. Badeer. Hemodynamics for medical students. *Advan in Physiol Edu*, 25:44–52, 2001.

[21] Seendy Jean-Louis, John V. Lovasik, and Helene Kergoat. Systemic hyperoxia and retinal vasomotor responses. *Investigative Ophthalmology & Visual Science*, 46(5):1714–1720, 2005.

[22] Edward D. Gilmore, Chris Hudson, David Preiss, and Joe Fisher. Retinal arteriolar diameter, blood velocity, and blood flow response to an isocapnic hyperoxic provocation. *American Journal of Physiology - Heart and Circulatory Physiology*, 288(6):H2912–H2917, 2005.

[23] Martin J. Dumskyj, Jesper E. Eriksen, Caroline J. Dore, and Eva M. Kohner. Autoregulation in the human retinal circulation: Assessment using isometric exercise, laser doppler velocimetry, and computer-assisted image analysis. *Microvascular Research*, 51:378–392, 1996.

[24] Peter Jeppesen, PernilleA Gregersen, and Toke Bek. The age-dependent decrease in the myogenic response of retinal arterioles as studied with the retinal vessel analyzer. *Graefe's Archive for Clinical and Experimental Ophthalmology*, 242:914–919, 2004.

[25] B. L. Justesen, P. Mistry, N. Chaturvedi, S. A. Thom, N. Witt, D. Kohler, A. D. Hughes, and A. K. Sjolie. Retinal arterioles have impaired reactivity to hyperoxia in type 1 diabetes. *Acta Ophthalmologica*, 88(4):453–457, 2010.

[26] K. E. Pyke and M. E. Tschakovsky. The relationship between shear stress and flow-mediated dilation: implications for the assessment of endothelial function. *J Physiol*, 568(2):357–369, 2005.

[27] M. C. Corretti, T. J. Anderson, E. J. Benjamin, D. Celermajer, F. Charbonneau, M. A. Creager, J. Deanfield, H. Drexler, M. Gerhard-Herman, D. Herrington, P. Vallance, J. Vita, and R. Vogel. Guidelines for the ultrasound assessment of endothelial dependent flow-mediated vasodilation of the brachial artery. *Journal of the American College of Cardiology*, 39(2):257–265, 2002.

[28] J. A. Panza, A. A. Quyyumi, J. E. Brush, and S. E. Epstein. Abnormal endothelium-dependent vascular relaxation in patients with essential hypertension. *The New England Journal of Medicine*, 323:22–27, 1990.

[29] Stefano Taddei, Agostino Virdis, Paola Mattei, Lorenzo Ghiadoni, Alessandra Gennari, Ciro Basile Fasolo, Isabella Sudano, and Antonio Salvetti. Aging and endothelial function in normotensive subjects and patients with essential hypertension. *Circulation*, 91(7):1981–1987, 1995.

[30] J. A. Panza, P. R. Casino, C. M. Kilcoyne, and A. A. Quyyumi. Role of endothelium-derived nitric oxide in the abnormal endothelium-dependent vascular relaxation of patients with essential hypertension. *Circulation*, 87:1468–1474, 1993.

[31] L. Lind, S. Granstam, and J. Millgard. Endothelium-dependent vasodilation in hypertension: A review. *Blood Pressure*, 9:4–15, 2000.

[32] Martin McIntyre, David F. Bohr, and Anna F. Dominiczak. Endothelial function in hypertension: The role of superoxide anion. *Hypertension*, 34(4):539–545, 1999.

[33] J Cai and M Boulton. The pathogenesis of diabetic retinopathy: old concepts and new questions. *Eye*, 16(3):242–260, 2002.

[34] Julio A. Panza, Arshed A. Quyyumi, Timothy S. Callahan, and Stephen E. Epstein. Effect of antihypertensive treatment on endothelium-dependent vascular relaxation in patients with essential hypertension. *Journal of the American College of Cardiology*, 21(5):1145–1151, 1993.

[35] Lorenzo Ghiadoni, Agostino Virdis, Armando Magagna, Stefano Taddei, and Antonio Salvetti. Effect of the angiotensin II type 1 receptor blocker candesartan on endothelial function in patients with essential hypertension. *Circulation*, 35(1):501–506, 2000.

[36] Guido T. Dorner, Gerhard Garhofer, Barbara Kiss, Elzbieta Polska, Kaija Polak, Charles E. Riva, and Leopold Schmetterer. Nitric oxide regulates retinal vascular tone in humans. *American Journal of Physiology - Heart and Circulatory Physiology*, 285(2):H631–H636, 2003.

[37] R. Heitmar and R. J. Summers. Assessing vascular function using dynamic retinal diameter measurements: A new insight on the endothelium. *Thrombosis and Haemostasis*, 107:1019–1026, 2012.

[38] R. Roberts, H. Luan, and B. A. Berkowitz. Blocking ET-1 receptors does not correct subnormal retinal oxygenation response in experimental diabetic retinopathy. *Investigative Ophthalmology & Visual Science*, 47(8):3550–3555, 2006.

[39] Mohammad M. Rahman and Ismail Laher. Structural and functional alteration of blood vessels caused by cigarette smoking: An overview of molecular mechanisms. *Current Vascular Pharmacology*, 5:276–292, 2007.

[40] Susanne Dallinger, Guido T. Dorner, Roland Wenzel, Ursula Graselli, Oliver Findl, Hans-Georg Eichler, Michael Wolzt, and Leopold Schmetterer. Endothelin-1 contributes to hyperoxia-induced vasoconstriction in the human retina. *Investigative Ophthalmology & Visual Science*, 41(3):864–869, 2000.

[41] Subha T. Venkataraman, Chris Hudson, Joseph A. Fisher, Lisa Rodrigues, Alexandra Mardimae, and John G. Flanagan. Retinal arteriolar and capillary vascular reactivity in response to isoxic hypercapnia. *Experimental Eye Research*, 87:535–542, 2008.

[42] Berthold Pemp, Günther Weigert, Katharina Karl, Ursula Petzl, Michael Wolzt, Leopold Schmetterer, and Gerhard Garhofer. Correlation of flicker-induced and flow-mediated vasodilatation in patients with endothelial dysfunction and healthy volunteers. *Diabetes Care*, 32:1536–1541, 2009.

[43] Peter Jeppesen, Javad Sanye-Hajari, and Toke Bek. Increased blood pressure induces a diameter response of retinal arterioles that increases with decreasing arteriolar diameter. *Investigative Ophthalmology & Visual Science*, 48(1):328–331, 2007.

[44] F Robinson, C E Riva, J E Grunwald, B L Petrig, and S H Sinclair. Retinal blood flow autoregulation in response to an acute increase in blood pressure. *Investigative Ophthalmology & Visual Science*, 27(5):722–6, 1986.

[45] H Tachibana, F Gotoh, and Y Ishikawa. Retinal vascular autoregulation in normal subjects. *Stroke*, 13(2):149–55, 1982.

[46] C E Riva, J E Grunwald, and S H Sinclair. Laser doppler velocimetry study of the effect of pure oxygen breathing on retinal blood flow. *Investigative Ophthalmology & Visual Science*, 24(1):47–51, 1983.

[47] Gerhard Garhofer, Hemma Resch, Stefan Sacu, Gunther Weigert, Doreen Schmidl, Michael Lasta, and Leopold Schmetterer. Effect of regular smoking on flicker induced retinal vasodilatation in healthy subjects. *Microvascular Research*, 82(3):351 – 355, 2011.

[48] Edgar Nagel, Walthard Vilser, and Ines Lanzl. Age, blood pressure, and vessel diameter as factors influencing the arterial retinal flicker response. *Investigative Ophthalmology & Visual Science*, 45(5):1486–1492, 2004.

[49] Kaija Polak, Leopold Schmetterer, and Charles E. Riva. Influence of flicker frequency on flicker-induced changes of retinal vessel diameter. *Investigative Ophthalmology & Visual Science*, 43(8):2721–2726, 2002.

[50] Epilepsy Action (British Epilepsy Association). Photosensitive epilepsy. Online, March 2012. http://goo.gl/3gUlE.

[51] Barbara Kiss, Elzbieta Polska, Guido Dorner, Kaija Polak, Oliver Findl, Gabriele Fuchsjager Mayrl, Hans-Georg Eichler, Michael Wolzt, and Leopold Schmetterer. Retinal blood flow during hyperoxia in humans revisited: Concerted results using different measurement techniques. *Microvascular Research*, 64(1):75 – 85, 2002.

[52] A Luksch, G Garhofer, A Imhof, K Polak, E Polska, G T Dorner, S Anzenhofer, M Wolzt, and L Schmetterer. Effect of inhalation of different mixtures of O_2 and CO_2 on retinal blood flow. *British Journal of Ophthalmology*, 86(10):1143–1147, 2002.

[53] Leopold Schmetterer, Franz Lexer, Oliver Findl, Ursula Graselli, Hans-Georg Eichler, and Michael Wolzt. The effect of inhalation of different mixtures of O_2 and CO_2 on ocular fundus pulsations. *Experimental Eye Research*, 63:351–355, 1996.

[54] H. O. Sieker and J. B. Hickham. Normal and impaired retinal vascular reactivity. *Circulation*, 7(1):79–83, 1953.

[55] F. Lacombe, M. Glanc, J. Le Gargasson, C. Bellmann, M. Paques, and J. Sahel. Direct measurements of blood cells density and velocity in retinal micro vessels. *Ophthalmic Technologies XVI*, 6138(1):61381, 2006.

[56] Leopold Schmetterer and Gerhard Garhofer. How can blood flow be measured? *Survey of Ophthalmology*, 52(6, Supplement):S134 – S138, 2007.

[57] L Schmetterer, S Dallinger, O Findl, K Strenn, U Graselli, H G Eichler, and M Wolzt. Noninvasive investigations of the normal ocular circulation in humans. *Investigative Ophthalmology & Visual Science*, 39(7):1210–20, 1998.

[58] Alexandra Luksch, Michael Lasta, Kaija Polak, Gabriele Fuchsjager-Mayrl, Elzbieta Polska, Gerhard Garhofer, and Leopold Schmetterer. Twelve-hour reproducibility of retinal and optic nerve blood flow parameters in healthy individuals. *Acta Ophthalmologica*, 87(8):875–880, 2009.

[59] S. T. Venkataraman, C. Hudson, J. A. Fisher, and J. G. Flanagan. Novel methodology to comprehansively assess retinal arteriolar vascular reactivity to hypercapnia. *Microvascular Research*, 72:101–107, 2006.

[60] B Wimpissinger, H Resch, F Berisha, G Weigert, L Schmetterer, and K Polak. Response of choroidal blood flow to carbogen breathing in smokers and non-smokers. *British Journal of Ophthalmology*, 88(6):776–781, 2004.

[61] Marcus Langhans, Georg Michelson, and Michael J M Groh. Effect of breathing 100 per cent oxygen on retinal and optic nerve head capillary blood flow in smokers and non-smokers. *British Journal of Ophthalmology*, 81(5):365–369, 1997.

[62] J. D. Briers. Laser doppler, speckle and related techniques for blood perfusion mapping and imaging. *Physiol. Meas*, 22:R35–R66, 2001.

[63] Yasuhiro Tamaki, Makoto Araie, Miyuki Nagahara, and Ken Tomita. Acute effects of cigarette smoking on tissue circulation in human optic nerve head and choroid-retina. *Ophthalmology*, 106(3):564 – 569, 1999.

[64] Yasuhiro Tamaki, Makoto Araie, Miyuki Nagahara, Ken Tomita, and Masao Matsubara. The acute effects of cigarette smoking on human optic nerve head and posterior fundus circulation in light smokers. *Eye*, 14(1):67–72, 2000.

[65] K. Polak, G. Dorner, B. Kiss, E. Polska, O. Findl, G. Rainer, H. Eichler, and L. Schmetterer. Evaluation of the Zeiss retinal vessel analyser. *Br J Ophthalmol*, 84:1285–1290, 2000.

[66] G. Gerhofer, T. Bek, A. G. Boehm, D. Gherghel, J. Grunwald, P. Jeppesen, H. Kergoat, K. Kotliar, I. Lanzl, J. V. Lovasik, E. Nagel, W. Vilser, S. Orgul, and L. Schmetterer. Use of the retinal vessel analyser in ocular blood flow research. *Acta Ophthalmologica*, 88:717–722, 2010.

[67] B. Seifert and W. Vilser. Retinal Vessel Analyser (RVA) – Design and function. *Biomed Tech*, 47, 2002.

[68] W. Vilser, E. Nagel, and I. Lanzl. Retinal vessel analysis – new possibilities. *Biomed Tech (Berl)*, 47:682–685, 2002.

[69] T. Kida, S. Harino, T. Sugiyama, K. Kitanishi, Y. Iwahashi, and T. Ikeda. Change in retinal arterial blood flow in the contralateral eye of retinal vein occlusion during glucose tolerance test. *Graefe's Archive for Clinical and Experimental Ophthalmology*, 240:342–347, 2002.

[70] Akitoshi Yoshida, Gilbert T Feke, Fumihiko Mori, Taiji Nagaoka, Naoki Fujio, Hironobu Ogasawara, Suguru Konno, and J.Wallace Mcmeel. Reproducibility and clinical application of a newly developed stabilized retinal laser doppler instrument. *American Journal of Ophthalmology*, 135(3):356–361, 2003.

[71] Kit Guan, Chris Hudson, and John G Flanagan. Variability and repeatability of retinal blood flow measurements using the canon laser blood flowmeter. *Microvascular Research*, 65(3):145–151, 2003.

[72] K. Guan, C. Hudson, T. Wong, M. Kisilevsky, R. K. Nrusimhadevara, W. K. Lam, M. Mandelcorn, R. G. Devenyi, and J. G. Flanagan. Retinal hemodynamics in early diabetic macular edema. *Diabetes*, 55:813–818, 2006.

[73] C. A. Girkin. Principles of confocal scanning laser ophthalmoscopy for the clinician. Online. http://goo.gl/wIhcX.

[74] David W. Arathorn, Qiang Yang, Curtis R. Vogel, Yuhua Zhang, Pavan Tiruveedhula, and Austin Roorda. Retinally stabilized cone-targeted stimulus delivery. *Opt. Express*, 15(21):13731–13744, Oct 2007.

[75] S J Pakola and J E Grunwald. Effects of oxygen and carbon dioxide on human retinal circulation. *Investigative Ophthalmology & Visual Science*, 34(10):2866–70, 1993.

[76] Mitra Sehi, Edmund Tsui, Richard Cheng, Jennifer Wan, Tien Wong, Stephanie Dorner, Joseph Fisher, and Christopher Hudson. Relative magnitude of vascular reactivity in the major arterioles of the retina. *Microvascular Research*, 83:200–204, 2012.

[77] Leopold F. Schmetterer, Franz Lexer, Christian J. Unfried, Harald Sattmann, and Adolf F. Fercher. Topical measurement of fundus pulsations. *Optical Engineering*, 34(3):711–716, 1995.

[78] Helene Kergoat and Caroline Faucher. Effects of oxygen and carbogen breathing on choroidal hemodynamics in humans. *Investigative Ophthalmology & Visual Science*, 40(12):2906–2911, 1999.

[79] S.B. Stevenson and A. Roorda. Correcting for miniature eye movements in high resolution scanning laser ophthalmoscopy. In Fabrice Manns, Per G. Soderberg, and Arthur Ho, editors, *Ophthalmic Technologies XV*, volume 5688A, pages 145–151. SPIE, 2005.

[80] Alfredo Dubra and Zachary Harvey. Registration of 2D images from fast scanning ophthalmic instruments. In Bernd Fischer, Benoat Dawant, and Cristian

Lorenz, editors, *Biomedical Image Registration*, volume 6204 of *Lecture Notes in Computer Science*, pages 60–71. Springer Berlin / Heidelberg, 2010.

[81] Susana Martinez-Conde, Stephen L. Macknik, and David H. Hubel. The role of fixational eye movements in visual perception. *Nature Reviews Neuroscience*, 5:229–240, March 2004.

[82] Lorrin A. Riggs, John G. Flanagan C. Armington, and Floyd Ratliff. Motions of the retinal image during fixation. *J. Opt. Soc. Am.*, 44(4):315–321, Apr 1954.

[83] M. Ezenman, P.E Hallett, and R.C. Frecker. Power spectra for ocular drift and tremor. *Vision Research*, 25(11):1635 – 1640, 1985.

[84] Joseph W. Goodman. *Introduction to Fourier Optics*. Roberts & Company Publishers, third edition.

[85] J.P. Lewis. Fast template matching. *Vision Interface*, pages 120–123, 1995.

[86] Curtis R. Vogel, David W. Arathorn, Austin Roorda, and Albert Parker. Retinal motion estimation in adaptive optics scanning laser ophthalmoscopy. *Opt. Express*, 14(2):487–497, Jan 2006.

[87] N Chapman, N Witt, X Gao, A A Bharath, A V Stanton, S A Thom, and A D Hughes. Computer algorithms for the automated measurement of retinal arteriolar diameters. *British Journal of Ophthalmology*, 85(1):74–79, 2001.

[88] Shruti A. Japee, Christopher G. Ellis, and Roland N. Pittman. Flow visualization tools for image analysis of capillary networks. *Microcirculation*, 11(1):39–54, 2004.

[89] Y. Sato, Jian Chen, R.A. Zoroofi, N. Harada, S. Tamura, and T. Shiga. Automatic extraction and measurement of leukocyte motion in microvessels using spatiotemporal image analysis. *Biomedical Engineering, IEEE Transactions on*, 44:225–236, 1997.

[90] Johnny Tam and Austin Roorda. Speed quantification and tracking of moving objects in adaptive optics scanning laser ophthalmoscopy. *Journal of Biomedical Optics*, 16(3):036002–036002–11, 2011.

[91] Johnny Tam, Joy A. Martin, and Austin Roorda. Noninvasive visualization and analysis of parafoveal capillaries in humans. *Investigative Ophthalmology & Visual Science*, 51(3):1691–1698, 2010.

[92] S M B Rassam, V Patel, H C Chen, and E M Kohner. Regional retinal blood flow and vascular autoregulation. *Eye*, 10:331–337, 1996.

[93] W E Sponsel, K L DePaul, and S R Zetlan. Retinal hemodynamic effects of carbon dioxide, hyperoxia, and mild hypoxia. *Investigative Ophthalmology & Visual Science*, 33(6):1864–9, 1992.

[94] K. Lorentz, A. Zayas-Santiago, S. Tummala, and J.J. Kang Derwent. Scanning laser ophthalmoscope-particle tracking method to assess blood velocity during hypoxia abd hyperoxia. *Adv. Exp. Med Biol.*, 614:253–261, 2008.

[95] Rebekka Heitmar, Andrew Blann, Robert P Cubbidge, Gregory Lip, and Doina Gherghel. Continuous retinal vessel diameter measurements - the future of retinal vessel assessment? *Investigative Ophthalmology & Visual Science*, 51(11):5833–39, 2010.

[96] Hak Sung Chung, Alon Harris, Paul J. Halter, Larry Kagemann, Emma J. Roff, Hanna J. Garzozi, Sarah L. Hosking, and Bruce J. Martin. Regional differences in retinal vascular reactivity. *Investigative Ophthalmology & Visual Science*, 40(10):2448–2453, 1999.

[97] TA Deutsch, JS Read, J Ernest, and TK Goldstick. Effects of oxygen and carbon dioxide on the retinal vasculature in humans. *Archives of Ophthalmology*, 101(8):1278–1280, 1983.

[98] N Chapman, G Haimes, A V Stanton, S A Thom, and A D Hughes. Acute effects of oxygen and carbon dioxide on retinal vascular network geometry in hypertensive and normotensive subjects. *Clin. Sci.*, 99:483–488, 2000.

[99] G T Feke, H Tagawa, D M Deupree, D G Goger, J Sebag, and J J Weiter. Blood flow in the normal human retina. *Investigative Ophthalmology & Visual Science*, 30(1):58–65, 1989.

[100] C E Riva, J E Grunwald, S H Sinclair, and B L Petrig. Blood velocity and volumetric flow rate in human retinal vessels. *Investigative Ophthalmology & Visual Science*, 26(8):1124–32, 1985.

[101] CA Giller, G Bowman, H Dyer, L Mootz, and W Kripper. Cerebral arterial diameters during changes in blood pressure and carbon dioxide during craniotomy. *Neurosurgery*, 32:737–741, 1993.

[102] World Health Organisation. Who report on the global tobacco epidemic, 2011: warning about the dangers of tobacco. (online), www.who.int/tobacco/globalreport/2011, May 2012.

[103] Yoram Solberg, Mordechai Rosner, and Michael Belkin. The association between cigarette smoking and ocular diseases. *Survey of Ophthalmology*, 42(6):535 – 547, 1998.

[104] M. Chiba and R. Masironi. Toxic and trace elements in tobacco and tobacco smoke. *Bulletin of the World Healthy Organization*, 70(2):269–275, 1992.

[105] John A Ambrose and Rajat S Barua. The pathophysiology of cigarette smoking and cardiovascular disease: An update. *Journal of the American College of Cardiology*, 42(10):1731–1737, 2004.

[106] F Robinson, B L Petrig, and C E Riva. The acute effect of cigarette smoking on macular capillary blood flow in humans. *Investigative Ophthalmology & Visual Science*, 26(5):609–13, 1985.

[107] Hedwig J Kaiser, Andreas Schoetzau, and Josef Flammer. Blood flow velocity in the extraocular vessels in chronic smokers. *British Journal of Ophthalmology*, 81(2):133–135, 1997.

[108] A. C. Pearce and R. M. Jones. Smoking and anesthesia: Preoperative abstinence and perioperative morbidity. *Anesthesiology*, 61:576–584, 1984.

[109] Neal L. Benowitz. The role of nicotine in smoking-related cardiovascular disease. *Preventive Medicine*, 26:412–417, 1997.

[110] CL Sarin, JC Austin, and WO Nickel. Effects of smoking on digital blood-flow velocity. *JAMA*, 229(10):1327–1328, 1974.

[111] B. Waeber, M. D. Schaller, J. Nussberger, J. P. Bussien, K. G. Hofbauer, and H. R. Brunner. Skin blood flow reduction induced by cigarette smoking: role of vasopressin. *American Journal of Physiology - Heart and Circulatory Physiology*, 247(6):H895–H901, 1984.

[112] G. Monfrecola, G. Riccio, C. Savarese, G. Posteraro, and E.M. Procaccini. The acute effect of smoking on cutaneous microcirculation blood flow in habitual smokers and nonsmokers. *Dermatology*, 197:115–118, 1998.

[113] P. Lehtovirta and M. Forss. The acute effect of smoking on intervillous blood flow of the placenta. *BJOG: An International Journal of Obstetrics & Gynaecology*, 85(10):729–731, 1978.

[114] RL Rogers, JS Meyer, TG Shaw, KF Mortel, and J Thornby. The effects of chronic cigaretter smoking on cerebrovascular responsiveness to 5% CO_2 and 100% O_2 inhalation. *J AM Geriatr Soc.*, 6:415–20, 1984.

[115] A.M. Zeiher, V. Schachinger, and J. Minners. Long-term cigarette smoking impairs endothelium-dependent coronary arterial vasodilator function. *Circulation*, 92:1094–1100, 1995.

[116] D S Celermajer, K E Sorensen, D Georgakopoulos, C Bull, O Thomas, J Robinson, and J E Deanfield. Cigarette smoking is associated with dose-related and potentially reversible impairment of endothelium-dependent dilation in healthy young adults. *Circulation*, 88(5):2149–55, 1993.

[117] D.S. Celermajer, M.R. Adams, P. Clarkson, J. Robinson, R. McCredie, A. Donald, and J. E. Deanfield. Passive smoking and impaired endothelium-dependent arterial dilation in healthy young adults. *The New England Journal of Medicine*, pages 150–154, 1996.

[118] Rajat S. Barua, John A. Ambrose, Lesley-Jane Eales-Reynolds, Mary C. DeVoe, John G. Zervas, and Dhanonjoy C. Saha. Dysfunctional endothelial nitric oxide biosynthesis in healthy smokers with impaired endothelium-dependent vasodilatation. *Circulation*, 104:1905–1910, 2001.

[119] Pavel Poredos, Marta Orehek, and Erika Tratnik. Smoking is associated with dose-related increase of intima-media thickness and endothelial dysfunction. *Angiology*, 50(3):201–208, 1999.

[120] J. Lekakis, C. Papamichael, C. Vemmos, J. Nanas, D. Kontoyannis, S. Stamatelopoulos, and S. Moulopoulos. Effect of acute cigarette smoking on endothelium-dependent brachial artery dilation in healthy individuals. *The American Journal of Cardiology*, 79:529–531, 1997.

[121] R. G. Ijzerman, E.H. Serne, M.M. VanWeissenbruch, R.T. DeJongh, and C.D.A. Stehouwer. Cigarette smoking is associated with an acute impairment of microvascular function in humans. *Clinical Science*, 104:247–252, 2003.

[122] R Cubbidge, RJ Summers, and R Heitmar. Retinal vessel reactivity after cigarette smoking. *Acta Ophthalmologica*, 90:0–0, 2012.

[123] Barbara Wimpissinger, Hemma Resch, Fatmire Berisha, Gunther Weigert, Kaija Polak, and Leopold Schmetterer. Effects of isometric exercise on subfoveal choroidal blood flow in smokers and nonsmokers. *Investigative Ophthalmology & Visual Science*, 44(11):4859–4863, 2003.

[124] Pedro B. Morgado, Hean C. Chen, Vinod Patel, Luke Herbert, and Eva M. Kohner. The acute effect of smoking on retinal blood flow in subjects with and withour diabetes. *Ophthalmology*, 101:1220–1226, 1994.

[125] A. Light, C. Grass, D. Pursley, and J. Krause. Carboxyhemoglobin levels in smokers vs. non-smokers in a smoking environment. *Respir Care*, 52(11):1576, 2007.

[126] Barbara Wimpissinger, Hemma Resch, Fatmire Berisha, Ganther Weigert, Leopold Schmetterer, and Kaija Polak. Response of retinal blood flow to systemic hyperoxia in smokers and nonsmokers. *Graefe's Archive for Clinical and Experimental Ophthalmology*, 243:646–652, 2005.

[127] J. Reddy Kambam, Lily H. Chen, and Steve A. Hyman. Effect of short-term smoking halt on carboxyhemoglobin levels and p50 values. *Anesthesia & Analgesia*, 65(11):1186–1188, 1986.

[128] A K Armitage, C T Dollery, C F George, T H Houseman, P J Lewis, and D M Turner. Absorption and metabolism of nicotine from cigarettes. *British Medical Journal*, 4:313–316, 1975.

[129] N L Benowitz, P Jacob, R T Jones, and J Rosenberg. Interindividual variability in the metabolism and cardiovascular effects of nicotine in man. *The American Society for Pharmacology*, 221:368–372, 1982.

[130] Andrew D Blann, Ursula Kirkpatrick, Carol Devine, Salina Naser, and Charles N McCollum. The influence of acute smoking on leucocytes, platelets and the endothelium. *Atherosclerosis*, 141:133–139, 1998.

[131] Tom H. Williamson, Gordon D. O. Lowe, and Grant M. Baxter. Influence of age, systemic blood pressure, smoking, and blood viscosity on orbital blood velocities. *British Journal of Ophthalmology*, 79:17–22, 1995.

[132] Robert D. Steigerwalt, Giuseppe Laurora, Lucrezia Incandela, Maria Rosaria Cesarone, Gianni V. Belcaro, and Maria Teresa De Sanctis. Ocular and orbital blood flow in cigarette smokers. *Retina*, 20:394–397, 2000.

[133] I. Gul, H. Karapinar, M. Yarioglues, I. Ozdogru, M. G. Kaya, A. Yilmaz, O. O. Turgut, I. Tandogan, and N. K. Eryol. Acute effects of passive smoking on endothelial function. *Angiology*, 63(3):245–247, 2011.

[134] T. Kato, T. Inoue, T. Morooka, N. Yoshimoto, and K. Node. Short-term passive smoking causes endothelial dysfunction via oxidative stress in nonsmokers. *Canadian Journal of Physiology and Pharmacology*, 84(5):523–529, 2006.

[135] J. Lekakis, C. Papamichael, C. Vemmos, K. Stamatelopoulos, A. Voutsas, and S. Stamatelopoulos. Effects of acute cigarette smoking on endothelium-dependent arterial dilation in nornal subjects. *The American Journal of Cardiology*, 81(10):1225–1228, 1998.

[136] M. Sarabi and L. Lind. Short-term effects of smoking and nicotine chewing gum on endothelium-dependent vasodilation in young healthy habitual smokers. *Journal of Cardiovascular Pharmacology*, 35(3):451–456, 2000.

[137] Jin-Yan Zhang, Yong-Xiao-Cao, Cang-Bao Xu, and Lars Edvinsson. Lipid-soluble smoke particles damage endothelial cells and reduce endothelium-dependent dilation in rat and man. *BMC Cardiovascular Disorders*, 6(3), 2006.

[138] M. A. Hassan Talukder, Wesley M. Johnson, Saradhadevi Varadharaj, Jiarui Lian, Patrick N. Kearns, Mohamed A. El-Mahdy, Xiaoping Liu, and Jay L. Zweier. Chronic cigarette smoking causes hypertension, increased oxidative stress, impaired no bioavailability, endothelial dysfunction, and cardiac remodeling in mice. *American Journal of Physiology - Heart and Circulatory Physiology*, 300(1):388–396, 2011.

[139] G E McVeigh, L Lemay, D Morgan, and J N Cohn. Effects of long-term cigarette smoking on endothelium-dependent responses in humans. *Am J Cardiol*, 78:668–672, 1996.

[140] J. Marin and M. A. Rodriguez-Martinez. Age-related changes in vascular responses. *Experimental Gerontology*, 34:503–512, 1999.

[141] Michael F. O'Rourke and Junichiro Hashimoto. Mechanical factors in arterial aging: A clinical perspective. *Journal of the American College of Cardiology*, 50:1–13, 2007.

[142] P. Moreau, L. V. d'Uscio, and T. F. Luscher. Structure and reactivity of small arteries in aging. *Cardiovascular Reseach*, 37:247–253, 1998.

[143] J. M. Muller-Delp. Aging-induced adaptations of microvascular reactivity. *Microcirculation*, 13:301–314, 2006.

[144] M. Barton, F. Cosentino, R. P. Brandes, P. Moreau, S. Shaw, and T. F. Lüscher. Anatomic heterogeneity of vascular aging: Role of nitric oxide and endothelin. *Hypertension*, 30:817–824, 1997.

[145] A. J. Donato, L. B. Gano, I. Eskurza, A. E. Silver, P. E. Gates, K. Jablonski, and D. R. Seals. Vascular endothelial dysfunction with aging: endothelin-1 and endothelial nitric oxide synthase. *American Journal of Physiology - Heart and Circulatory Physiology*, 297(1):H425–H432, July 2009.

[146] M. R. Tschudi, M. Barton, N. A. Bersinger, P. Moreau, F. Cosentino, G. Noll, T. Malinski, and T. F. Luscher. Effect of age on kinetics of nitric oxide release in rat aorta and pulmonary artery. *The American Society for Clinical Investigation*, 98(4):899–905, 1996.

[147] J. E. Grunwald, J. Piltz, N. Patel, S. Bose, and C. E. Riva. Effect of aging on retinal macular microcirculation: A blue field suimulation study. *Investigative Ophthalmology & Visual Science*, 34(13):3609–3613, 1993.

[148] J. E. Grunwald, S. M. Hariprasad, and J. DuPont. Effect of aging on foveolar choroidal circulation. *Arch Ophthalmol*, 116:150–154, 1998.

[149] A. G. Boehm, A. U. Koeller, and L. E. Pillunat. The effct of age on optic nerve head blood flow. *Investigative Ophthalmology & Visual Science*, 46(4):1291–1295, 2005.

[150] M. J. Groh, G. Michelson, and J. Harazny. Influences of age on retinal and optic nerve head blood circulation. *Ophthalmology*, 103(3):529–34, 1996.

[151] Tien Yin Wong, Ronald Klein, A.Richey Sharrett, Teri A Manolio, Larry D Hubbard, Emily K Marino, Lewis Kuller, Gregory Burke, Russell P Tracy, Joseph F Polak, John S Gottdiener, and David S Siscovick. The prevalence and risk factors of retinal microvascular abnormalities in older persons: the cardiovascular health study. *Ophthalmology*, 110:658–666, 2003.

[152] S J Embleton, S L Hosking, E J Roff Hilton, and I A Cunliffe. Effect of senescence on ocular blood flow in the retina, neuroretinal rim and lamina cribrosa, using scanning laser doppler flowmetry. *Eye*, 16(2):156–162, 2002.

[153] M. Blum, K. Bachmann, and J. Strobel. [age-correlation of blood pressure induced myogenic autoregulation of human retinal arterioles in 40 volunteers]. *Klin Monbl Augenheilkd*, 217(4):225–30, October 2000.

[154] M. Blum, C. Scherf, K. Bachmann, and J. Strobel. Alterskorrelierte kontraktilitatt retinaler arteriolen bei sauerstoffatmung. *Der Ophthalmologe*, 98:265–268, 2001.

[155] M. Kneser, T. Kohlmann, J. Pokorny, and F. Tost. Age related decline of microvascular regulation measured in healthy individuals by retinal dynamic vessel analysis. *Med Sci Monit*, 15(8):436–441, 2009.

[156] K. Kamiya, K. Shimizu, and F. Ohmoto. Effect of aging on corneal biomechanical parameters using the ocular response analyser. *J Refract Surg*, 25(10):888–93, 2009.

[157] R. David, L. Zangwill, D. Stone, and Y. Yassur. Epidemiology of intraocular pressure in a population screened for glaucoma. *British Journal of Ophthalmology*, 71:776–771, 1987.

[158] L. Bonomi, G. Marchini, M. Marraffa, P. Bernardi, I. De Franco, S. Perfetti, A. Varotto, and V. Tenna. Prevalence of glaucoma and intraocular pressure distribution in a defined population. *Ophthalmology*, 105(2):209–215, 1998.

[159] World Health Organisation. Cardiovascular diseases (CVDs): Fact sheet. Online, March 2013. http://www.who.int/mediacentre/factsheets/fs317/en/index.html.

[160] World Health Organisation. 2003 world health organisation (WHO)/International Society of Hypertension (ISH) statement on management of hypertension. *Journal of Hypertension*, 21:1983–1992, 2003.

[161] *Basic and Clinical Science Course: Retina and Vitreous*. San Francisco: American Academy of Ophthalmology, 2006-2007.

[162] B Williams, N R Poulter, M J Brown, M Davis, G T McInnes, J F Potter, P S Sever, and S McG Thom. Guidelines for management of hypertension: report of the fourth working party of the british hypertension society, 2004–BHS IV. *J Hum Hypertens*, 18:139–185, 2004.

[163] A. D. Hughes. The clinical assessment of retinal microvascular structure and therapeutic implications. *Current Treatment Options in Cardiovascular Medicine*, 9(3):236–241, 2007.

[164] Marcus Gunn. On ophthalmoscopic evidence of general arterial disease. *Trans Ophthalmol Soc UK*, pages 356–81, 1898.

[165] N. M. Keith, H. P. Wagener, and N. W. Barker. Some different types of essential hypertension: Their course and prognosis. *AM J MED SCI*, pages 332–43, 1939.

[166] B. H. van den Born, C. A. A. Hulsman, J. B. L. Hoekstra, R. O. Schlingemann, and G. A van Montfrans. Value of routine funduscopy in patients with hypertension: systematic review. *BMJ*, 331:73–6, 2005.

[167] Tien Yin Wong, Jie Jin Wang, Elena Rochtchina, Ronald Klein, and Paul Mitchell. Does refractive error influence the association of blood pressure and retinal vessel diameters? the blue mountains eye study. *American Journal of Ophthalmology*, 137(6):1050–1055, 2004.

[168] Thanh T. Nguyen and Tien Y. Wong. Retinal vascular manifestations of metabolic disorders. *Trends in Endocrinology & Metabolism*, 17(7):262–268, 2006.

[169] Tien Yin Wong, Ronald Klein, Barbara E.K Klein, James M Tielsch, Larry Hubbard, and F.Javier Nieto. Retinal microvascular abnormalities and their relationship with hypertension, cardiovascular disease, and mortality. *Survey of Ophthalmology*, 46(1):59–80, 2001.

[170] Noyan Gokce, John F. Keaney, Liza M. Hunter, Michael T. Watkins, James O. Menzoian, and Joseph A. Vita. Risk stratification for postoperative cardiovascular events via noninvasive assessment of endothelial function: A prospective study. *Circulation*, 105(13):13, 2002.

[171] Tien Yin Wong, Ronald Klein, F.Javier Nieto, Barbara E.K Klein, A.Richey Sharrett, Stacy M Meuer, Larry D Hubbard, and James M Tielsch. Retinal microvascular abnormalities and 10-year cardiovascular mortality: A population-based case-control study. *Ophthalmology*, 110(5):933 – 940, 2003.

[172] World Health Organisation. Diabetes: Fact Sheet. Online, March 2013. http://who.int/mediacentre/factsheets/fs312/en/index.html.

[173] T. Y. Wong, R. Klein, A. R. Sharrett, M. I. Schmidt, J. S. Pankow, D. J. Couper, B. E. K. Klein, L. D. Hubbard, and B. B. Duncan. Retinal arteriolar narrowing and risk of diabetes mellitus in middle-aged persons. *JAMA*, 287(19):2528–2533, 2002.

[174] Rudy W. Bilous. *Understanding Diabetes*. Family Doctor Publications Limited in association with the British Medical Association, 2009.

[175] Retina Panel Preferred Practice Patterns Committee. Preferred practice pattern guidelines. diabetic retinopathy. *San Francisco: American Academy of Ophthalmolgy*, 2008.

[176] A.M. Joussen. *Retinal Vascular Disease*. Springer, 2007.

[177] J.J. Kanski. *Clinical Ophthalmology: A systematic Approach*. Butterworth-Heinemann, 2007.

[178] M. V. van Hecke, J. M. Dekker, G. Nijpels, A. C. Moll, R. J. Heine, L. M. Bouter, B. C. P. Polak, and C. D. A. Stehouwer. Inflammation and endothelial dysfunction are associated with retinopathy: the hoorn study. *Diabetologia*, 48:1300–1306, 2005.

[179] Aleksandra Mandecka, Jens Dawczynski, Marcus Blum, Nicolle Müller, Christoph Kloos, Gunter Wolf, Walthard Vilser, Heike Hoyer, and Ulrich Alfons Müller. Influence of flickering light on the retinal vessels in diabetic patients. *Diabetes Care*, 30(12):3048–3052, 2007.

[180] T. Nagaoka, E. Sato, A. Takahashi, H. Yokota, K. Sogowa, and A. Yoshida. Impaired retinal circulation in patients with type 2 diabetes mellitus: Retinal laser doppler velocimetry study. *Investigative Ophthalmology & Visual Science*, 51(12):6729–6734, 2010.

[181] Thanh T. Nguyen, Ryo Kawasaki, Jie Jin Wang, Andreas J. Kreis, Jonathan Shaw, Walthard Vilser, and Tien Y. Wong. Flicker light–induced retinal vasodilation in diabetes and diabetic retinopathy. *Diabetes Care*, 32(11):2075–2080, 2009.

[182] J E Grunwald, C E Riva, J Baine, and A J Brucker. Total retinal volumetric blood flow rate in diabetic patients with poor glycemic control. *Investigative Ophthalmology & Visual Science*, 33(2):356–63, 1992.

[183] M. Hammer, T. Heller, S. Jentsch, J. Dawczynski, D. Schweitzer, S. Peters, K. Schmidtke, and U. Muller. Retinal vessel oxygen saturation under flicker light stimulation in patients with nonproliferative diabetic retinopathy. *Investigative Ophthalmology & Visual Science*, 53(7):4063–4068, 2012.

[184] E. D. Gilmore, C. Hudson, R. K. Nrusimhadevara, R. Ridout, P. T. Harvey, M. Mandelcorn, W. Lam, and R. G. Devenyi. Retinal arteriolar hemodynamic response to a combined isocapnic hyperoxia and glucose provocation in early sight-threatening diabetic retinopathy. *Investigative Ophthalmology & Visual Science*, 49(2):699–705, 2008.

[185] M. E. J. Lott, J. E. Slocomb, V. Shivkumar, B. Smith, R. A. Gabbay, D. Quillen, T. W. gardner, and K. Bettermann. Comparison of retinal vasodilator and constrictor responses in type 2 diabetes. *Acta Ophthalmologica*, 90(6):e434–41, 2012.

[186] A. J. Jaap, M. S. Hammersley, A. C. Shore, and J. E. Tooke. Reduced microvascular hyperaemia in subjects at risk of developing type 2 (non-insulin-dependent) diabetes mellitus. *Diabetologia*, 37(2):214–6, 1994.

[187] A. J. Jaap, A. C. Shore, and J. E. Tooke. Relationship of insulin resistance to microvascular dysfunction in subjects with fasting hyperglycaemia. *Diabetologia*, 40(2):238–243, 1997.

[188] A E Caballero, S Arora, R Saouaf, S C Lim, P Smakowski, J Y Park, G L King, F W LoGerfo, E S Horton, and A Veves. Microvascular and macrovascular reactivity is reduced in subjects at risk for type 2 diabetes. *Diabetes*, 48(9):1856–1862, 1999.

[189] S Vehkavaara, A Seppälä-Lindroos, J Westerbacka, P H Groop, and H Yki-Järvinen. In vivo endothelial dysfunction characterizes patients with impaired fasting glucose. *Diabetes Care*, 22(12):2055–2060, 1999.

[190] M. J. Dumskyj and E. M. Kohner. Retinal blood flow regulation in diabetes mellitus: Impaired autoregulation and no detectable effect of autonomic neuropathy using laser doppler velocimetry, computer assisted image analysis, and isometric exercise. *Microvascular Research*, 57:353–356, 1999.

[191] G Garhöfer, C Zawinka, H Resch, P Kothy, L Schmetterer, and G T Dorner. Reduced response of retinal vessel diameters to flicker stimulation in patients with diabetes. *British Journal of Ophthalmology*, 88(7):887–891, 2004.

[192] Toke Bek, Javad Hajari, and Peter Jeppesen. Interaction between flicker-induced vasodilatation and pressure autoregulation in early retinopathy of type 2 diabetes. *Graefe's Archive for Clinical and Experimental Ophthalmology*, 246:763–769, 2008.

[193] S E Bursell, A C Clermont, B T Kinsley, D C Simonson, L M Aiello, and H A Wolpert. Retinal blood flow changes in patients with insulin-dependent diabetes mellitus and no diabetic retinopathy. *Investigative Ophthalmology & Visual Science*, 37(5):886–97, 1996.

[194] B.I. Levy, G. Ambrosio, A.R. Pries, and H.A.J. Struijker-Boudier. Microcirculation in hypertension: A new target for treatment? *Cir*, 104(6):735–740, 2001.

[195] P. S. Jensen, P. Jeppesen, and T. Bek. Differential diameter responses in macular and peripheral retinal arterioles may contribute to the regional distribution of diabetic retinopathy lesions. *Graefe's Archive for Clinical and Experimental Ophthalmology*, 249:407–412, 2011.

[196] Tien Yin Wong, Ronald Klein, Barbara E. K. Klein, Stacy M. Meuer, and Larry D. Hubbard. Retinal vessel diameters and their associations with age and blood pressure. *Investigative Ophthalmology & Visual Science*, 44(11):4644–4650, 2003.

[197] Harry Leung, Jie Jin Wang, Elena Rochtchina, Ava G. Tan, Tien Y. Wong, Ronald Klein, Larry D. Hubbard, and Paul Mitchell. Relationships between age, blood pressure, and retinal vessel diameters in an older population. *Investigative Ophthalmology & Visual Science*, 44(7):2900–2904, 2003.

[198] A. Richey Sharrett, Larry D. Hubbard, Lawton S. Cooper, Paul D. Sorlie, Rosemary J. Brothers, F. Javier Nieto, Joan L. Pinsky, and Ronald Klein. Retinal arteriolar diameters and elevated blood pressure: The atherosclerosis risk in communities study. *American Journal of Epidemiology*, 150(3):263–270, 1999.

[199] M. Kamran Ikram, Frank Jan de Jong, Johannes R. Vingerling, Jacqueline C. M. Witteman, Albert Hofman, Monique M. B. Breteler, and Paulus T. V. M. de Jong. Are retinal arteriolar or venular diameters associated with markers for cardiovascular disorders? the rotterdam study. *Investigative Ophthalmology & Visual Science*, 45(7):2129–2134, 2004.

[200] T Y Wong, L D Hubbard, R Klein, E K Marino, R Kronmal, A R Sharrett, D S Siscovick, G Burke, and J M Tielsch. Retinal microvascular abnormalities and

blood pressure in older people: the cardiovascular health study. *British Journal of Ophthalmology*, 86(9):1007–1013, 2002.

[201] W. Smith, J. J. Wang, T. Y. Wong, E. Rochtchina, R. Klein, S. R. Leeder, and P. Mitchell. Retinal arteriolar narrowing is associated with 5-year incident severe hypertension: The Blue Mountains eye study. *Hypertension*, 44:442–447, 2004.

[202] M. K. Ikram, J. C. M. Witteman, J. R. Vingerling, M. M. B. Breteler, A. Hofman, and P. T. V. M. de Jong. Retinal vessel diameters and risk of hypertension: The Rotterdam study. *Hypertension*, 47:189–194, 2006.

[203] T. Y. Wong, R. Klein, A. R. Sharrett, B. B. Duncan, D. J. Couper, B. E. Klein, L. D. Hubbard, and F. J. Nieto. Retinal arteriolar diameter and risk of hypertension. *Ann Intern Med*, 140(4):248–55, 2004.

[204] T. Y. Wong, A. Shankar, R. Klein, B. E. K. Klein, and L. D. Hubbard. Prospective cohort study of retinal vessel diameters and risk of hypertension. *BMJ*, 2004.

[205] Christian Delles, Georg Michelson, Joanna Harazny, Sebastian Oehmer, Karl F. Hilgers, and Roland E. Schmieder. Impaired endothelial function of the retinal vasculature in hypertensive patients. *Stroke*, 35(6):1289–1293, 2004.

[206] François Feihl, Lucas Liaudet, Bernard I. Levy, and Bernard Waeber. Hypertension and microvascular remodelling. *Cardiovascular Research*, 78(2):274–285, 2008.

[207] A. D. Hughes, A. V. Stanton, A. S. Jabbar, N. Chapman, M. E. Martinez-Perez, and S. A.McG Thom. Effect of antihypertensive treatment on retinal microvascular changes in hypertension. *Journal of Hypertension*, 26:1703–1707, 2008.

[208] E. Nagel, W. Vilser, A. Fink, T. Riemer, and I. Lanzl. Blood pressure effects on retinal vessel diameter and flicker response: a 1.5-year follow-up. *Eur J Ophthalmol*, 16(4):560–5, 2006.

[209] C Thuillez and V Richard. Targeting endothelial dysfunction in hypertensive subjects. *J Hum Hypertens*, 19:S21–S25, 2005.

[210] Lorenzo Ghiadoni, Armando Magagna, Daniele Versari, Isabella Kardasz, Yale Huang, Stefano Taddei, and Antonio Salvetti. Different effect of antihypertensive drugs on conduit artery endothelial function. *Hypertension*, 41(6):1281–1286, 2003.

[211] T Wong, A Shankar, R Klein, BK Klein, and LD Hubbard. Retinal arteriolar narrowing, hypertension, and subsequent risk of diabetes mellitus. *Archives of Internal Medicine*, 165(9):1060–1065, 2005.

[212] Thanh T. Nguyen, Jie Jin Wang, F.M. Amirul Islam, Paul Mitchell, Robyn J. Tapp, Paul Z. Zimmet, Richard Simpson, Jonathan Shaw, and Tien Y. Wong.

Retinal arteriolar narrowing predicts incidence of diabetes: The Australian diabetes, obesity and lifestyle (AusDiab) study. *Diabetes*, 57(3):536–539, 2008.

[213] R. Klein, C. E. Myers, K. E. Lee, R. Gangon, and B. E. K. Klein. Changes in retinal vessel diameter and incidence and progression of diabeic retinopathy. *Arch Ophthalmol*, 130(6):749–755, 2012.

[214] J. E. Grunwald, C. E. Riva, S. H. Sinclair, A. J. Brucker, and B. L. Petrig. Laser doppler velocimetry study of retinal circulation in diabetes mellitus. *Archives of Ophthalmology*, 104(7):991–996, 1986.

[215] G. Tikellis, J.J. Wang, R. Tapp, R. Simpson, P. Mitchell, P.Z. Zimmet, J. Shaw, and T.Y. Wong. The relationship of retinal vascular calibre to diabetes and retinopathy: the australian diabetes, obesity and lifestyle (ausdiab) study. *Diabetologia*, 50(11):2263–2271, 2007.

[216] M. Kamran Ikram, Joop A.M.J.L. Janssen, Anna M.E. Roos, Ingrid Rietveld, Jacqueline C.M. Witteman, Monique M.B. Breteler, Albert Hofman, Cornelia M. van Duijn, and Paulus T.V.M. de Jong. Retinal vessel diameters and risk of impaired fasting glucose or diabetes: The rotterdam study. *Diabetes*, 55(2):506–510, 2006.

[217] Sophie Louise Rogers, Gabriella Tikellis, Ning Cheung, Robyn Tapp, Jonathan Shaw, Paul Z. Zimmet, Paul Mitchell, Jie Jin Wang, and Tien Yin Wong. Retinal arteriolar caliber predicts incident retinopathy: The australian diabetes, obesity and lifestyle (ausdiab) study. *Diabetes Care*, 31(4):761–763, 2008.

[218] M. Lorenzi, G. T. Feke, E. Cagliero, L. Pitler, D. A. Schaumberg, F. Berisha, D. M. Nathan, and J. W. McMeel. Retinal haemodynamics in individuals with well-controlled type 1 diabetes. *Diabetologia*, 51(2):361–364, 2008.

[219] Aleksandra Mandecka, Jens Dawczynski, Walthard Vilser, Marcus Blum, Nicolle Muller, Christoph Kloos, Gunter Wolf, and Ulrich Alfons Muller. Abnormal retinal autoregulation is detected by provoked stimulation with flicker light in well-controlled patients with type 1 diabetes without retinopathy. *Diabetes Research and Clinical Practice*, 86(1):51–55, 2009.

[220] J. E. Grunwald, C. E. Riva, A. J. Brucker, S. H. Sinclair, and B. L. Petrig. Altered retinal vascular response to 100% oxygen breathing in diabetes mellitus. *Ophthalmology*, 91(12):1447–52, 1984.

[221] M. Blum, U. Kubetschka, W. Hunger-Dathe, K. Bachmann, U. A. Muller, and J. Strobel. [autoregulation retinaler arteriolen bei patienten mit diabetes mellitus und normalprobanden] autoregulation of retinal arterioles in diabetics and normals subjects. *Klin Monbl Augenheilkd*, 216(1):40–44, 2000.

[222] T. A. Gardiner, A. W. Stitt, H. R. Anderson, and D. B. Archer. Selective loss of vascular smooth muscle cells in the retinal microcirculation of diabetic dogs. *British Journal of Ophthalmology*, 78:54–60, 1994.

[223] G F Watts, S F O'Brien, W Silvester, and J A Millar. Impaired endothelium-dependent and independent dilatation of forearm resistance arteries in men with diet-treated non-insulin-dependent diabetes: role of dyslipidaemia. *Clin. Sci.*, 91(5):567–573, 1996.

[224] G.E. McVeigh, G.M. Brennan, G.D. Johnston, B.J. McDermott, L.T. McGrath, W.R. Henry, J.W. Andrews, and J.R. Hayes. Impaired endothelium-dependent and independent vasodilation in patients with type 2 (non-insulin-dependent) diabetes mellitus. *Diabetologia*, 35(8):771–776, 1992.

[225] S. J. Morris, A. C. Shore, and J. E. Tooke. Responses of the skin microcirculation to acetylcholine and sodium nitroprusside in patients with NIDDM. *Diabetologia*, 38(11):1337–44, 1995.

[226] S. Makimattila, M. Liu, J. Vakkilainen, A. Schlenzka, S. Lahdenpera, M. Syvanne, M. Mantysaari, P. Summanen, R. Bergholm, M. Taskinen, and H. Yki-Jarvinen. Impaired endothelium-dependent vasodilation in type 2 diabetes. *Diabetes Care*, 22:973–981, 1999.

[227] J. Goodfellow, M . W. Ramsey, L. A. Luddington, C. J. H. Jones, P. A. Coates, F. Dunstan, M. J. Lewis, Owens D. R, and A. H. Henderson. Endothelium and inelastic arteries: an early marker of vascular dysfunction in non-insulin dependent diabetes. *BMJ*, 312:744–5, 1996.

[228] J. Topping. *Errors of Observation and Their Treatment*. Chapman and Hall, Science Paperbacks, fourth edition, 1972.

[229] M. Bland. *An introduction to medical statistics*. Oxford University Press, third edition, 2000.